ISEL
INSTITUTO SUPERIOR DE ENGENHARIA DE LISBOA
DEPARTAMENTO DE ENGENHARIA QUÍMICA

Liquified biomass utilization in water co-electrolysis for Synthesis gas production

DIOGO MIGUEL MOUTA RODRIGUES MARTINS

(Licenciado em Engenharia Química e Biológica)

Trabalho final de Mestrado para obtenção do grau de Mestre em Engenharia Química e Biológica – Processos Químicos

Orientadores:

Doutor Jaime Filipe Borges Puna

Doutor Rui Galhano Dos Santos

Júri:

Presidente: Doutor Rui Manuel Gouveia Filipe

Vogais:

Doutor José Valério Nascimento Palmeira

Doutor Nelson Guerreiro Cortez Nunes

Doutor Jaime Filipe Borges Puna

setembro 2023

“Education is a progressive discovery of our own ignorance”

Will Durant

ACKNOWLEDGMENTS

As overly pessimistic person, over the last few years, as I worked and wrote this thesis, I never really believed that I would get to the end of this journey. Thankfully, I was lucky to have the support of people that helped me better believe in myself and get to the point where I am now. I would like to express my sincere appreciation and gratitude to the following individuals and organizations who have supported me throughout this.

First and foremost, I want to thank my supervisor, Prof. Jaime Puna, for his guidance, mentorship, and unwavering support. Although, he was constantly busy with other functions, he would always find time to answer my call and help me. I also need to express my gratitude for Prof. João Gomes, that while not an official supervisor, nevertheless provided much valuable assistance. His expertise, insightful feedback, and continuous encouragement have been instrumental in shaping this research.

I'm very thankful for Project "CLEANFOREST", ref. PCIF/GVB/0167/2018 funded through the *Fundação para a Ciência e Tecnologia* (FCT, I.P.), in which I have been integrated as part of its research group, for the opportunities granted and for financing my presentations at CEMMEERS-23 and Chempor-23. This insightful experience helped me better realize my potential and enriched my set of skills by exposing me to the world of academic research.

To my colleagues and great friends Tiago Cabrita, Ailton Gonçalves and Ana Rita Marçalo, I owe a lot. Your support and assistance were a crucial motivation throughout this journey. Their insightful discussions, encouragement, and camaraderie have been invaluable in shaping my ideas and refining my research.

Lastly, I would like to express my deepest gratitude to my family and friends for their unwavering support, understanding, and encouragement throughout this entire endeavor. Their love, patience, and belief in me have been my constant motivation, and I am incredibly fortunate to have them by my side. My mother, father and dear sister that were always there, with their support when I needed the most. My old friend Ricardo Ribeiro for his (although unusual) methods to push me into keep going and believe in myself. My dear girlfriend, Madalena for her never-ending support. And to all friends that I made along the way, Rafael Augusto, Miguel Andre and some more, I am grateful to have known in my life.

Finally, although I might risk sounding somewhat arrogant, I want to thank myself for never giving up, even in the hardest times. Before writing this I never thought I was good enough or even able to write a final thesis that I would be proud, but throughout it all I chose to keep going until the end.

To all of you, thanks for being there

ABSTRACT

Over the last decades, the increase in the World's energy needs resulted in growing consumption of non-renewable fuel sources and, consequently, greater environmental impacts. For this reason, there is an increasing commitment to develop alternative sustainable energy sources (biomass, solar and wind energy, among others).

Developed within the scope of an R&DT project by the start-up GSYF, Lda, this 1 kW pilot unit aims at the recovery of previously liquefied biomass from lignocellulosic forest residues, later used as a carbon source for co-electrolysis to produce synthesis gas (H_2, O_2, CO, and CO_2), also known as syngas. In turn, this will be transformed into other value-added products, such as methane, methanol or biodiesel. This research focuses on further developing this unit through optimization tests to determine the ideal conditions for syngas production to be used as a feedstock for methane production.

The experimental work was divided into two main parts, first a set of tests without any addition of biomass and with a wider range of conditions (3, 4 and 5 bar gauge and 90, 100 and 110 ºC using 1M NaOH or KOH electrolyte) acting as a baseline for the second set of tests where two samples of liquified biomass were tested (labelled as Acacia and Energreen). The syngas produced should have a low O_2 content, a CO_2:H_2 ratio close to the 1:4 found in the Sabatier reaction, and a good energy spent per amount of gas produced relation.

In the first part, higher pressures and temperatures beneficiated the process. Additionally, from the two electrolytes tested, the NaOH solution proved himself as the better choice due to the lower energy expenditure and being easier to work with. With these results, a narrower range of conditions was chosen (4 and 5 bar(g), and 100 and 110 ºC using only the 1M NaOH electrolyte) to be used in future tests.

In the second part, the additions of liquified biomass boosted CO_2 production which as a consequence also lowered O_2 concentrations. Acacia is better at lowering O_2 content while Energreen had a lower energy consumption. When considering each biomass strengths, both showed the best results at 4 bar(g) at 110 ºC with 2.5 % of biomass.

Keywords: Syngas, Biomass, Water Electrolysis, Electrochemical process, Renewable energy, Biodiesel, methane production.

RESUMO

Nas últimas décadas, o aumento das necessidades energéticas mundiais resultou num consumo crescente de fontes de energia não renováveis e, consequentemente, em graves impactes ambientais. Por esta razão, existe uma aposta cada vez maior no desenvolvimento de fontes alternativas de energia sustentáveis (biomassa, energia solar e eólica, entre outras).

Desenvolvida no âmbito de um projeto de I&DT pela start-up GSYF, Lda, esta unidade piloto de 1 kW visa a recuperação de biomassa previamente liquefeita de resíduos florestais lignocelulósicos, para uso como fonte de carbono em co-eletrólise para produção de gás de síntese (H_2, O_2, CO, e CO_2), também conhecido como syngas. Por sua vez, este será transformado noutros produtos de valor acrescentado, como o metano, o metanol ou o biodiesel. Esta investigação centra-se no desenvolvimento desta unidade através de testes de otimização para determinar as condições ideais para a produção de syngas, destinado a ser utilizado como matéria-prima para a produção de metano.

O trabalho experimental dividiu-se em duas partes principais, sendo a primeira um conjunto de ensaios sem adição de biomassa e com uma gama mais alargada de condições (3, 4 e 5 bar relativos, e 90, 100 e 110 ºC usando eletrólito 1M NaOH ou KOH) que serviram de base para o segundo conjunto de ensaios onde foram testadas duas amostras de biomassa liquefeita (designadas por Acácia e Energreen). O gás de síntese produzido deve ter um baixo teor de O_2, um rácio CO_2:H_2 próximo do rácio 1:4 encontrado na reação de Sabatier e uma boa relação entre a energia gasta e a quantidade de gás produzido.

Na primeira parte, pressões e temperaturas mais elevadas favoreceram o processo. Além disso, dos dois eletrólitos testados, a solução de NaOH provou ser a melhor escolha devido ao menor gasto de energia e por ser mais fácil de trabalhar. Com estes resultados, foi escolhida uma gama de condições mais restrita (4 e 5 bar relativos, e 100 e 110 ºC utilizando apenas o eletrólito NaOH 1M) para ser utilizada em testes futuros.

Na segunda parte, as adições de biomassa liquefeita aumentaram a produção de CO_2, o que, consequentemente, também reduziu as concentrações de O_2. A Acacia é melhor na redução do teor de O_2, enquanto a Energreen tem um consumo de energia mais baixo. Ao considerar os pontos fortes de cada biomassa, ambas apresentaram os melhores resultados a 4 bar de pressão a 110 ºC com 2,5 % de biomassa.

Palavras-chave: Syngas, Biomassa, Eletrólise da água, Processo eletroquímico, Energia renovável, Biodiesel, Produção de metano.

TABLE OF CONTENTS

FIGURE INDEX

Index of Tables

LIST OF ACRONYMS

(R)WGS	Reverse Water-Gas Shift Reaction
AEM	Anion Exchange Membrane
bar(g)	Bar gauge
BASF	Badische Anilin & Soda Fabrik
BCE	Before the Common era
bio-DME	bio-dimethyl ether
CIS	Commonwealth of independent states
DC	Direct current
DME	Dimethyl-Ether
EJ	Exajoules
EU	European Union
F	Flow of gas produced
FTIR	Fourier-transform infrared
GHG	greenhouse gases
GISS	Goddard Institute of Space Studies
GMST	Global mean surface temperature
GSYF Lda	GreenSynFuel
CO_2: H_2	unit of hydrogen molecules per molecule of CO_2
HFCs	hydrofluorocarbons
I	Current Intensity
ICI	Imperial Chemical Industries
IEA	International Energy Agency
IPCC	Intergovernmental Panel on Climate Change
IRENA	International Renewable Energy Agency
JRC	Joint Research center
LULUCF	Land use, land-use change, and forestry
M	Mols per liter
$M_{elect.}$	Molar mass of the electrolyte
m	Mass
w/w	weight of solute per weight of solvent
Mt CO_2 /yr	Mega tons of CO2 emmitted per year
MTBE	Methyl Ter-Butyl Ether
MTG	methanol-to-gasoline

MTO	methanol-to-olefins
n	number of moles
NAEI	National Atmospheric Emissions Inventory
NASA	National Aeronautics and Space Administration
NO_x	nitrogen oxides
OHC	Ocean Heat Content
P	Pressure
PBL	Publication
PEM	Proton Exchange Membrane
PFCs	perfluorocarbons
R&Dt	Research and development
SMR	Steam Methane Reforming
SNG	Synthetic Natural Gas
SOEC	Solid oxide electrolysis cell
T	Temperature
UK	United Kingdom
UN	United Nations
UNCED	United Nations Conference on environment and development
UNCHE	United Nations Conference on the Environment
V	Voltage
V/cell	Voltage per cell
W/F	Energy expenditure
WGS	water-gas shift
WMO	World Metrologic Organization

1. State of the art

1.1. Global energetic consumption and modern context

In order to produce most goods and services, energy consumption (on any form) is required. Thus, the more developed we get as a civilization, the higher our total energetic consumption becomes. Unfortunately, this increase in consumption has led to an increase in carbon emissions and the discharge of other pollutants, thus placing tremendous pressure on the environment and putting in question our future energy supplies (Ma & Fu, 2020).

As an economic system becomes more developed it becomes easier to fund smaller companies, allowing them to scale-up faster, resulting in higher energetic consumption. On the other hand, consumers in more financially stable areas tend to have more disposable income which enhances the consumption of non-essential products, such as luxury goods, cars, and electrical appliances, thus elevating the energy demand. This increase in consumption of products and services, results in an increase in total energy needs and, consequently, increasing its environmental impact (Yue et al., 2019).

As a result, there has been an increase in the World's yearly energy consumption over the last 50 years. In Europe alone, the total consumption in exajoules (EJ) has risen from 44.69 in 1965, to 82.38 in 2021, or in other words, an increase of 84.34 % (B.P. Statistical Review, 2022). While this increase is correlated to the civilization's development in the last century, it also puts into question the sustainability of our current energy supply and the impacts that we might have on the global environment (Dessie et al., 2023).

The following graph (Figure 1-1), using data from B.P. Statistical Review (2022), shows the gradual increase in primary energy consumption worldwide. It is important to note that the pronounced decrease in 2020 resulted from the lockdowns and restrictions imposed by the Covid-19 pandemic, temporarily reducing primary energy consumption and emissions (B.P. Statistical Review, 2022).

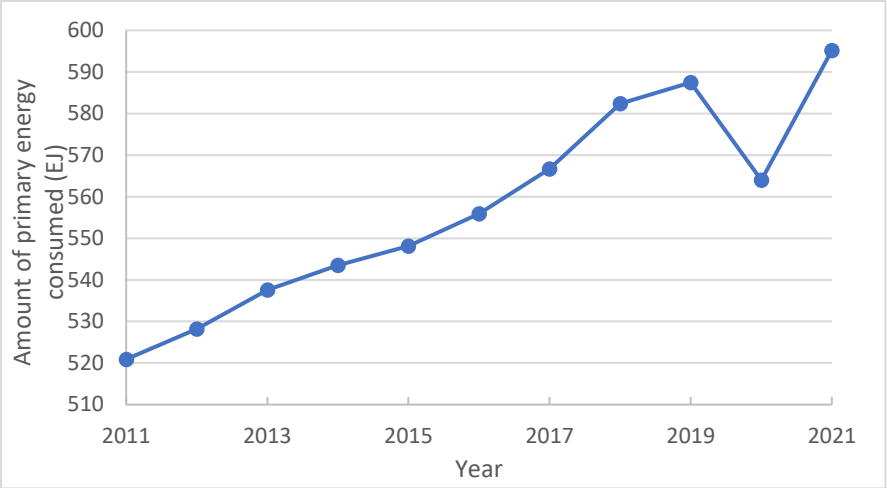

Figure 1-1: Total Primary energy consumed worldwide over the last 10 years (B.P. Statistical Review, 2022)*;*

In terms of energy sources, these can be divided into three distinctive classes: primary, secondary, and final energy (Senior, 2008):

- Primary sources correspond to any type of energy in its raw and natural forms not converted into any other forms of energy;
- Secondary sources: includes the vast group of products obtained from petroleum, such as Diesel fuel, gasoline, kerosene, etc;
- Final sources: other sources that cannot be directly sourced from nature and obtained by converting primary and secondary sources into other forms of energy.

A short list of various primary, secondary and final sources has been compiled in the Table 1-1 presented below:

Table 1-1: Examples of the different energy sources adapted from (Senior, 2008)*;*

Type of energy source	**Primary**	**Secondary**	**Final**
Examples	Biomass Oil Natural gas Solar, geothermal, and hydroelectric energy Wind power	Diesel Gasoline Kerosene Liquified petroleum gas (also known as LPG)	Electricity Heat

Additionally, primary energy sources can be classified as renewable and nonrenewable (or exhaustible) sources depending on their ability to renew their availability in the scale of a human lifetime. Renewable sources include solar, geothermal, and hydroelectric energy, as well as wind power, while non-renewable include finite resources such as oil, natural gas, mineral

coal, uranium, and plutonium (Güney, 2019; *Primary, Secondary, Final, and Useful Energy: Why Are There Different Ways of Measuring Energy? - Our World in Data*, n.d.).

As the name implies, non-renewable sources such as oil pose an expectable problem when it comes to the finite nature of their reserves and the resultant problematic shortages that we might have in the future if we overly rely on them. On the other hand, renewable energies come from practically unlimited and almost infinite sources, and, as such, can offer a better and more sustainable alternative to most exhaustible sources used for energy production. For this same reason, in the last few decades, primary energy consumption has been slowly replacing exhaustible sources in choice of renewable alternatives (Güney, 2019; *Primary, Secondary, Final, and Useful Energy: Why Are There Different Ways of Measuring Energy? - Our World in Data*, n.d.).

Even though renewable sources provide better chances for a more sustainable future, our society is still at a point where we depend mainly on exhaustible resources like oil and coal due to being energy-rich and relatively cheap to process and transform into other forms of energy. Even though research and development have been pushing for the use of more sustainable alternatives, as can be concluded from the data from B.P. Statistical Review(2022) (in Figure 1-2), in terms of primary energy consumption, most of it is still sourced from exhaustible sources (B.P. Statistical Review, 2022; Kim & Park, 2016).

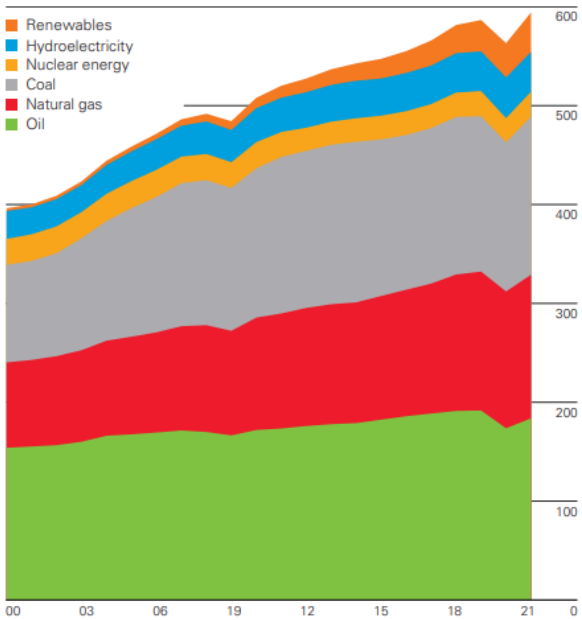

Figure 1-2: Primary energy consumption over the last 20 years in exajoules adapted from (B.P. Statistical Review, 2022)*;*

According to the data presented in Figure 1-2, by the year 2021, from a total primary energy consumption of 595.15 EJ, 514.97 EJ (86.53 %) were sorted from non-renewable

sources, while only 80.17 EJ (13.47 %) is originated from renewable ones. Furthermore, among all primary sources, oil was the most consumed with 184.21 EJ (or 30.95 % of the total energy consumption) followed up by natural gas with 145.35 EJ (or 24.42 %). Once again, this illustrates that, despite all the recent advancements in the field of renewable energies and the attempts of promoting their use, when considering the worldwide context, society is still dependent on exhaustible resources (B.P. Statistical Review, 2022).

1.2. Emissions and associated problems

Besides its exhaustible nature, fossil fuel consumption results in massive carbon emissions and other harmful products resulting from their use. When used as a source of energy, fossil sources such as oil, coal, and natural gas produce a secondary product residue in the form of gas emissions and solid substances that cannot be reprocessed further in the industry, thus polluting the environment. Among the effects of these pollutants, the two most concerning, at present, are the decrease in the quality of life due to air pollution (particularly associated with coal burning emissions), and climate changes, which are mainly due to the greenhouse effect (Güney, 2019).

Akin to a greenhouse, where sun light enters and the heat is retained, the greenhouse effect (as the name implies) refers to a similar phenomenon where a specific group of gases, designated as greenhouse gases (GHGs), act as the glass wall of a greenhouse, thus raising global temperatures. According to the Kyoto protocol, the main GHGs include carbon dioxide (CO_2), methane (CH_4), nitrogen dioxide (NO_2), hydrofluorocarbons (HFCs), perfluorocarbons (PFCs), sulfur hexafluoride (SF_6) and nitrogen trifluoride (NF_3). The figure below (Figure 1-3), based on data from the UN Emissions Gap report 2022, shows the total yearly anthropogenic GHGs emissions, for each respective group of gases, including specific CO_2 emitted from land use, land-use change, and forestry (LULUCF), which, as the name implies, designates the sector covering emissions and removals of GHGs resulting from direct human-induced land use, land use, change and forestry activities (Scheiner, 2023; UN Enviroment Programme, 2022).

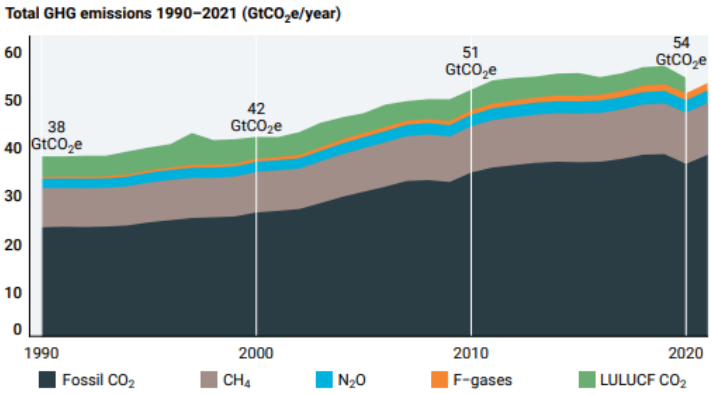

Figure 1-3: Total GHG emissions by gas from 1990 to 2021(GtCO2e/year) adapted from (UN Enviroment Programme, 2022)*;*

As shown in Figure 1-3, among this particular group, Fossil CO_2 is the main contributor to global warming followed by CH_4, making it the main focus of most climate change initiatives (*Overview of Greenhouse Gases - NAEI, UK*, n.d.). Beyond this, in the last three decades alone the total anthropogenic CO_2 emissions have risen by approximately 67 % (JRC, 2022). Further data confirming this increase in emissions, the respective division by sector, and other important details can be found in Figure 1-4.

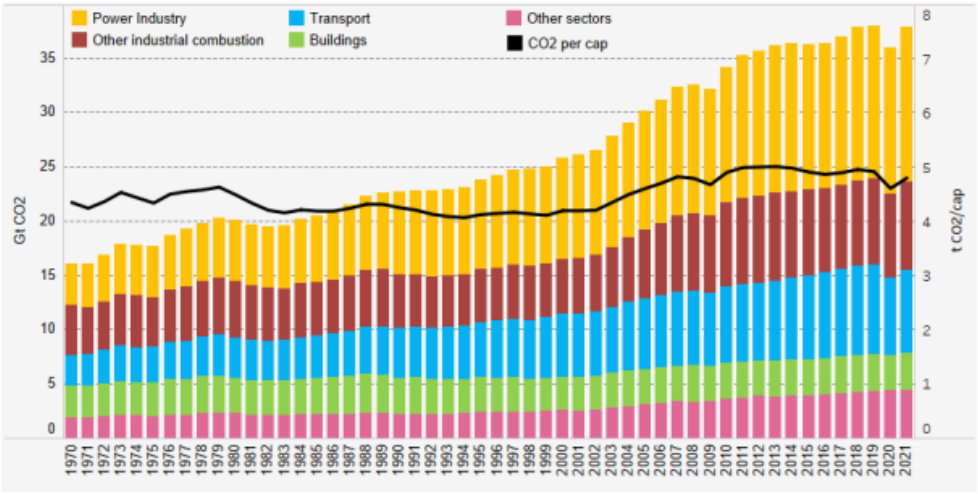

Figure 1-4: Fossil fuel CO_2 emissions by sector, CO_2 emission per capita from 1970 to 2021 adapted from (JRC, 2022)*;*

Table 1-2: Specific values from Figure 1-4 for the years 1990, 2005, 2020, and 2021 (JRC, 2022)*;*

Year	CO_2 emissions Mt CO_2/yr	CO_2 emissions per capita tCO_2/cap/yr	Estimated world Population
2021	37857.58	4.811	7.87E+09
2020	35960.67	4.618	7.79E+09
2005	30161.58	4.614	6.54E+09
1990	22717.73	4.264	5.33E+09

From among all the individual sectors in Figure 1-4, the power industry presents the highest volume in emissions and the most noticeable growth over the years, having experienced an increase of approximately 87 %, since 1990, in contrast to the previously referred growth of 67 % in total global CO_2 emissions. Once again, this proves that the current development, as a society, has resulted in a continual increase in energy consumption and, as a consequence, provoked side effects in the form of pollution that will, in the long run, put on more strain, and can destroy a balanced environment and even possibly harm future generations in a not so distant future (W. C. Lu, 2017).

While it is true that most developed countries have been trying to decrease their carbon footprint (by decreasing their CO_2 emission and slowly relying on more renewable alternatives), on a global scale there is still an annual growth correlated to a few countries like China and India that still depend on sources such as mineral coal for their energy production. As a comparison, while the European Union (EU) as a whole, has progressed from emitting 3819.2 $MtCO_2$/yr in 1990 to 2774.9 $MtCO_2$/yr in 2021 (or in other words, approximately 27 % less), China alone went from 2425.6 $MtCO_2$/yr to 12466.3 $MtCO_2$/yr, for the same period (approximately 414 % More) (JRC, 2022). Figure 1-5 displays the Fossil CO_2 emissions of the six major emitting economies according to JRC/IEA/PBL 2022 Report.

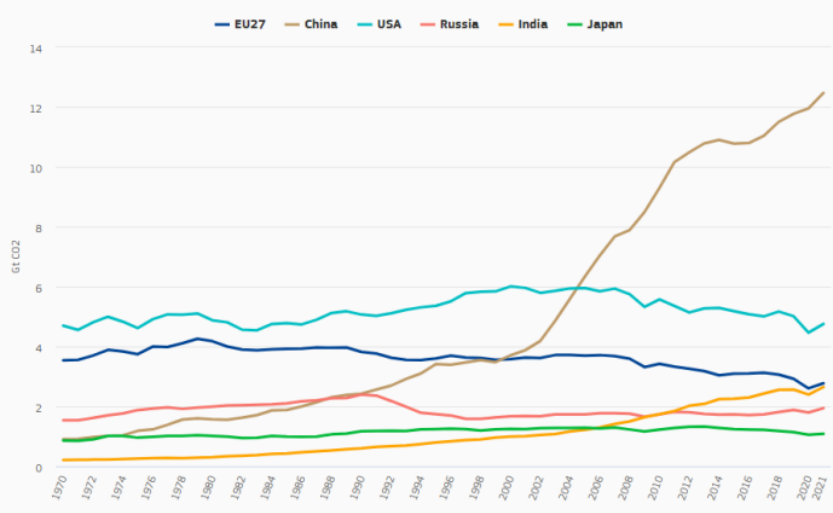

Figure 1-5: Fossil CO2 emissions of the major emitting economies from 1970 to 2021(JRC, 2022)*;*

The main problem resulting from these emissions is their direct correlation with the increase of the greenhouse effect and, consequentially, global warming and climate change in general. According to the World Metrologic Organization (WMO), in January-September 2022 the Global mean surface temperature (GMST) was 1,15±0.13 ºC warmer when compared to the established pre-industrial baseline. While this number may appear low, it results into multiple

negative side effects for the environment and signals future consequences that might still have a chance to be avoided (Jarvis et al., 2009; *Provisional State of the Global Climate 2022*, n.d.).

Figure 1-6 (Taken directly from WMO, Provisional State of the Global Climate 2022) displays the direct effects of increased CO_2 concentration in the atmosphere, as well as the corresponding risks that might affect mankind directly if no specific measures towards more sustainable development are pursued.

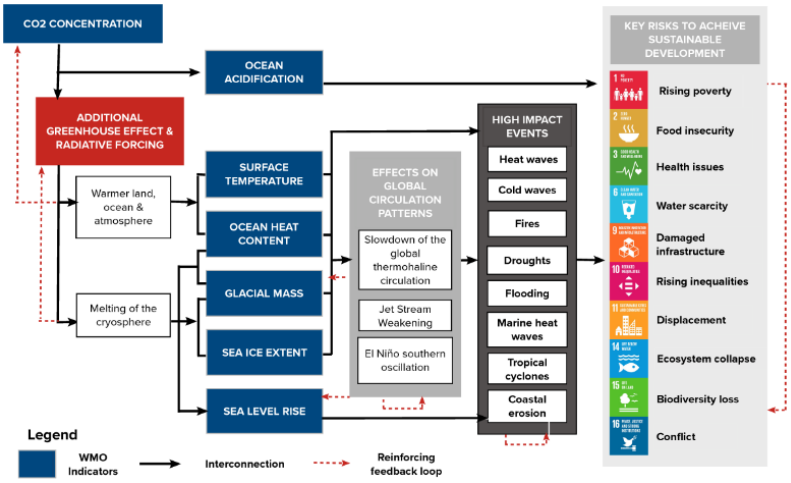

Figure 1-6: Impacts of High CO_2 concentrations and key risks adapted from(Provisional State of the Global Climate 2022, n.d.*);*

The gradual rise of global temperatures caused by the greenhouse effect that took place in the last decade, the warmest one recorded, is threatening the planet and, thus, the civilization as we know it over the last decades, global warming has intensified and created various environmental problems, such as increased desertification and drought in some areas of the globe, changes in the patterns of snow and rainfall, glaciers melting and, as a consequence, rise in sea levels, and changing the behavior or even endanger entire species of animal and plants (*Provisional State of the Global Climate 2022*, n.d.; Rehman et al., 2017).

Figure 1-7 presents the difference in temperature from a pre-industrial baseline (1880-1910) to the current year (2022) according to NASA Goddard Institute for Space Studies (GISS) Surface Temperature Analyses tool (*Data.GISS: GISS Surface Temperature Analysis (v4): Global Maps*, n.d.).

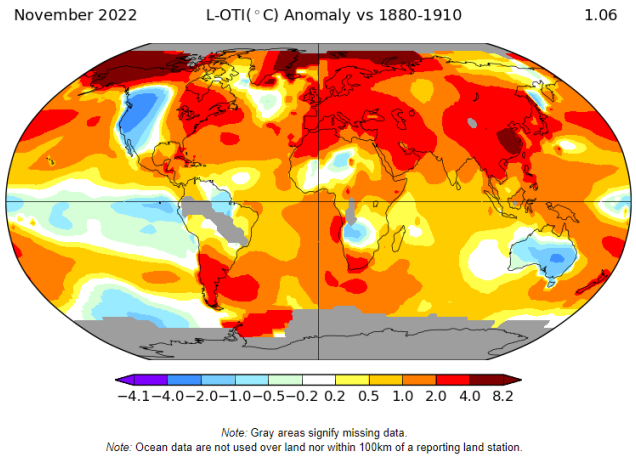

Figure 1-7: Temperature anomaly from 1880-1910 average to 2022 adapted from (*Data.GISS: GISS Surface Temperature Analysis (v4): Global Maps*, n.d.)*;*

From the whole energy accumulated on earth due to the greenhouse effects, around 90 % is absorbed by the oceans. This heat accumulation is measured through a unit designated Ocean Heat Content (OHC), being measured at various depths up to 2000 meters deep (Cai et al., 2023; *Provisional State of the Global Climate 2022*, n.d.).

As the data from Figure 1-8 shows, the last two decades alone show a strong noticeable increase in this value, which carries significant consequences not only to aquatic biodiversity but to the entire planet too (*Provisional State of the Global Climate 2022*, n.d.).

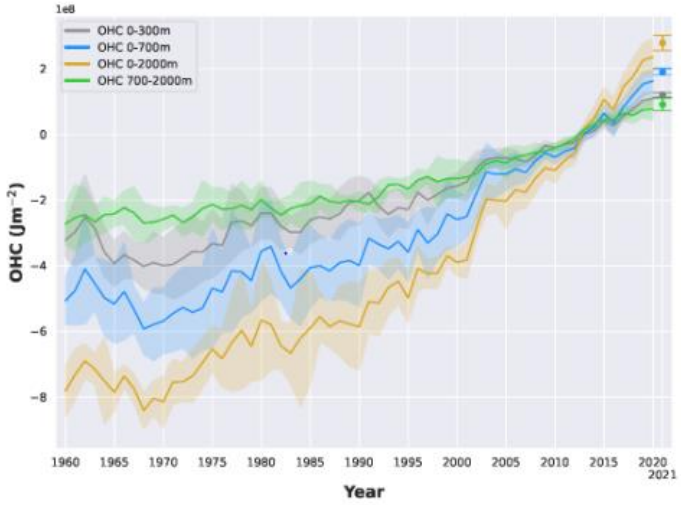

Figure 1-8: OCH values up to the depth of 2000 meters from 1960 to 2021 adapted from(*Provisional State of the Global Climate 2022*, n.d.)*;*

The rise in the temperature of sea waters carries numerous consequences that might not affect mankind directly, but will result in further indirect problems down the line. One key example is the risk it presents to coral reefs, as their extreme sensitivity to temperature changes

makes them one of the most vulnerable ecosystems when facing climate change. If seawater gets too warm coral will release the micro-algae present in their structure, leaving them with a "bleached" appearance, designating this phenomenon as "Coral Bleaching". Coral health is quite important as reefs are important habitat for numerous ecosystems, and act as a natural protection for coastlines against erosion and storms, and also serve as a source of tourism (Shlesinger & van Woesik, 2023; Thangal et al., 2022).

On the other hand, rising anthropogenic CO_2 concentration in the atmosphere also significantly impacts Ocean water's pH level since around 23 % of the CO_2 emitted to the atmosphere is absorbed by the oceans. While this helps, to some degree, to alleviate climate change, when combined with seawater, CO_2 forms Carbonic Acid (H_2CO_3), leading to the acidification of sea water (Thangal et al., 2022).

Figure 1-9 displays the steady decline of Global mean ocean pH experienced since 1985.

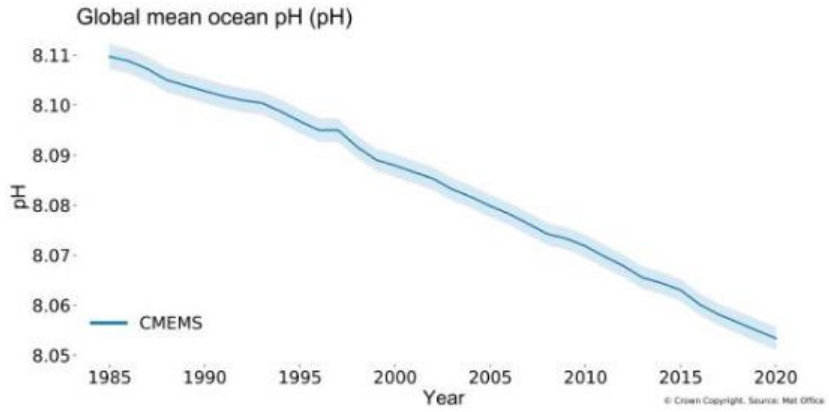

Figure 1-9: Global Mean Ocean pH from 1985 to 2020 adapted from (*Provisional State of the Global Climate 2022*, n.d.)*;*

The decrease in global mean pH, may endanger key organisms such as fish and coral, and, consequently, expose them in order to damage the entire ecosystem, potentially affecting food supplies and worsening already existing problems such as world hunger. It is estimated that by 2100, oceans' pH could be down to 7.8 due to the continual release of CO_2 by multiple anthropogenic sources such as the gas industry, burning of fossil fuels, deforestation, and many others (*Provisional State of the Global Climate 2022*, n.d.; Thangal et al., 2022).

While the negative development footprint society left on the planet is undeniable, there are still measures to be taken to remedy global warming or, at least, mitigate its impacts. Taking urgent action to combat climate change is a priority due to the risk it presents to millions of people (*Climate Change - United Nations Sustainable Development*, n.d.; Kvamme, 2023).

In 1972, the United Nations Conference on the Environment (UNCHE) held in Stockholm, Sweden marked itself as the first international gathering focusing on human activities concerning the environment and paved the path for what would become the modern discourse for environmental action at an international level (Vasseur, 1973).

Until the 1980s, the environmental approach was primarily centered on a sectoral and restorative way with the objective of rectifying damages already caused. However, from the 1990s on, this perspective shifted to the prevention and reduction of eco-disasters and environmental damage. Additionally, in 1992 the United Nations Conference on environment and development (UNCED), held in Rio de Janeiro, Brazil proposed a new approach, more focused on a social dimension and the necessity to create the tools required for more sustained development. In other words, sustainable development and the protection of the environment would be treated as "global" priorities, and as such, should be taken into consideration when planning future economic and social development (Barcena, 1992).

As shown previously in Figure 1-1, except for 2020, primary energy consumption has risen consistently over the years and most predictions point out to the same behavior in the future as a by-product of economic and population development. While this is almost unavoidable, as the society progresses to a better compromise between the needs for energy production and environmental protection, it may be possible to decrease energy loss during energy production and, gradually substitute the use of exhaustible energy sources with cleaner renewable ones (B.P. Statistical Review, 2022).

Focusing on the increase in the use of renewable sources in the last two decades, Figure 1-10 shows the percentual share of global primary use according to the BP Statistical review of world energy, 2022:

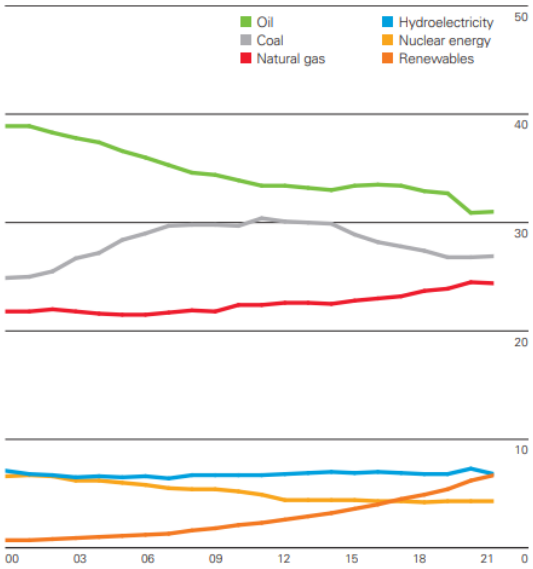

Figure 1-10: Shares (%) of global primary energy over the last decade (2001-2021) adapted from (B.P. Statistical Review, 2022)*;*

As the data confirms, in the period between 2001 and 2021, the use of renewable sources (not counting hydroelectric energy as the data separates the two) showed a significant increase in global shares, surpassing nuclear energy and reaching approximately 6.7 % in 2021. Nevertheless, despite their continual decrease in use as energy sources, the two sources with the biggest share are still oil and coal respectively with global shares of approximately 31.0 % and 26.9 %.

Now analyzing on a regional basis, Figure 1-11 shows regional patterns of primary energy consumption in 2021:

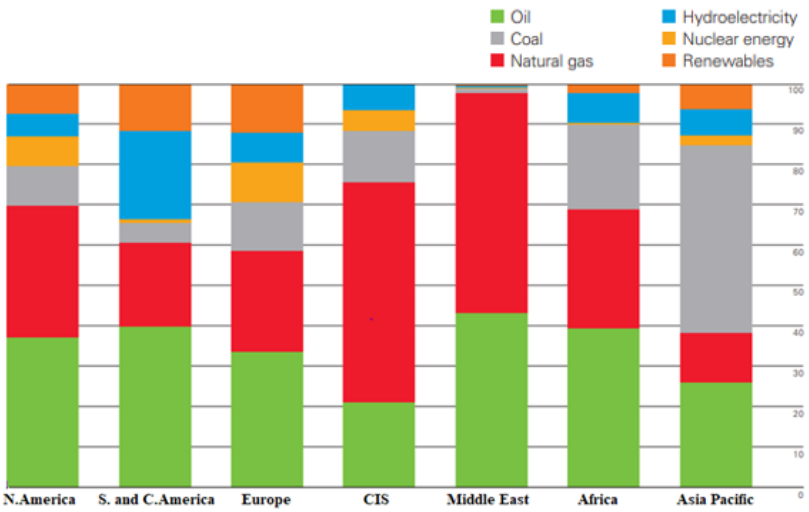

Figure 1-11: Regional consumption patterns of 2021adapted from(B.P. Statistical Review, 2022)*;*

By considering the distribution of the primary energy consumption in each region in 2021, it can be concluded that:

- Oil is the dominant source in North America (with a share of approximately 37.0 %), South and Central America (39.8 %), Europe (33.5 %), and Africa (39.3 %). Additionally, oil is the second most consumed source on the Commonwealth of independent states (CIS) (21.0 %), Middle East (43.1 %), and Asia Pacific (25.9 %)(B.P. Statistical Review, 2022);
- Natural gas, on the other hand, is the dominant source in the CIS (54.5 %) and Middle East (54.7 %) and is second to oil in North America (32.7 %), Europe (25.0 %), and Africa (29.6 %)(B.P. Statistical Review, 2022);
- At last Coal is a dominant fuel in Pacific Asia (46.8 %) due to high exploration of the existent mines (more specifically in China), making this region responsible for approximately 79.7 % of global coal consumption (B.P. Statistical Review, 2022).

According to the latest assessment report from the IPCC, if greenhouse gas emissions continue to increase at their current rate, the global average temperature is likely to rise by more than 1.5 °C above pre-industrial levels by the end of the century. This temperature increase could lead to a wide range of impacts, including more frequent heatwaves, more intense and frequent extreme weather events, sea level rise, and marked changes in the distribution and abundance of plants and animals. To limit the risks of these impacts, the IPCC recommends reducing greenhouse gas emissions to keep the global average temperature increase to below 2 °C, preferably below 1.5 °C. Therefore it is imperative that for “us”, as a society, to take action and steer energy production to a more sustainable future, by finding cleaner and more sustainable sources and reducing the emissions produced in their use (IPCC, n.d.).

1.3. Electrolysis

1.3.1. Water Electrolysis

Water electrolysis is an electrochemical process in which water (H_2O) is decomposed into hydrogen (H_2) and oxygen (O_2) gases by passing an electric current through it. The process is based on the fact that water is an electricity conductor, and can be decomposed into its constituent elements, hydrogen, and oxygen when an electric current is passed through it (Gerloff, 2021).

In general, the global reaction is: $H_2O \rightarrow H_2 + \frac{1}{2}O_2$ (1-1)

1.3.1.1. Brief historical background

The process of electrolysis has been known since the early 19th century, but it was not until the 20th century that it began to be used on a large scale as a means of producing hydrogen. The first recorded observation of the decomposition of water into hydrogen and oxygen using electricity was made in 1800 by William Nicholson and Anthony Carlisle, who passed an electric current through water and observed the production of hydrogen and oxygen. However, it was not until the development of the voltaic pile, a device that could produce a sustained electric current, that electrolysis became a practical method for producing hydrogen (IRENA, 2020).

In the early 20th century, the electrolysis of water was primarily used for the production of hydrogen for use in the manufacturing of ammonia for fertilizers. It was not until the energy crisis of the 1970s that the use of electrolysis for the production of hydrogen as a fuel began to gain widespread attention as a potential alternative to fossil fuels. Today, electrolysis is used in a variety of applications, including the production of hydrogen for use in fuel cells, the production of chlorine and caustic soda for the chemical industry, and the purification of metals (IRENA, 2020).

The historical progress of water electrolysis and its important steps over the last two centuries are displayed in a summarized form in Figure 1-12:

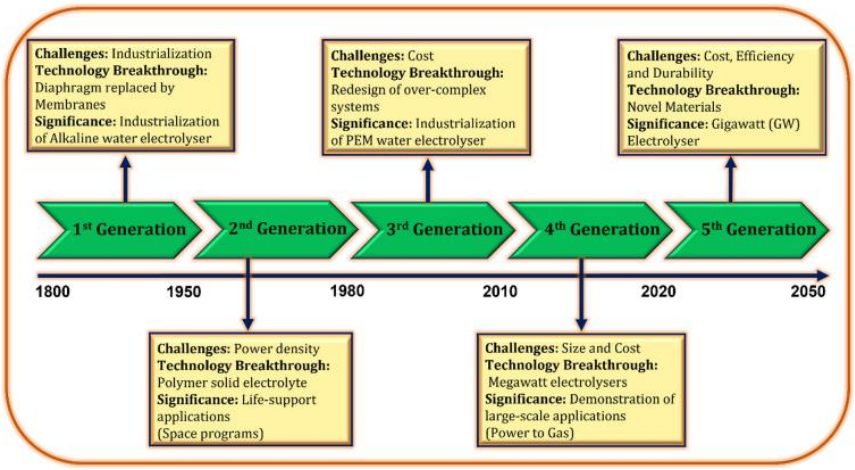

Figure 1-12: Generations of water electrolysis development adapted from (Shiva Kumar & Lim, 2022)*;*

1.3.1.2. The importance of water electrolysis and hydrogen in the modern industry

As the lightest and most abundant chemical substance in the universe, hydrogen is an important component of modern industry and is used in a variety of applications. Some of the key uses of hydrogen include (Gerloff, 2021; Lavate et al., 2023):

- Transportation: hydrogen can be used as fuel for vehicles, as several hydrogen-powered cars are already on the market. Hydrogen has the advantage of being a clean-burning fuel that does not produce harmful emissions, making it a potential alternative to gasoline and diesel;
- Electricity generation: hydrogen can be used to generate electricity through fuel cells, which use a chemical reaction between hydrogen and oxygen to produce electricity. Fuel cells are used in a variety of applications, including portable electronic devices, backup power systems, and even in some vehicles as already referred to;
- Industrial processes: hydrogen is used in a variety of industrial processes, including the production of fertilizers, plastics, and other chemicals. It is also used in the refining of petroleum and the production of steel;
- Energy vector: As hydrogen can store large amounts of energy in a compact form, it can be produced when excess electricity is available, such as from renewable sources like wind or solar power. This hydrogen can then be stored and used later for energy production when needed.

Overall, hydrogen is an important component of the modern industry due to its versatility and ability to be used as a clean-burning fuel. Its importance is expected to continue to grow in the coming years as the demand for clean energy sources increases (Kelly, 2014).

Hydrogen is classified according to a color code system-based production technology, source of energy used, and environmental impact. The meaning of each color code can be found below in Figure 1-13:

Hydrogen Color	Technology	Source	Products	Cost ($ kg/H_2)	CO_2 emissions
Brown Hydrogen	Gasification	Brown coal (Lignite)	$H_2 + CO_2$	1.2–2.1	High
Black Hydrogen	Gasification	Black coal (Bituminous)	$H_2 + CO_2$	1.2–2.1	High
Grey Hydrogen	Reforming	Natural gas	$H_2 + CO_2$ (Released)	1–2.1	Medium
Blue Hydrogen	Reforming + carbon capture	Natural gas	$H_2 + CO_2$ (Captured 85-95%)	1.5–2.9	Low
Green Hydrogen	Electrolysis	Water	$H_2 + O_2$	3.6–5.8	Minimal

Figure 1-13: Hydrogen color codes and their Technology, cost, and CO2 emissions (Shiva Kumar & Lim, 2022)*;*

Water electrolysis is one of the primary methods used to produce hydrogen in an environmentally friendly way. It uses electric current (more specially DC current) to split water molecules into hydrogen and oxygen. The electric energy used in the process can be generated

directly from renewable sources such as solar or wind power. This makes water electrolysis a way to produce hydrogen that does not contribute to climate change. As a result, water electrolysis is an important technology for producing clean hydrogen fuel and reducing our reliance on fossil fuels (Kelly, 2014; Shiva Kumar & Lim, 2022).

There are currently several challenges to the widespread adoption of green hydrogen, including the high cost of production and the lack of infrastructure for storing and distributing hydrogen. However, as renewable energy prices continue to decline and technology improves, green hydrogen is expected to become more competitive with fossil fuels and could play a major role in the energy mix of the future (Mazzeo et al., 2022).

1.3.2. Principal of water electrolysis and modern technologies

With the development of the technology, several variations of water electrolysis were introduced. Out of these, the main four are Alkaline water electrolysis, Proton Exchange Membrane (PEM) electrolysis, Solid oxide water electrolysis (SOEC), and Anion Exchange Membrane (AEM) electrolysis (Shiva Kumar & Lim, 2022).

1.3.2.1. Alkaline water electrolysis

In this type of electrolysis, two electrodes are submerged in an alkaline electrolyte solution, usually composed of sodium hydroxide (NaOH) or potassium hydroxide (KOH). This alkaline solution ensures an increased ionic concentration of the water, so that the electric conductivity is substantially increased to promote the electrochemical reaction (Lehner & Hart, 2022; Shiva Kumar & Lim, 2022).

The two electrodes are separated by a diaphragm responsible mainly for the separation of the gases produced as it helps to prevent the ions and gases produced at the anode and cathode from mixing, which is important for maintaining the purity of the hydrogen and oxygen gases. In general, when working with an alkaline electrolyzer, these diaphragms are composed of Asbestos/Zirfon/Nickel coated perforated stainless steel (Shiva Kumar & Lim, 2022).

For a better understanding of the structure of an alkaline water electrolyzer, Figure 1-14 shows a possible schematic sketch.

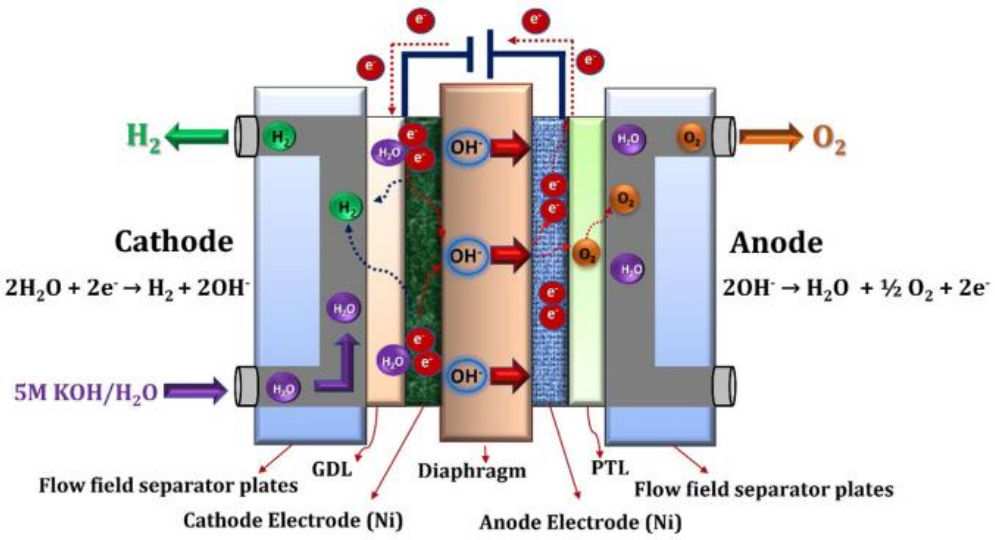

Figure 1-14: Schematic illustration of alkaline water electrolysis working principle adapted from (Shiva Kumar & Lim, 2022)*;*

Cathode reaction: $2H_2O + 2e^- \rightarrow H_2 + 2OH^-$ (1-2)

Anode reaction: $2OH^- \rightarrow H_2O + \frac{1}{2}O_2 + 2e^-$ (1-3)

There are several advantages to using alkaline water electrolysis. It is a relatively simple, well-established, and low-cost technology that is already used in modern industry, it offers good long-term stability and does not require the use of noble metal electrocatalysts. However, it also bears some limitations, such as requiring high operating voltages and the partial intermixing of generated gases caused by the commonly-used thick diaphragms that increase ohmic resistance (Lehner & Hart, 2022; Shiva Kumar & Lim, 2022).

1.3.2.2. PEM electrolysis

In this type of water electrolysis, the water used as an electrolyte is introduced into the anode section, where the electrochemical dissociation happens. The protons formed to pass through a membrane into the anode where they combine to form hydrogen while the oxygen formed is unable to cross the membrane, therefore separating the two gases produced (Thomassen et al., 2022).

A schematic representation of the electrolyzer and the reactions happening in the anode and cathode is shown in Figure 1-15:

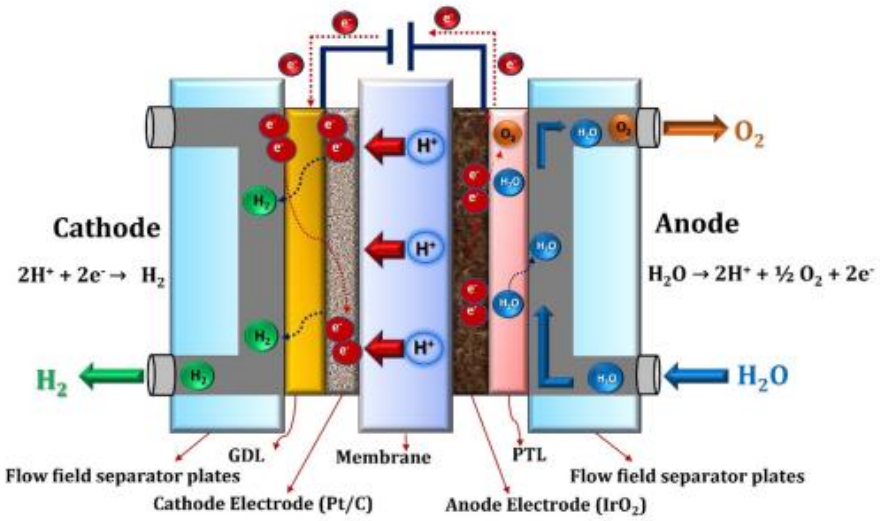

Figure 1-15: Schematic illustration of PEM water electrolysis working principle adapted from (Shiva Kumar & Lim, 2022)*;*

$$\text{Cathode reaction: } 2H^+ + 2e^- \rightarrow H_2 \qquad (1\text{-}4)$$

$$\text{Anode reaction: } H_2O \rightarrow 2H^+ + \frac{1}{2}O_2 + 2e^- \qquad (1\text{-}5)$$

As a method of hydrogen production through electrochemical means, PEM electrolysis offers multiple advantages, such as its higher operating current density when compared to alkaline electrolysis (translating into lower energy consumption), producing high-purity hydrogen due to the use of the membrane and relatively compact design-wise. On the other hand, the membranes used increase significantly the capital cost of the installation and lack of long-term durability. Additionally, its electrochemical catalysts are composed of precious metals such as platinum (Pt) resulting once again in a higher capital cost for the process (Shiva Kumar & Lim, 2022; Thomassen et al., 2022).

1.3.2.3. Solid oxide water electrolysis

A Solid oxide electrolysis cell (SOEC) is constituted of three main components, a porous anode and a porous cathode, and a solid dense ceramic electrolyte capable of passing Oxide ions (O^{2-}). Similarly, to an alkaline process the oxygen ions (in this case O^{2-}) pass through the electrolyte while the hydrogen gas formed is carried by steam stream, although, in this case, the electric energy used to split the water is substituted by a thermal source instead, thus requiring a heat source (Shiva Kumar & Lim, 2022; X. Wei et al., 2023).

A schematic representation of a SOEC electrolyzer as well as the reactions happening in the anode and cathode are shown in Figure 1-16.

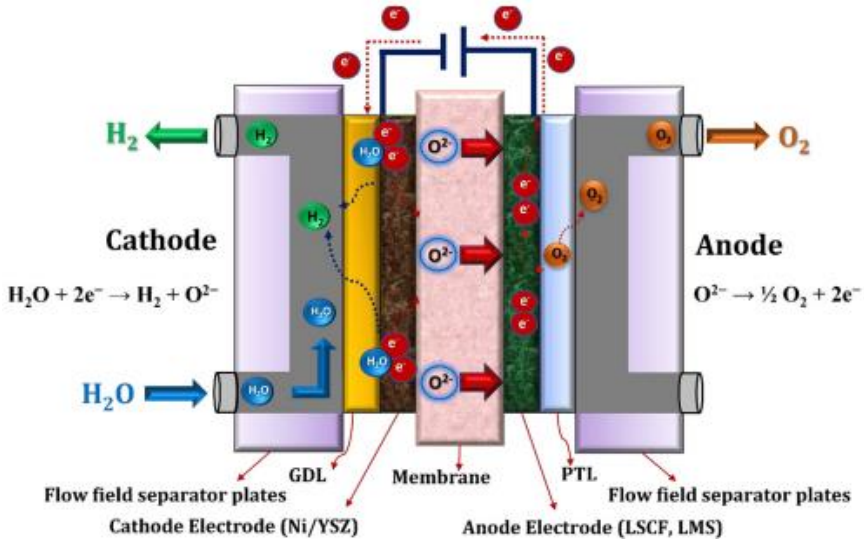

Figure 1-16: Schematic illustration of SOEC water electrolysis working principle adapted from (Shiva Kumar & Lim, 2022)*;*

Cathode reaction: $H_2O + 2e^- \rightarrow H_2 + O^{2-}$ (1-6)

Anode reaction: $O^{2-} \rightarrow + \frac{1}{2}O_2 + 2e^-$ (1-7)

In terms of advantages, this process is highly efficient and does not require the use of a noble metal catalyst and can function at higher temperatures. Nevertheless, it is still a process under development and does present some challenges such as long-term stability due to the lacking durability of the solid electrolyte (Shiva Kumar & Lim, 2022; X. Wei et al., 2023).

1.3.2.4. AEM water electrolysis

The working principle of an AEM electrolyzer has some of the specifications of the conventional alkaline system. However, the key difference between the two is the replacement of the conventional diaphragm used is alkaline electrolysis, with an anion exchange membrane. Hydroxide ions can pass through the membrane and collect at the cathode, while oxygen ions are not and collect at the anode (Mamlouk, 2022).

The electric current applied to the alkaline electrolyte causes the water molecules to break down into hydrogen ions (H^+) and hydroxide (HO^-). Then, the anion exchange membrane separates the two by allowing the passage of the formed hydroxide while retaining the hydrogen in the cathode half-cell and later releasing it via a gas diffusion layer. After crossing into the anode half-cell, the hydroxide reacts to produce oxygen that is released via a liquid gas diffusion layer (*Anion Exchange Membrane Water Electrolysis: How It Works - Enapter*, n.d.; Shiva Kumar & Lim, 2022).

A schematic representation of an AEM electrolyzer, as well as the reactions happening in the anode and cathode are shown in Figure 1-17.

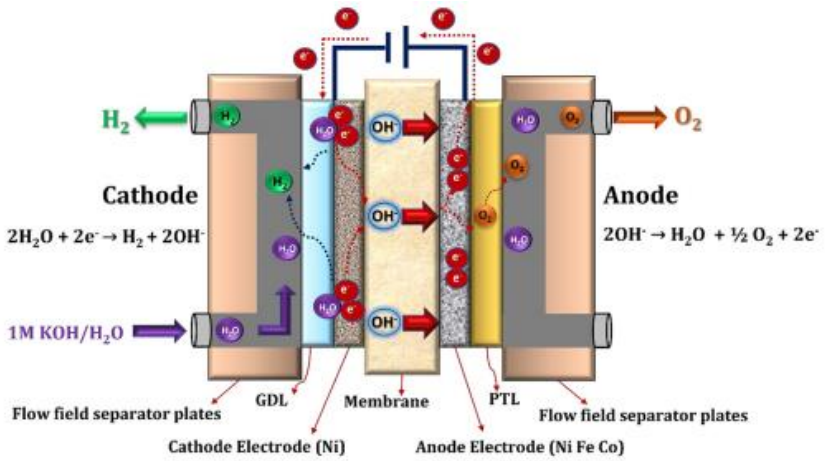

Figure 1-17: Schematic illustration of AEM water electrolysis working principle adapted from (Shiva Kumar & Lim, 2022)*;*

$$\text{Cathode reaction: } 2H_2O + 2e^- \rightarrow H_2 + 2OH^- \quad (1\text{-}8)$$

$$\text{Anode reaction: } 2OH^- \rightarrow H_2O + \frac{1}{2}O_2 + 2e^- \quad (1\text{-}9)$$

From all the methods of electrolysis shown, AEM is the most recent technology and still under development. It was introduced to overcome some of the drawbacks related to alkaline and PEM water electrolysis such as the need for noble metal electrocatalysts as well as high concentrations of liquid alkaline electrolyte. Nevertheless, as it is still at the beginning of its development stage, several innovations/improvements are still needed to overcome the major

challenges and allow the scale-up of this technology, namely, membrane performance and durability (Mamlouk, 2022; Shiva Kumar & Lim, 2022).

1.4. Synthesis gas

Synthesis gas (syngas) is a mixture of hydrogen (H_2), carbon monoxide (CO) and often carbon dioxide (CO_2) in variable percentage. It can be used as a intermediate for the production of chemicals, fuels, and other products, such as methane, methanol, hydrogen, synthetic natural gas, ammonia, acetic acid and liquid fuels through Fisher-Tropsch (such as diesel and gasoline) (Chen et al., 2018).

1.4.1. Technologies for Syngas production

The technologies used to produce syngas through carbon-based substances are the following (Chen et al., 2018; Moulijn et al., 2013):

- Reforming of natural gas, also designated as Steam methane reforming (SMR);
- Gasification of coal or biomass;
- Co-electrolysis of water;

1.4.2.1. Steam methane reforming:

Steam methane reforming is a chemical process that converts methane, the main component of natural gas, into hydrogen gas and carbon monoxide. The process involves reacting methane with steam under high temperatures and pressures in the presence of a catalyst, typically a metal such as nickel. By itself, natural gas is composed of a mixture of hydrocarbons, of which the main is methane (Moulijn et al., 2013). The reactions that can occur in this process are shown in Table 1-3:

Table 1-3: Reactions occurring during SMR, adapted from (Moulijn et al., 2013)

Reaction	ΔH^0_{298}(kJmol^{-1})	
$CH_4 + H_2O \rightleftharpoons CO + 3H_2$	206	(1-10)
$CH_4 + 2H_2O \rightleftharpoons CO_2 + 4H_2$	-41	(1-11)
$CH_4 + CO_2 \rightleftharpoons 2CO + 2H_2$	247	(1-12)
$CH_4 \rightleftharpoons C + 2H_2$	75	(1-13)
$2CO \rightleftharpoons C + CO_2$	-173	(1-14)
$CH_4 + {}^1/_2\, O_2 \rightleftharpoons CO + 2H_2$	-36	(1-15)
$CH_4 + 2O_2 \rightleftharpoons CO_2 + 2H_2O$	-803	(1-16)
$CO + {}^1/_2\, O_2 \rightleftharpoons CO_2$	-284	(1-17)
$H_2 + {}^1/_2\, O_2 \rightleftharpoons H_2O$	-242	(1-18)

When focusing on the conversion of methane in the presence of steam the most important reactions are the steam reforming reaction (1-10) and the water-gas shift (WGS) (1-11). Additional production of CO is carried out through a methane and carbon dioxide in a reaction known as CO_2 reforming (1-12). Furthermore, this may be accompanied by secondary reactions, such as (Moulijn et al., 2013):

- the formation of coke, either by the decomposition of methane (1-13) or by the disproportionation of carbon monoxide (1-14). This rection is undesired as the formation of coke leads to deactivation of the catalyst;
- in the presence of oxygen, methane suffers partial oxidation (1-15) also producing syngas;
- the complete oxidation of methane in to carbon dioxide and H_2O (1-16);
- the oxidation of formed carbon monoxide (1-17) and hydrogen (1-18);

Focusing on the thermodynamics of the process, the steam reforming reaction is highly endothermic with the use of a nickel base catalyst, while the reactions involving methane and oxygen are moderate to extremely exothermic. Hence, the operation can be allothermal (with a steam feed with no or little oxygen added and the requirement of an external heat source) or autothermal (with both steam and oxygen added in the feed and heat generated by the exothermic reactions within the reactor), depending on the steam/oxygen ratio (Moulijn et al., 2013).

For a clearer understanding of the process, Figure 1-18, displays a simplified schematic of a steam reforming plant.

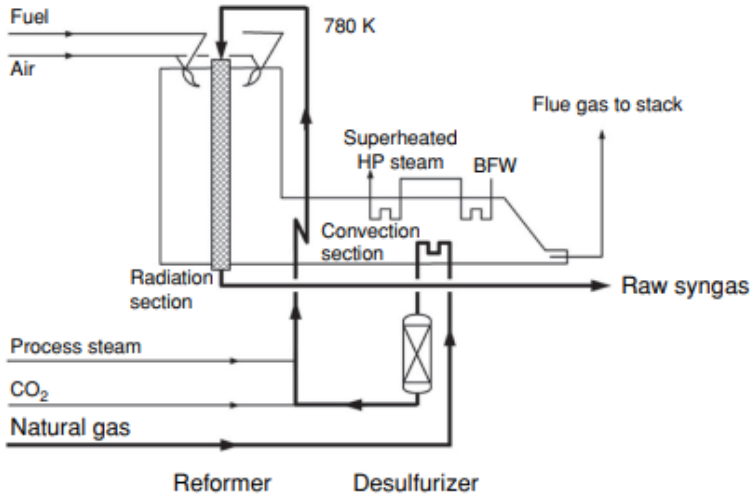

Figure 1-18: Simplified flow scheme of the steam reforming process, adapted from (Moulijn et al., 2013)*;*

1.4.2.2. *Coal and biomass Gasification*

Gasification designates a process in which coal, biomass, oil, and other gaseous compounds are converted into syngas through reactions involving oxygen and steam. It occurs due to thermal degradation in temperatures above 700-800 ºC and its first recorded use was in the early 19th century, when coal was gasified to produce a gas that was used for street lighting. This product, known as "town gas," was used in many cities around the world until the early 20th century. Nowadays, it is used in a variety of applications throughout the industry, including the production of electricity, fertilizers, and other chemical products and the treatment of waste materials. It is also being explored as a way to produce hydrogen (Akkala et al., 2023; Moulijn et al., 2013).

Taking the specific example of the gasification of coal, Table 1-4 showcases the main reactions occurring during the process, in which coal is expressed carbon (C), in a simplified manner.

Table 1-4: Reactions occurring during coal gasification, adapted from (Moulijn et al., 2013)*;*

Reaction	ΔH^0_{800}(kJmol^{-1})	
Heterogeneous reactions		
$\mathbf{C + H_2O \rightleftharpoons CO + H_2}$	136	(1-19)
$\mathbf{C + CO_2 \rightleftharpoons 2CO}$	173	(1-20)
$\mathbf{2C + O_2 \rightleftharpoons 2CO}$	-222	(1-21)
$\mathbf{C + O_2 \rightleftharpoons CO_2}$	-394	(1-22)
$\mathbf{C + 2H_2 \rightleftharpoons CH_4}$	-87	(1-23)
Homogeneoyus reactions		
$\mathbf{2CO + O_2 \rightleftharpoons 2CO_2}$	-572	(1-24)
$\mathbf{CO + H_2O \rightleftharpoons CO_2 + H_2}$	-37	(1-25)

1.4.2.3. *Co-electrolysis of water*

Water co-electrolysis is an electrochemical process by which carbon dioxide and steam are transformed into syngas through the use of a solid oxide cell, similarly to normal SOEC electrolysis. Unlike normal SOEC or other methods of exclusively water electrolysis, co-electrolysis can be used to recover and reuse CO_2 produced from other processes (Dittrich et al., 2019; Zheng et al., 2017).

A simplified schematic of a water co-electrolysis electrolyzer for syngas production is showed in Figure 1-19.

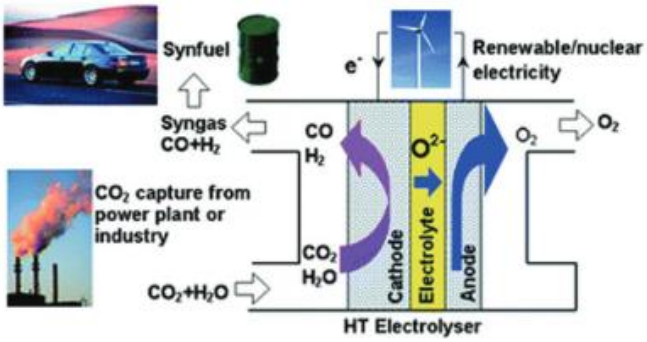

Figure 1-19: Schematic diagram of CO2/H2O co-electrolysis using a solid oxide electrolysis cell (SOEC) for syngas production, adapted from (IRENA, 2020) (Zheng et al., 2017)*;*

Considering the thermodynamic of the process, the reactions that take place at the electrodes during co-electrolysis are the following:

- At the cathode interface, water and CO_2 reduction occur (Dittrich et al., 2019).

Water reduction: $H_2O + 2e^- \rightarrow H_2 + O^{2-}$ (1-6)

CO_2 reduction: $CO_2 + 2e^- \rightarrow CO + O^{2-}$ (1-26)

- On the other hand, at the anode interface, two secondary reactions occur producing syngas, the Reverse water-gas shift reaction ((R)WGS) (1-27) and the Sabatier reaction (1-28) (Zheng et al., 2017).

(R)WGS: $H_2 + CO_2 \rightleftharpoons CO + H_2O$ (1-27)

Sabatier reaction: $CO + 3H_2 \rightleftharpoons CH_4 + H_2O$ (1-28)

1.4.2. Synthesis gas applications

Syngas has several potential uses in the modern industry, as it can be converted into other synthetic fuels, both gaseous like methane or liquid such as gasoline and diesel, through processes such as Fischer-Tropsch or the methanol-to-gasoline conversion. It can also be used as a feedstock for the production of a wide range of chemicals products, including methanol, ammonia, and acetic acid. In addition, syngas can be burned to generate electricity in gas turbines or internal combustion engines and substitute more expensive or scarce feedstocks in refinery processes, such as the hydrogen production for petroleum refining (S. Lu et al., 2020).

Figure 1-20 displays the applications and subproducts of syngas:

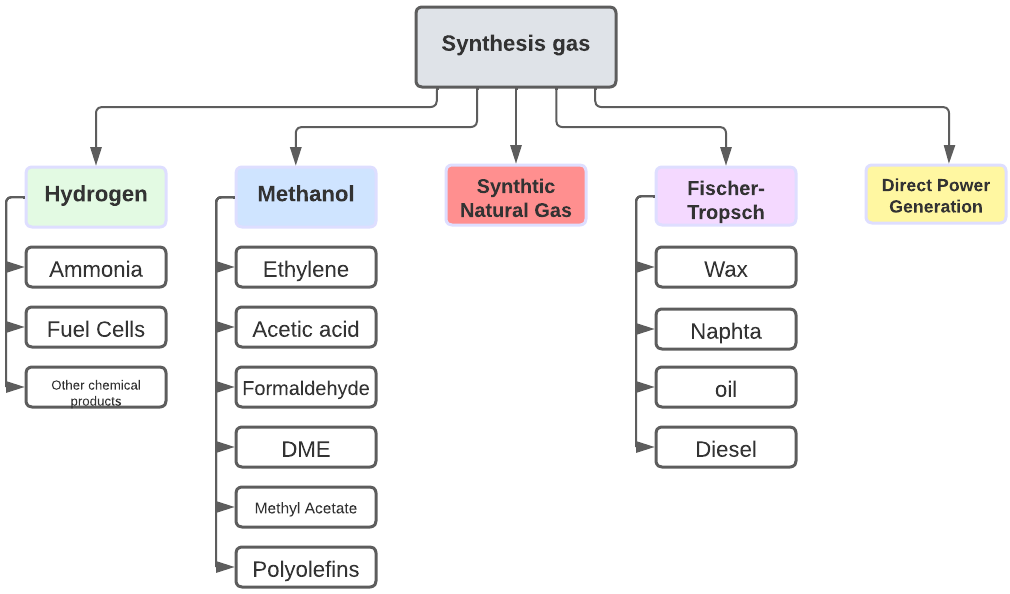

Figure 1-20: Diagram of syngas uses and subproducts;

1.4.2.4. Synthetic fuel production using syngas

Synthetic fuels, are liquid or gaseous man-made energy sources produced from a variety of raw materials, including coal, natural gas, and biomass, either from converting them directly into fuel or indirectly through the use of an intermediate feedstock like syngas that is later converted to other fuels with the use of processes like Fischer-Tropsch (Chen et al., 2018).

The Fischer-Tropsch process is a chemical reaction in which syngas is converted into liquid hydrocarbons. It was first developed by Franz Fischer and Hans Tropsch in Germany in the 1920s and was used on an industrial scale in Germany during World War II as a means of producing synthetic fuel from coal. After the war, the process was also used in other countries, including South Africa, where it was used to produce fuel from coal during the apartheid era. Today, the Fischer-Tropsch process is used on a smaller scale in several countries as a means of producing synthetic fuels and chemical products from a variety of feedstocks, including syngas, natural gas, coal, and biomass (Khodakov et al., 2007; Speight, 2020).

Fischer-Tropsch is a heterogeneous catalytic process, requiring the use of a metallic catalyst, typically iron or cobalt, at high pressures and temperatures to produce a mixture of liquid hydrocarbons. While all group VIII metals have some capacity to act as a catalyst in the hydrogenation of carbon monoxide to produce hydrocarbons, only iron (Fe), cobalt (Co), and ruthenium (Ru) base catalysts meet the requirements to be used on an industrial level (Chen et al., 2018; Speight, 2020).

Iron-based catalysts are often preferred due to their low cost and availability, and they have been used in the majority of commercial-scale Fischer-Tropsch plants. These catalysts typically consist of iron oxides or iron carbides, and they are typically supported on a solid substrate, such as alumina. The exact composition of the catalyst can vary, but it is typically composed of a mixture of iron and other metals such as chromium or nickel, which can affect the properties of the catalyst and its ability to convert syngas into hydrocarbons (Chen et al., 2018).

Cobalt-based catalysts are also used in the Fischer-Tropsch process, and they have some advantages over iron-based catalysts. Cobalt-based catalysts tend to have a higher activity and selectivity for the production of longer-chain hydrocarbons, which can lead to higher yields of diesel and jet fuel. However, cobalt is a more expensive metal than iron, and it is also less abundant, which can make cobalt-based catalysts more costly than iron-based catalysts (Chen et al., 2018).

Additionally, ruthenium-based catalysts can also be used in the Fischer-Tropsch process. These catalysts are generally considered to be more active and selective than iron or cobalt, but they are also much more expensive and as a result, they aren't as used on an industrial scale (Chen et al., 2018).

Catalyst performance, especially activity and selectivity, is also largely influenced by reaction conditions like temperature, and pressure. The optimal conditions for the Fischer-Tropsch process, such as temperature and pressure, depend on the specific catalyst being used. In general, higher temperatures and pressures tend to increase the activity of the catalyst, but can also lead to the formation of unwanted byproducts possibly leading to the deactivation of the catalyst. As such, the selection of the conditions and catalyst depend on the desired product. In the case of iron catalysts, they have more industrial uses within the production of olefins, while cobalt catalysts are more used to produce paraffins (Chen et al., 2018)

The primary reactions taking place during this process to produce hydrocarbons are the following (Chen et al., 2018):

$$\mathrm{nCO} + 2\mathrm{nH_2} \rightarrow \mathrm{C_nH_{2n}} + \mathrm{nH_2O} \quad (1\text{-}29)$$

$$\mathrm{nCO} + (2\mathrm{n}+1)\mathrm{H_2} \rightarrow \mathrm{C_nH_{2n+1}} + \mathrm{nH_2O} \quad (1\text{-}30)$$

1.4.2.5. Methanol production and applications

Also known as methyl alcohol, Methanol ($\mathrm{CH_3OH}$) is a clear colorless, and volatile liquid with a distinct, sweet smell. It is an alcohol widely used in industry and laboratory settings. Methanol is a key component in the production of many chemical products, including methyl ter-butyl ether (MTBE), dimethyl terephthalate, dimethyl-ether (DME), formaldehyde,

and acetic acid. It is also used as an antifreeze, solvent, and fuel. However, methanol is toxic when consumed in large quantities, and can cause blindness or death. It is also known to be used as a denaturant, added to industrial denatured alcohols to render them undrinkable (Ott et al., 2012).

Methanol has a long history of use in a variety of industrial and household applications. It is believed to have been discovered in 1661 by Sir Robert Boyle through the rectification of crude wood vinegar. His molecular composition and structure were first defined in the 1820s by the French chemist Jean-Baptiste Dumas, and later in 1834 by the German chemist Justus von Liebig. The commercial production of methanol began in the late 1800s, being initially used as a fuel and solvent. Later in the early 20th century, it became a key ingredient in the production of formaldehyde and other chemicals. During World War II, methanol was used as a fuel for aircraft, and it continues to be used as a fuel for racing cars and boats (Ott et al., 2012).

Up to 1923, the only commercial source of methanol was "wood alcohol" obtained from dry distillation of wood. Around the year 1913, Alwin Mittasch and his co-workers at Badische Anilin und Soda Fabrik (BASF) developed a new way to synthesize methanol, from carbon monoxide and hydrogen (syngas) in the presence of iron oxide catalysts. However, the decisive step to allow industrial scale production came later in the early 1920s with the development of a sulfur-resistant zinc/chromium oxide catalysts ($Z_nO - C_{r2}O_3$) at high pressures (25-35 MPa) and at 320-450 ºC (Ott et al., 2012).

A breakthrough method for producing methanol was developed by ICI in the 1960s, using the reaction of sulfur-free syngas with a high concentration of carbon dioxide on highly selective copper oxide catalysts ($Cu - ZnO$). This technique, as well as others similar, are characterized by relatively mild reaction conditions (5-10 MPa, 200-300 ºC) and still serve as the foundation for modern industrial methanol production (Ott et al., 2012).

Nowadays all commercially available catalyst systems are built on a basis of Cu-ZnO-Al_2O_3 or Cr_2O_3 with a variety of promoters and additives to improve process performance/ efficiency. Zn, Cr, Mg, and rare metals are essential components promoting significantly the mobility of the Cu particles on the catalytic surface, their dispersion, and their size (Ott et al., 2012).

Table 1-5: Summary of copper-containing catalysts for low-pressure methanol synthesis Adapted from (Ott et al., 2012)*;*

Manufacturer	Components	Content, atom %
IFP	Cu	25-80
	Zn	10-50
	Al	4-25
Sud Chemie	Cu	65-75
	Zn	18-23
	Al	8-12
Shell	Cu	71
	Zn	24
	Rare earth oxide	5
ICI	Cu	61
	Zn	30
	Al	9
BASF	Cu	65-75
	Zn	20-30
	Al	5-10
Du Pont	Cu	50
	Zn	19
	Al	31
United Catalysts	Cu	62
	Zn	21
	Al	17
Haldor Topsøe	Cu	37
	Zn	15
	Al	48

The main reactions occurring during the catalytic process currently used to produce methanol are the following:

Table 1-6:Main reactions occurring during methanol production adapted from (Moulijn et al., 2013)*;*

Reaction	ΔH^0_{298}(kJmol^{-1})	
$CO + 2H_2 \rightleftharpoons CH_3OH$	-90.8	(1-31)
$CO_2 + 3H_2 \rightleftharpoons CH_3OH + H_2O$	-49.6	(1-32)

Both reactions resulting in the synthesis of methanol are exothermic and induce a reduction of volume. As such by analyzing their thermodynamics, it is clear, the process is favored by low temperatures and high pressures (although the development of previously referred copper-based catalysts allowed for lowers pressures due to their higher activity) (Moulijn et al., 2013).

Furthermore, out of the two, reaction (1-31) is considered the main one while (1-32) is a secondary, seen as modern copper-based catalysts promote (1-31). Knowing this, the optimal ratio for converting syngas is 2.02-2.04 H_2:CO but in the case of the syngas feed used not meeting these requirements, its composition can be manipulated by installing a (R)WGS (1-27) reactor before the main synthesis reactor, to decrease CO concentration. On the other hand, the presence CO_2 up to a concentration of 3 % promotes the activity of the catalyst with higher concentrations hindering its performance (Moulijn et al., 2013).

Methanol has been considered a potential environmentally friendly alternative to other fossil fuels. It is a clean-burning fuel that produces lower emissions of harmful pollutants compared to gasoline and diesel as it does not contribute to nitrogen oxides (NO_x) emissions. Additionally, methanol can be produced from a variety of renewable feedstocks such as wood, biomass, and waste, rather than being derived from fossil fuels. It can also be used as a feedstock to produce of other chemicals and transportation fuels through processes such as the methanol-to-gasoline (MTG) process or the methanol-to-olefins (MTO) process. These processes convert methanol into transportation fuels and chemicals such as gasoline, diesel, and ethylene (Calam et al., 2020; Ott et al., 2012).

1.4.2.6. Methane

Methane is a hydrocarbon compound composed of one carbon atom and four hydrogen atoms (CH_4). It is a colorless, odorless, and flammable gas that is the primary component of natural gas. It is also a powerful greenhouse gas, which means that it can trap heat in the atmosphere and contribute to global warming. In addition to being a byproduct of human activities such as agriculture and fossil fuel extraction, methane is also produced by natural processes such as the breakdown of organic matter by microbes in wetlands and in the stomachs of ruminant animals (H. M. Bolt, 2022; Lundegard, 1964).

Its history can be traced back to ancient times, as it has been known for centuries that certain types of rocks and soils would emit a flammable gas when ignited. However, the first recorded discovery of methane was made by the ancient Greek philosopher Empedocles in the 5th century BCE, who observed that certain types of earth would emit a flammable gas when heated. In 1776, Italian chemist and physicist Alessandro Volta identified it and discovered that could be obtained from marsh gas (*Museo Galileo - In Depth - Methane*, n.d.).

Methane can be found in a variety of locations on Earth. Some of the most significant sources of methane include (Masyagina & Menyailo, 2020; Saunois et al., 2020):

- Natural gas deposits: methane is the primary component of natural gas, which can be found in underground reservoirs and can be extracted through drilling;
- Wetlands: marshes, swamps, and other wetlands are natural sources of methane, which is produced by microbes that break down organic matter;
- Landfills: as organic material in landfills decomposes, it produces methane. This constitutes a significant source of methane emissions;
- Coal mines: methane is often found in coal mines, and it can be a significant safety hazard if it accumulates in large enough quantities;
- Ruminant animals: Livestock such as cows and sheep produce methane as a byproduct of their digestion;
- Arctic permafrost: as permafrost melts, it releases methane trapped in the ground;
- Methane hydrates: methane hydrates are ice-like substances that form when methane molecules become trapped in the structure of water molecules. They can be found in deep ocean sediments and permafrost regions.
- Industrial processes: methane is a byproduct of many industrial processes, such as the production of coal, oil, and natural gas, and the treatment of wastewater.

In the modern industry, methane is primarily used as a source of energy, being used to generate electricity in power plants, heat buildings and homes, and power vehicles such as buses and trucks. It is also used as a raw material in the production of chemicals and fertilizers (Franz et al., 2021).

Methane is also used in the oil and gas industry as a means of enhanced oil recovery, where it is injected into oil reservoirs to increase the amount of oil extraction. Additionally, it is used in the production of hydrogen fuel, through Steam methane reforming (Franz et al., 2021).

In recent years, there has been increasing interest in the use of methane as a feedstock for the production of chemicals and liquid fuels, such as methanol and dimethyl ether, as a way to reduce greenhouse gas emissions by capturing and utilizing methane rather than allowing it to be released into the atmosphere (Franz et al., 2021).

The rising cost of natural gas in recent years, and more noticeably in the last months due to the recent conflicts in Ukraine, has led to the need, and as result research, for new ways to produce it in order to meet the increasing demand for energy. Seen as methane is the primary component in natural gas, it can be used as an option to produce Synthetic Natural Gas (SNG).

In comparation to other fuel sources like coal or normal natural gas, synthetic methane is considered a “cleaner fuel” source as it burns at lower temperatures and produces less carbon dioxide per heat unit. The production of synthetic methane cand be done through hydrogenation of carbon monoxide during the Fischer-Tropsch process as a side product (as it was previously shown) or through hydrogenating carbon dioxide using the Sabatier process (A. Bolt et al., 2020).

1.4.2.7. Sabatier Process

The Sabatier process, also known as the Sabatier-Senderens reaction, is a chemical reaction that uses hydrogen and carbon dioxide (or in other words syngas) to produce methane and water. The reaction is catalyzed by a metal catalyst, typically nickel or ruthenium and it was invented by French chemist Paul Sabatier and his student, Jean Senderens, in the early 20th century. The process has been studied extensively as a potential method for producing methane as a source of renewable energy, as well as a means of reducing carbon dioxide levels in the atmosphere (A. Bolt et al., 2020).

The key reactions occurring throughout the process are show in Table 1-7:

Table 1-7: Sabatier reactions, adapted from (A. Bolt et al., 2020)*;*

Reaction	ΔH^0_{298} **(kJmol^{-1})**	
$\mathbf{CO_2 + 4H_2 \rightarrow CH_4 + H_2O}$	-164.9	(1-33)
$\mathbf{CO + 3H_2 \rightarrow CH_4 + H_2O}$	-206.3	(1-34)

From the main reactions, (1-33) is the main on to take in consideration, while (1-34) is the result of traces of CO reactive catalytically, generating methane. In both cases, the reactions are highly exothermic leaving the process limited by his thermodynamic equilibrium. Typically, conditions include temperatures around 250-400 °C, allowing for higher CO_2 conversion and higher CH_4 selectivity and avoiding catalyst sintering (resultant from the released heat). Furthermore, in terms of pressure, both reaction result in the loss of occupied volume, which translates in to the necessity of high pressures to promote better conversion (above 1 atm) (Junaedi et al., 2011).

On the other hand, the following side reactions can occur:

(R)WGS: $CO_2 + H_2 \rightarrow CO + H_2O$ (1-27)

Bosh reaction: $CO_2 + 2H_2 \rightarrow C(s) + 2H_2O$ (1-35)

In both cases these reactions are undesirable as they reduce the selectivity towards methane formation and in the specific case of bosh reaction the carbon produced can deposit on the catalyst surface, thus reducing the catalyst activity and performance as well as increasing the pressure drop. Additionally the presence of O_2 also results in catalyst deactivation reducing its efficiency significantly (Junaedi et al., 2011).

The most common catalysts used in the Sabatier process are nickel and ruthenium. nickel-based catalysts are widely used, due to their high activity and selectivity, as well as their relatively low cost. They are typically used in the form of nickel powders or supported on a variety of supports such as alumina, silica, or carbon. On the other hand, ruthenium-based catalysts have also been shown to be active and selective in the Sabatier process, and they have the advantage of being more resistant to deactivation by CO_2 but they are also more expensive in comparation to nickel-based catalysts (A. Bolt et al., 2020; Junaedi et al., 2011).

Other metal catalysts that have been investigated for the Sabatier process include cobalt, palladium, and platinum. These catalysts have also shown promising results in terms of activity and selectivity, but they are significantly more expensive than nickel and ruthenium. Research breakthroughs are expected to result in new catalysts that are more active, selective and resistant to deactivation, and also more cost-effective and environmentally friendly (A. Bolt et al., 2020).

1.5. Biomass and its potential as a feedstock

Biomass refers to any organic matter derived from plants, animals, and microorganisms that can be used as a source of energy. It is a renewable and widely available resource that has been used for thousands of years by humans in various forms. It can be categorized into different types, including agricultural crops, forestry residues, organic waste materials, and dedicated energy crops. Examples of biomass resources include wood, crop residues, animal manure, food waste, algae, and energy crops like switchgrass or miscanthus (Ozturk et al., 2017; Yang et al., 2015).

The energy contained within biomass can be harnessed through various processes. One common method is combustion, where it is burned to produce heat, which can be used directly for heating applications or converted into electricity through steam turbines. In alternative, it can also be converted into liquid or gaseous fuels through processes like fermentation, pyrolysis, liquification or gasification. These fuels, such as bioethanol or biogas, can be used as alternative feedstocks to produce energy (Mateus et al., 2016).

Figure 1-21 shows a variety of methods to convert biomass into other more accessible fuel sources and their applications.

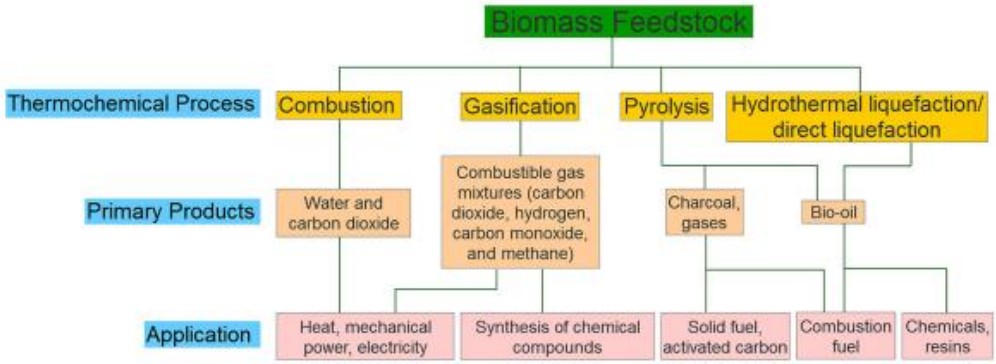

Figure 1-21: Primary products and applications from the conversion of biomass, adapted from (Jiang et al., 2018)*;*

The use of biomass as an energy source offers several advantages (Mateus et al., 2016; Ozturk et al., 2017):

- It is a renewable resource and likely a sustainable source of energy, making it a preferable alternative to fossil fuels;
- It can be sourced locally, reducing dependence on imported fossil fuels and enhancing energy security;
- Provides an opportunity to utilize organic waste materials, reducing landfill waste and associated environmental issues;

- The biofuels produced using it have a negligible concentration of sulfur, meaning that they don't contribute to sulfur dioxide emissions;

1.5.1. Lignocellulosic biomass

Lignocellulosic biomass refers to a type of biomass that is primarily composed of lignin, cellulose, and hemicellulose. It is the most abundant form of biomass on Earth, being derived from woody plants, agricultural residues, dedicated energy crops, and certain types of algae (Ge et al., 2018).

Structurally, the components found in lignocellulosic biomass are as follows (Dessie et al., 2023; H. Wei et al., 2017):

- Lignin: a complex polymer that provides structural support to plants, acting as a glue-like substance, binding cellulose and hemicellulose fibers together. Lignin is highly resistant to degradation and contributes to the robustness and durability of plant cell walls;
- Cellulose: a polysaccharide composed of glucose units linked together. It forms long, linear chains and represents the most abundant organic compound on Earth. Cellulose provides rigidity and strength to plant cell walls, and is a valuable component of lignocellulosic biomass that can be broken down into glucose through various enzymatic and chemical processes;
- Hemicellulose: a group of polysaccharides that are more branched and less rigid compared to cellulose. It consists of different sugar units, such as xylose, mannose, and glucose. Hemicellulose acts as a cementing material in the plant cell wall and contributes to its structural integrity.
- Other components: Besides lignin, cellulose, and hemicellulose, lignocellulosic biomass may contain small amounts of extractives, proteins, and other minor constituents. Extractives are non-structural compounds found in plant tissues, including oils, waxes, and pigments.

This type of biomass is of great interest for bioenergy and bioproducts due to its abundance and potential as a sustainable feedstock. However, the complex nature of lignocellulosic materials poses challenges in their efficient conversion into fuels and chemicals. Research and development efforts are focused on developing cost-effective technologies to break down the complex structure of lignocellulosic biomass and unlock its energy and value-added potential (Qian, 2014).

1.6. Project Clean Forest

Started in 2020, with the aim of formulating new ways to minimize the occurrence of wildfires, Clean Forest objective is to valorize forestal biomass waste, (growing in lands of higher wildfire susceptibility) by using it as carbon source in the production of 2nd generation synthetic biofuels, such bio-methanol, bio-dimethyl ether (bio-DME), and biogas (Gomes et al., 2022).

The project is financed by the Portuguese Fundação da Ciência e Tecnologia (FCT), under grant PCIF/GVB/0167/2018, and it is coordinated by ISEL, Lisbon Polytechnic Institute, partnered with, CERENA—Center for Environment and Natural Resources, from the University of Lisbon and the School of Agriculture, also, from the University of Lisbon (Gomes et al., 2022).

The cleaning of forests through the removal of these residues' benefits ecosystems, preserving them as an essential source of carbon dioxide capture and oxygen release. On the other hand, it instills economic dynamism in these interior regions, more disadvantaged and isolated of Portugal, allowing in some way, to minimize the desertification of these territories. The biogas produced can be valorized through its burning, originating heat and/or electricity for these regions, for domestic/industrial purposes, using, for example, cogeneration engines (*Clean Forest | Instituto Superior de Engenharia de Lisboa*, n.d.).

1.6.1. The pilot co-electrolysis unit

In cooperation with the company GSYF, Lda, current research (and the main topic of this study) focuses on the development of a pilot (patented) system to produce syngas without separation of the generated gases. This novel process, intended as a positive contribution for reducing the dependence on fossil fuels, combines alkaline water electrolysis with the addition of a carbon source in the form of graphite composing the disks inside the stack and, also, added liquified biomass obtained from forest residues to produce more eco-friendly syngas (*GSYF - Equipamentos Para Energia, Lda | Www.Pvinfo.Pl*, n.d.).

Although still in a developmental stage, the main objective of this system is to eventually provide both a use for biomass waste, that would otherwise increase the risk of wildfires if left to accumulate, and an ecological alternative to produce syngas. In comparison to the previously mention thermo-chemical processes, this one is based on electrochemistry with the possibility of sourcing all energy needed to work from renewable means, such as solar power or wind turbines.

The production of synthesis gas via electrochemical means is based on the following known reactions (Guerra, Rossi, et al., 2018):

Cathode reactions: $2H_2O + 2e^- \rightarrow 2H_2 + 2OH^-$ (1-8)

Anode reactions: $2OH^- \rightarrow H_2O + \frac{1}{2}O_2 + 2e^-$ (1-9)

$$2C + O_2 \rightarrow 2CO \quad (1\text{-}20)$$

$$2CO + O_2 \rightarrow 2CO_2 \quad (1\text{-}36)$$

Global reaction: $2H_2O + C + W_e \rightarrow 2H_2 + CO_2$ (1-37)

(It is important to note that the "C", is used to represent the carbon supplied by the carbon source being used.)

In comparison to a normal alkaline electrolysis unit, this process has two main differences (Guerra, Moura, et al., 2018):

- In the anode, besides the production of O_2, there´s also the oxidation of the carbon source from (1-20) and (1-36), resulting in the additional production of CO and CO_2 (two key compounds of syngas);
- The stack has no membrane to separate the gases produced. Instead, the mixture formed is kept together to produce a syngas mixture.

All experimental work executed throughout this study was done in this prototype plant with the intent to advance its development.

2. Experimental work

2.1. Reagents used

To perform the experimental work several different reagents were used as follows.

For the alkaline electrolysis, two different electrolytes with the concentration of 1M (mol/L) were used, one with sodium hydroxide (NaOH) for his respective tests and potassium hydroxide (KOH) for the others. The sodium hydroxide used was in the form of pure pellets with a molar mass of 40.00 g/mol (LabChem). On the other, the potassium hydroxide was in the form of pellets 88.2 % (mass) pure and a molar mass of 56.10 g/mol (LabChem).

Throughout the optimization tests, two different types of liquified biomass were tested as an alternative carbon source, one produced using pieces of acacia supplied by Instituto Superior Técnico, and the other supplied by Secil.

2.2. Equipment used

The production of syngas from alkaline water electrolysis was carried out in in a pilot plant measuring 50x50x60 cm (shown in Figure 2-1). The electrolyte solution is fed into a cylinder-shaped tank, serving as both a recirculation system and a separator for the liquid phase (unreacted alkaline electrolyte solution) and the generated gas phase (syngas, steam and other trace components). The electrolyte enters the bottom part of the stacks in which the electrolysis reaction occurs. After exiting the top of the stack, one of the two upper connectors feeds the tank with the recirculating solution.

Figure 2-1: Photo of the current version of Pilot plant for the alkaline water electrolysis process for syngas production;

The stack in use is composed in total of 11 graphite disks 5mm high each and separated bey 10 O-rings, making a total of 12 cells. The disks have two larger holes (10 mm in diameter and separated by an angle of 60 º) allowing for most of the circulation and a smaller one (2 mm in diameter). In both cases their center is 95 mm from the center of the disk itself (showed in Figure 2-2).

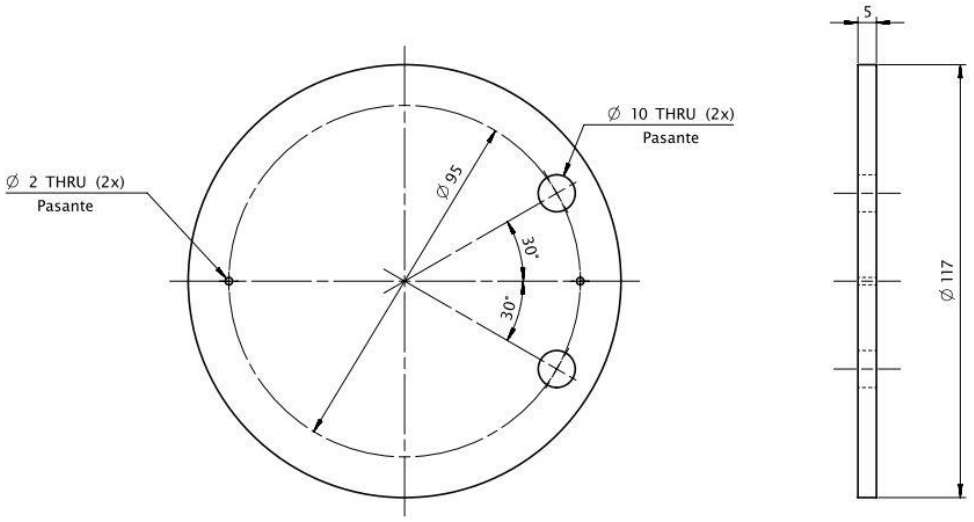

Figure 2-2: Graphite disks dimensions/specifications;

The top and bottom of the stack are composed of two steel disks, both with only one hole to allow the entrance/ exit of the solution and secured to the cylindrical structure by to two stainless steel rings bolted top to bottom with 12 metal rods. Each of the two steel disks have a screw connected to a cable used to transmit an electrical current with controlled potential difference which causes the circulation of current through the electrolyte solution in the stack and results in the desired electrochemical reaction inside.

The electrolyte solution together with the produced gaseous phase leave the stack from the top and are guided through the tubes into the initial tank where the liquid phase is recirculated while the gaseous phase is separated and leaves the tank through a pressure valve.

Since the produced gas phase leaving the tank still carries some concentration of steam, it needs to be passed through a cooling serpentine (a spiral shaped copper inserted in a cylindrical tank filled with water at room temperature) to condense the majority of the steam that is then collected in the following drainable reservoir. The remaining gas exists from a second hole on the top and is passed through a cylindrical tank filled with molecular sieve (2.0-5.0 mm) (Ambicare) to remove the remaining moisture. When the sieve is saturated with humidity (detected by the change in its color from blue to orange), it is possible to remove the tank to replace it.

Following the removal of most of his humidity, the gases enter a group of sensors (Madur, model Mamos, with an Accuracy of ± 0.2%), to analyze and determine remaining humidity as well as its composition (meaning H_2, CO_2, O_2, CO and CH_4 concentrations).

All connection pipes trough out the installation are made of PTFE (polytetrafluoroethylene) with elbows and T-sections connecting them together.

The control of parameters such as voltage applied to the stack and temperature of the process can be modified through a control panel attached to the back of the system as (shown in Figure 2-3).

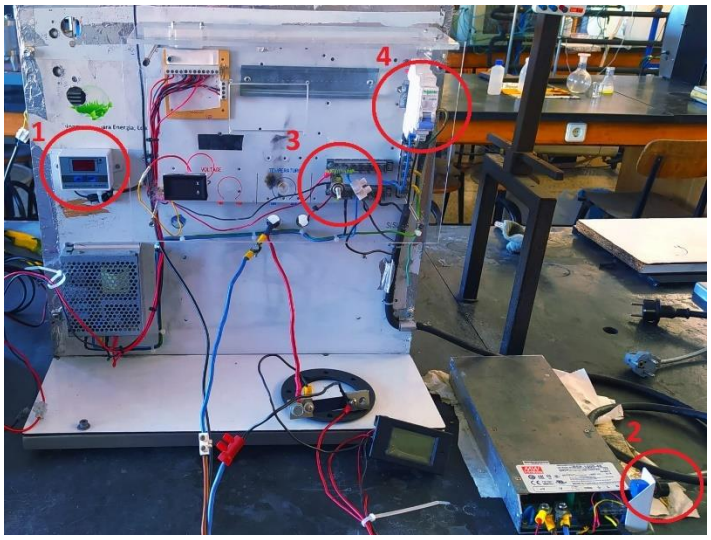

Figure 2-3: Prototype plant control panel

The analog panel on the left (1), displays the system temperature and the buttons right bellow allow the setup of the desired set point temperature; the knob on the power supply (Mean Well) on the right (2) changes the voltage at the extremities of the stack; the on-off knob (3) is used to turn on-off the water pump; and lastly, the on-off switch in the upper part of the panel (4) is used to turn on and off the entire system. At the start of each test, the initial voltage was manually adjusted to 40.00 V and later adjusted as necessary to achieve a current close to 15.00 A. This value was chosen on the basis of the energy required to promote oxidation during co-electrolysis, and is supported by previous experiments on the same prototype device.

Regarding temperature, heating is carried out mostly by the current passing through the stack (Joule heating) and partially by a heating coil placed between the pump and the stack. On the other hand, to cool down the system when needed, a fan is attached to the same section as the coil. The sensor responsible for measuring temperature(YF-B6, Unknown brand, with an Accuracy of ± 0.05 ºC) inside the system and a transmitting it in the form of a signal, is placed

in a section preceding the pump. Due to being placed before the system heat source, continuous recirculation is needed for measuring fluid temperature inside the stack.

Concerning pressure control, a pressure valve is placed right after the gas exit above the storage tank allowing for the manipulation of the pressure from that point backward. In the same section there's a sensor (EARU auto, with an Accuracy of ± 0.18 bar) responsible for determining system pressure.

For a more visual representation of the setup Figure 2-4 shows a simplified flowsheet.

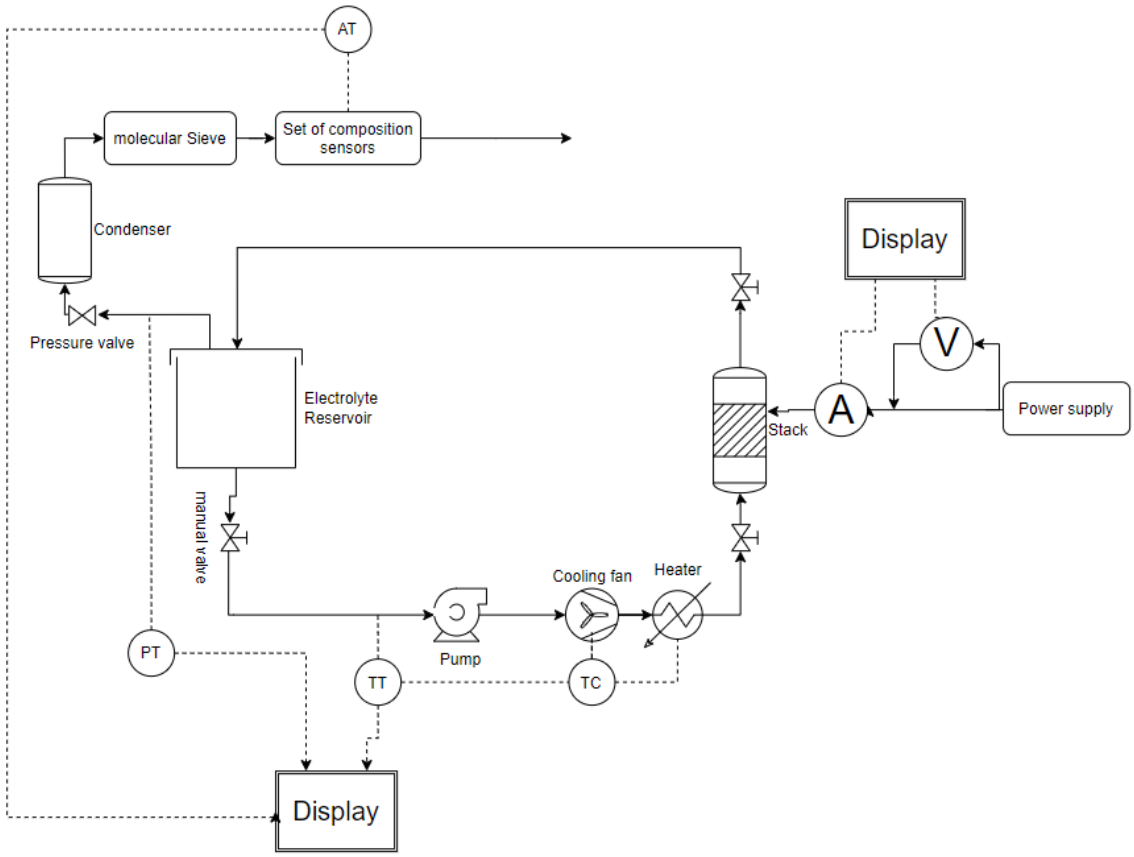

Figure 2-4: Flowsheet of the prototype process

Additional equipment was used throughout the experimental work, besides the ones directly connected to the electrolysis plant itself:

- An external switching power supply (Axiomet) to run tests of electrolyte conductivity;
- A Fourier-transform infrared (FTIR) spectrometer to obtain the absorbance and transmittance spectra of electrolyte and liquified biomass mixes;
- An additional gas analyzer to determine more precisely the composition of the gas outlet. Although, due to technical problems related its power supply, it was not used it in all tests.

2.3. Experimental procedure

With the intent of optimizing the production of syngas using liquified biomass as an alternative source of carbon, several tests were done at different operational condition. First without the use of biomass, two groups of tests were made using two different electrolyte solutions (having a concentration of 1 M), namely KOH and NaOH, each at different operational conditions variating relative pressure (3-5 bar) and temperature (90-110 ºC).

Foremost, the preparation of each electrolyte solution was done in two-liter batches with a new one being prepared when more was needed. In both cases 2 moles of KOH or NaOH were weighted and dissolved (in a volumetric flask) with enough distilled water to obtain two liters of solution. To determine the specific mass needed of KOH or NaOH needed for each electrolyte solution, the following equations were used:

For the 1M NaOH solution (and considering a molar mass of 40.00 g/mol):

$$Concentration = \frac{n}{L_{solution}} \; or \; n = C * L_{solution} \tag{2-1}$$

$$and \; n = \frac{m}{M_{elect.}} \; or \; m = n * M_{elect.} \tag{2-2}$$

Which means that for both solutions:

$$n_{NaOH/KOH} = 1_{mol/L} * 2L = 2 \; mol$$

- For the 1M NaOH solution (and considering a molar mass of 40.00 g/mol):

$$m_{NaOH} = 2_{mol} * 40.00 \frac{g}{mol} = 80 \; g$$

- For the 1M KOH solution (and considering a molar mass of 56.10 g/mol):

$$m_{KOH} = 2_{mol} * 56.10 \frac{g}{mol} = 112.2 \; g$$

Before starting each test, system circulation was turned on to first check the level of electrolyte solution inside the recirculated tank and if needed more would be added. Ideally, the tank should be filled between two thirds and half of his capacity to prevent potential operational issues.

It is also important to note that before proceeding with any tests requiring change of electrolyte solution, first all the system would be drained of most currently circulating electrolyte and then cleaned through circulating distilled water multiple times to remove any remaining.

In what regards the test methodology, the tests were performed within a suitable range of variating parameters (chosen based on testing done in previous studies) in every combination possible within that same range, first without the addition of liquified biomass. This domain of parameters includes:

- 3-5 (specifically 3, 4, and 5) bars(g) for the pressure;
- and 90-110 (90, 100, and 110) ºC for temperature;

After choosing a narrower range of conditions (based on the previous results) an additional set of tests were done, now using solutions of electrolyte mixed with one of two liquified biomass samples previously referred to in the reagents, first with a concentration of 2.5 % (w/w) and then with 5 % of diluted liquified biomass.

Before each test, all connections are checked to minimize the risk of leaks. Then the top of the tank is open, and circulation is turned on to evaluate electrolyte level. After that, the tank is closed, the temperature set point is adjusted into the control panel and the heating coil is turned on. As process temperature rises, the pressure valve is tightened to manually adjust the pressure to the specific test value. Only when the desired test conditions are achieved and maintained for a couple of minutes, can the test start.

Regarding the tests themselves, each one was executed over a period of 3 hours (chosen to follow the same procedure as previous works), whereas data such as relative pressure (bar(g)) temperature (ºC), current voltage (V) intensity (A), composition of the gases produced and its flow, was collected in 15 minutes intervals. For the measurement of produced gas flow, an improvised system was used, where an inverted graduated cylinder was placed over glass bowl and filled with water. The gas outlet is placed inside the cylinder to time how long it takes to displace 150 ml of its volume. For each collection, the flow rate was measured twice with concordant results, and later used to determine the arithmetic average of the two.

The analysis of electrolyte conductivity was carried out on every new batch of electrolyte and before and after each test (with most collections taken post one test being also considered the pre-test for the next one). On each test, a sample of approximately 200 ml of electrolyte is placed in a beaker where two spaced steel disks are half submerged and each connected to the anode or cathode of an external power source which applies voltages gradually increased from 0 to 5.0 (on a 0.5 interval) noting the resulting current intensity for each.

With the objective of analyzing the composition of the liquified biomasses used throughout the second set of tests, all electrolyte/liquified biomass solutions were subjected to FTIR analysis to. In each case, first a background spectrum was collected and only then analysis could carry on. A small film of the sample was placed on the proper holder for liquids, the lid was closed and the program was operated to obtain the absorbance/transmittance spectra and proceed with the composition analysis.

3. Results and discussion

3.1. Tests performed without addition of biomass

As previously mentioned, before the introduction of liquified biomass, an initial set of tests was carried out to analyze the performance of the electrolyzer without addition of any biomass under different conditions of pressure and temperature with two possible electrolytes (KOH and NaOH). In the case off temperature, it was tested within the range of 90-110 ºC with variations of 10 ºC between each test, resulting in three different tested temperatures (90, 100, and 110 ºC). On the other hand, for pressure, the range was 3-5 relative bars with variations of 1 bar, thus also resulting in three tested pressures (3, 4, and 5 bar). This way and considering all possible combinations of pressure, temperature, and electrolyte, there was a total of eighteen tests to be executed in the in the first set alone.

Concerning the current applied to the stack, seen as the system lacks automatic control for it, through out each procedure, the voltage applied was manually manipulated (using the knob in the power supply) with continual adjustments to keep current intensity on the desired range of 10-15 A. While their values are not necessarily kept consistent through a complete test, the comparison of the intensity obtained for the voltage applied and later the gas flow obtained per current applied are considered major factors in the choice of optimal conditions.

The Table 3-1; below shows the specific parameters established for each test;

Table 3-1:Test conditions without addition of liquified biomass;

Test	Electrolyte	Relative Pressure (bar(g))	Temperature (ºC)
1	KOH	3	90
2	KOH	3	100
3	KOH	3	110
4	KOH	4	90
5	KOH	4	100
6	KOH	4	110
7	KOH	5	90
8	KOH	5	100
9	KOH	5	110
10	NaOH	3	90
11	NaOH	3	100
12	NaOH	3	110
13	NaOH	4	90
14	NaOH	4	100
15	NaOH	4	110
16	NaOH	5	90
17	NaOH	5	100
18	NaOH	5	110

3.2. Results treatment

Throughout this sub-chapter the results directly obtained in the tests are be treated and used in the determinations of further data important to evaluate the performance of the electrolyzer at each set of working conditions. Before proceeding to the discussion and explanation of each individual test, the following equations are be explained to show how these additional parameters were calculated.

- **Voltage per cell (V/cell)**

Inside the stack, each pair of disks (either graphite or the steel disks on the top/bottom) and the existing space between them constitutes an individual cell with one disk acting as a cathode and the other as the anode. To evaluate the tension passing each individual cell in the sack the following equation (3-1) was used.

$$\mathrm{V/cell} = \frac{\text{Voltage applied}}{\text{nº of cells in the stack}} \qquad (3\text{-}1)$$

(Since there are 11 graphite disks inside the stack, the number of cells is equal to 12.)

- **Produced Gas outlet flow**

As previously explained in the experimental procedure, gas flow measurements were executed by measuring the time in which the outlet displaced 150 ml of water. Using this and using in equation (3-2) the flow was calculated and converted into more practical units.

$$\text{Gas flow} = \frac{\text{volume of produced gas}}{\text{time}} \text{ or in this case } \frac{150\text{ ml}}{\text{time(s)}} \qquad (3\text{-}2)$$

Conversions:

$$1\text{ ml/s} = \frac{1 * 60}{1000}\text{ l/min}$$

$$1\text{ ml/s} = \frac{1 * 3600}{1000}\text{ l/h}$$

- **Watt per gas flow (**$\mathrm{W/F}$)

  As a way to measure energy efficiency and compare the energy spent per unit of gas produced, the equation (3-2) was used:

$$\mathrm{W/F} = \frac{\mathrm{V{*}I}}{\text{Gas flow}} \qquad (3\text{-}2)$$

When considering and discussing the results obtained in each test, for each parameter, an average of the last three measurements was determined. In cases where one of the three values deviated significantly from the other two, it is considered as an outlier and left out of the average.

3.2.1. Tests and results, KOH electrolyte

3.2.1.1. 1M KOH, at 3 bar(g) and 90 ºC

Table 3-2: Conditions and collected results, 1M KOH, at 3 bar(g) and 90 ºC;

Time (min)	T (°C)	P (bar(g))	V (V)	I (A)	O_2 (%)	CO (%)	CO_2 (%)	H_2 (%)	F (l/h)	W/F (Wh/l)
0	90.4	3.3	37.36	15.64	7.0	2.0	26.8	64.2	45.17	12.94
15	89.4	3.3	37.34	15.65	6.5	2.0	28.3	63.2	49.16	11.89
30	89.1	2.6	37.34	15.45	6.5	2.0	31.5	60.0	50.40	11.45
45	89.6	2.9	37.35	15.59	6.6	2.0	30.4	61.0	49.56	11.75
60	90.1	2.9	37.34	15.64	6.4	2.0	31.3	60.3	48.45	12.05
75	90.0	2.9	37.34	14.88	6.3	2.0	31	60.7	46.69	11.90
90	90.0	2.9	37.33	15.25	6.4	2.0	31.7	59.9	46.98	12.12
105	89.4	3.0	37.34	14.9	6.4	2.0	31.9	59.7	46.11	12.06
120	89.2	3.0	37.34	15.12	6.4	2.0	31.8	59.8	45.44	12.43
135	89.4	3.0	37.34	15.13	6.4	2.0	31.6	60.0	45.59	12.39
150	89.6	3.1	37.34	15.01	6.4	2.0	31.6	60.0	46.02	12.18
165	89.2	2.9	37.33	14.99	6.4	2.0	31.7	59.9	47.08	11.89
180	89.8	3.0	37.34	15.07	6.4	2.0	31.8	59.8	44.03	12.78

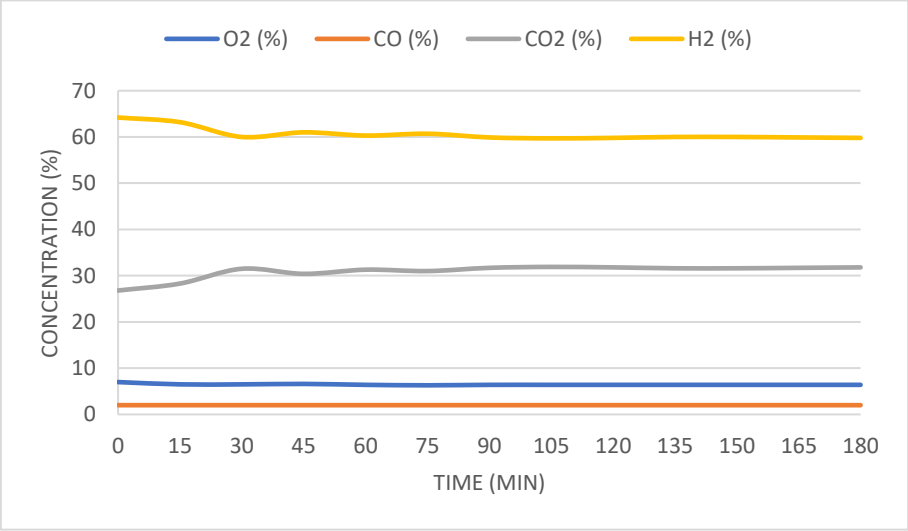

Figure 3-1: Gas outlet composition over the duration of the test, 1M KOH, at 3 bar(g) and 90 ºC;

Among the data obtained the key important parameters to note are:

- 6.4 % of oxygen in the outlet;
- 31.7 % of carbon dioxide;
- 59.9 % of hydrogen;
- 45.71 l/h of produced gas with an energetic cost of 12.28 Wh/l.

3.2.1.2. 1M KOH, at 3 bar(g) and 100 ºC

Table 3-3: Conditions and collected results, 1M KOH, at 3 bar(g) and 100 ºC;

Time (min)	T (°C)	P (bar(g))	V (V)	I (A)	O_2 (%)	CO (%)	CO_2 (%)	H_2 (%)	F (l/h)	W/F (Wh/l)
0	100.8	3.3	34.12	16.07	7.8	2.0	24.4	65.8	42.57	12.88
15	100.9	3.3	34.11	16.16	6.8	2.0	34.5	56.7	44.35	12.43
30	100.7	3.2	34.11	16.27	6.4	2.0	37.2	54.4	45.57	12.18
45	100.5	3.2	34.12	15.98	6.1	2.0	37.8	54.1	43.36	12.58
60	99.6	3.1	33.04	15.18	6.0	2.0	38.0	54.0	39.57	12.67
75	100.1	3.1	33.03	14.91	5.8	2.0	39.1	53.1	37.84	13.01
90	100.4	3.2	33.04	15.06	5.6	2.0	37.6	54.8	38.57	12.90
105	101.0	3.3	33.04	14.95	5.6	2.0	38.6	53.8	37.67	13.11
120	101.6	3.3	33.03	15.19	5.5	2.0	38.0	54.5	38.99	12.87
135	101.4	3.2	33.03	15.05	5.4	2.0	39.8	52.8	38.15	13.03
150	100.0	3.2	33.03	14.86	5.5	2.0	39.7	52.8	35.46	13.84
165	100.2	3.2	33.03	14.91	5.4	2.0	40.5	52.1	35.64	13.82
180	100.3	3.1	33.03	14.73	5.4	2.0	38.4	54.2	34.07	14.28

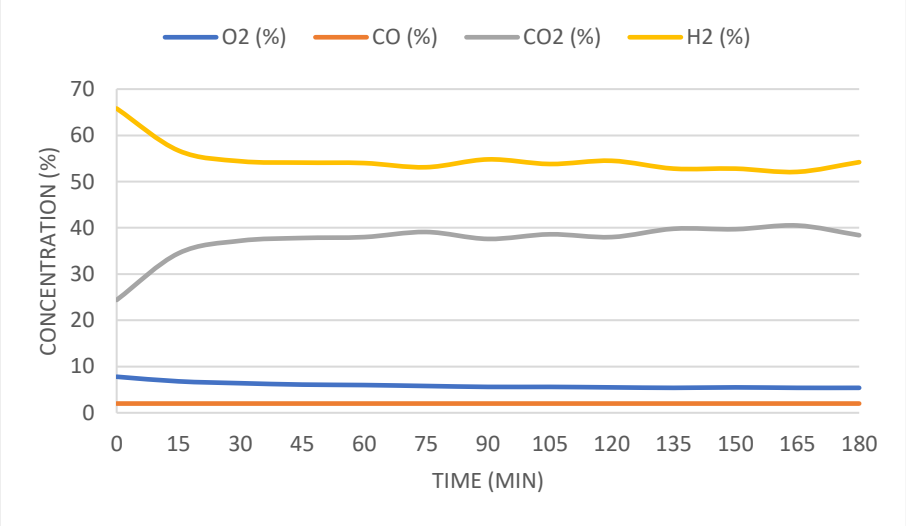

Figure 3-2: Gas outlet composition over the duration of the test, 1M KOH, at 3 bar(g) and 100 ºC;

Among the data obtained the key important parameters to note are:

- 5.4 % of oxygen in the outlet;
- 39.5 % of carbon dioxide;
- 53 % of hydrogen;
- 35.06 l/h of produced gas with an energetic cost of 13.98 Wh/l.

3.2.1.3. 1M KOH, at 3 bar(g) and 110 ºC

Table 3-4: Conditions and collected results, 1M KOH, at 3 bar(g) and 110 ºC;

Time (min)	T (°C)	P (bar(g))	V (V)	I (A)	O_2 (%)	CO (%)	CO_2 (%)	H_2 (%)	F (l/h)	W/F (Wh/l)
0	109.7	2.9	34.03	17.18	7.3	2.0	24.6	66.1	47.87	12.21
15	109.8	2.5	31.49	15.1	5.9	2.0	37.6	54.5	39.42	12.06
30	110.2	3.1	31.49	15.38	5.6	2.0	35.4	57.0	39.36	12.31
45	110.0	3.4	31.49	14.93	5.5	2.0	37.1	55.4	36.44	12.90
60	109.2	2.9	31.49	15.55	5.3	2.0	41.0	51.7	38.28	12.79
75	109.7	3.1	31.49	15.08	5.3	2.0	39.6	53.1	35.21	13.49
90	109.5	2.7	31.50	14.84	5.2	2.0	41.4	51.4	37.18	12.57
105	109.9	2.9	31.49	15.2	5.2	2.0	40.2	52.6	35.79	13.38
120	109.2	3.1	31.49	15.14	5.2	2.0	38.7	54.1	33.62	14.18
135	109.3	2.3	31.50	13.93	4.9	2.0	46.0	47.1	37.67	11.65
150	111.3	2.5	31.48	15.57	5.1	2.0	41.2	51.7	35.12	13.96
165	110.8	3.2	31.49	15.19	5.1	2.0	36.1	56.8	33.15	14.43
180	110.9	3.0	31.49	15.31	5.0	2.0	43.0	50.0	35.58	13.55

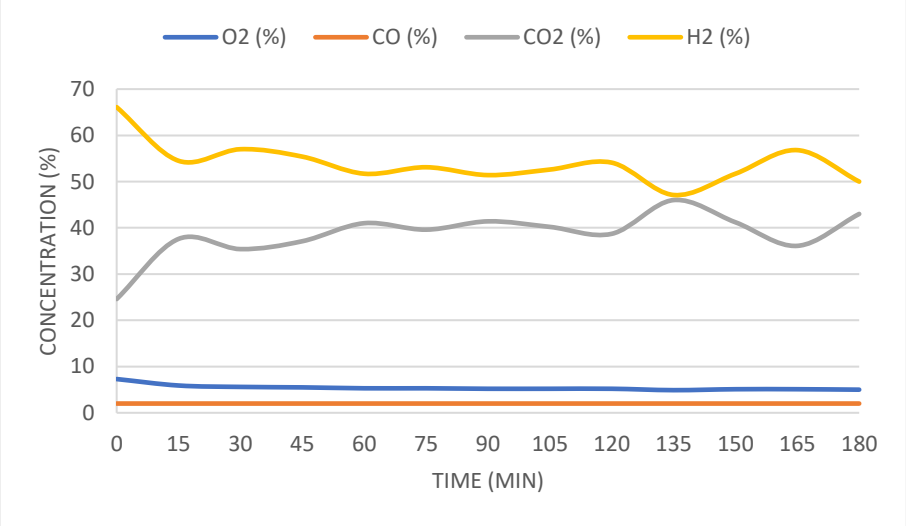

Figure 3-3: Gas outlet composition over the duration of the test, 1M KOH, at 3 bar(g) and 110 ºC;

Among the data obtained the key important parameters to note are:

- 5.1 % of oxygen in the outlet;
- 40.1 % of carbon dioxide;
- 52.8 % of hydrogen;
- 34.62 l/h of produced gas with an energetic cost of 13.98 Wh/l.

3.2.1.4. 1M KOH, at 4 bar(g) and 90 ºC

Table 3-5: Conditions and collected results, 1M KOH, at 4 bar(g) and 90 ºC;

Time (min)	T (°C)	P (bar(g))	V (V)	I (A)	O_2 (%)	CO (%)	CO_2 (%)	H_2 (%)	F (l/h)	W/F (Wh/l)
0	90.4	3.9	31.00	15.00	4.2	2.0	30.6	63.2	38.15	12.19
15	90.9	4.1	32.00	15.00	4.0	2.0	30.0	64.0	43.05	11.15
30	90.0	4.1	32.00	15.00	3.8	2.0	30.5	63.7	44.85	10.70
45	90.9	4.3	30.00	15.00	3.6	2.0	31.6	62.8	45.04	9.99
60	90.0	3.9	31.00	15.00	3.5	2.0	31.1	63.4	42.57	10.92
75	90.8	3.9	32.00	15.00	3.5	2.0	33.0	61.5	41.17	11.66
90	90.4	3.9	32.00	15.00	3.5	2.0	31.4	63.1	42.54	11.28
105	90.9	3.9	30.00	15.50	4.7	2.0	31.5	61.8	48.87	9.52
120	90.5	4.0	32.00	15.00	3.6	1.9	30.7	63.8	49.11	9.77
135	90.7	4.1	30.00	15.50	3.5	2.0	31.6	62.9	47.64	9.76
150	90.4	4.0	32.00	15.00	3.5	2.0	31.5	63.0	43.65	11.00
165	90.1	4.0	32.00	15.00	3.5	1.9	31.0	63.6	49.72	9.65
180	90.9	4.2	32.00	15.50	3.5	2.0	31.3	63.2	49.18	10.09

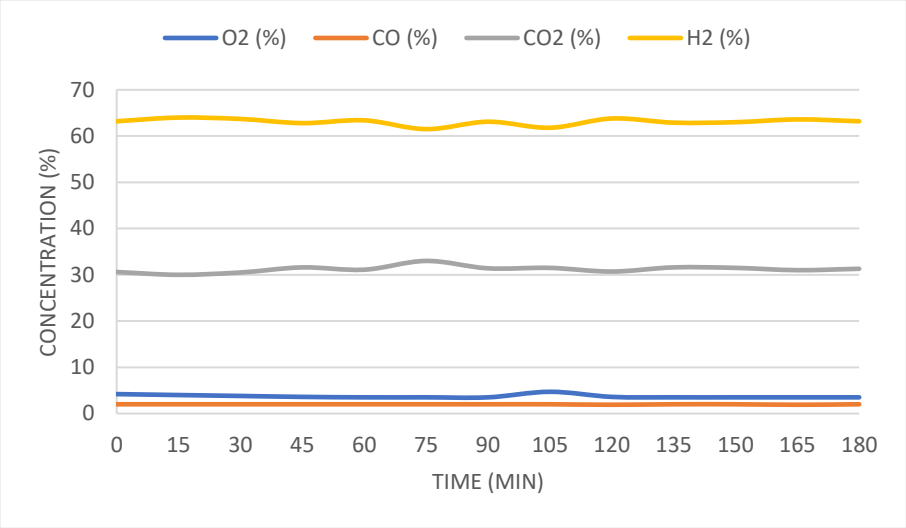

Figure 3-4: Gas outlet composition over the duration of the test, 1M KOH, at 4 bar(g) and 90 ºC;

Among the data obtained the key important parameters to note are:

- 3.5 % of oxygen in the outlet;
- 31.3 % of carbon dioxide;
- 63.3 % of hydrogen;
- 47.52 l/h of produced gas with an energetic cost of 10.24 Wh/l.

3.2.1.5. 1M KOH, at 4 bar(g) and 100 ºC

Table 3-6: Conditions and collected results, 1M KOH, at 4 bar(g) and 100 ºC;

Time (min)	T (°C)	P (bar(g))	V (V)	I (A)	O_2 (%)	CO (%)	CO_2 (%)	H_2 (%)	F (l/h)	W/F (Wh/l)
0	100.5	3.9	28.00	15.00	2.7	1.7	31.0	64.6	46.23	9.08
15	101.0	4.2	28.00	15.00	2.6	1.7	31.0	64.7	40.42	10.39
30	100.0	4.3	30.00	15.00	2.5	1.7	32.8	63.0	47.04	9.57
45	100.2	4.3	28.00	15.00	2.9	1.6	31.9	63.6	49.61	8.47
60	101.0	4.4	30.00	15.00	2.4	1.6	32.7	63.3	44.81	10.04
75	101.5	4.4	28.00	15.00	2.4	1.6	32.5	63.5	52.61	7.98
90	100.2	4.0	30.00	15.00	2.4	1.6	32.5	63.5	48.74	9.23
105	101.1	4.1	30.00	15.00	2.4	1.6	32.5	63.5	46.96	9.58
120	100.3	4.0	30.00	15.00	2.4	1.6	31.7	64.3	46.85	9.60
135	101.5	4.1	30.00	15.00	2.4	1.6	32.8	63.2	54.46	8.26
150	101.0	4.1	30.00	15.00	2.4	1.6	33.9	62.1	55.87	8.05
165	100.4	4.0	30.00	15.00	2.5	1.6	35.1	60.8	46.55	9.67
180	101.2	4.1	30.00	14.50	2.4	1.6	36.2	59.8	48.67	8.94

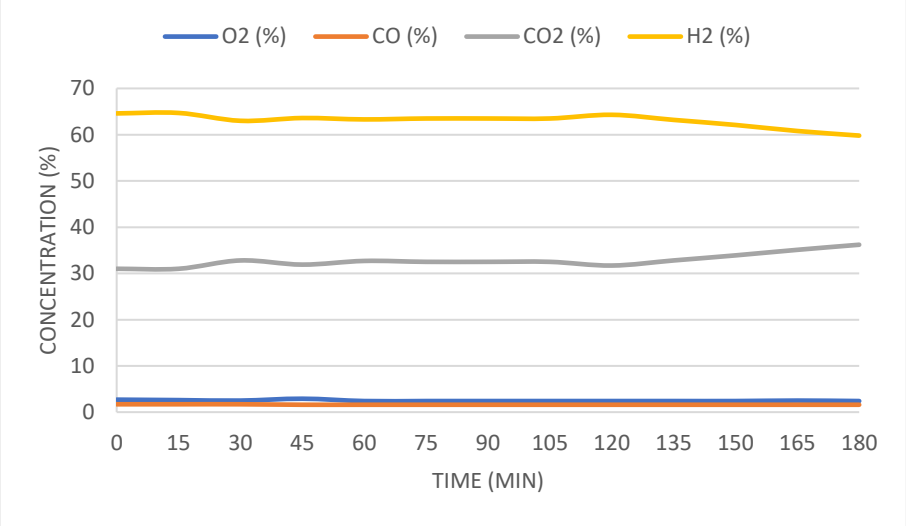

Figure 3-5: Gas outlet composition over the duration of the test, 1M KOH, at 4 bar(g) and 100 ºC;

Among the data obtained the key important parameters to note are:

- 2.4 % of oxygen in the outlet;
- 35.1 % of carbon dioxide;
- 60.9 % of hydrogen;
- 50.36 l/h of produced gas with an energetic cost of 8.89 Wh/l.

3.2.1.6. 1M KOH, at 4 bar(g) and 110 ºC

Table 3-7: Conditions and collected results, 1M KOH, at 4 bar(g) and 110 ºC;

Time (min)	T (°C)	P (bar(g))	V (V)	I (A)	O_2 (%)	CO (%)	CO_2 (%)	H_2 (%)	F (l/h)	W/F (Wh/l)
0	110.6	4.4	28.00	17.50	2.5	1.5	30.9	65.1	69.95	7.01
15	109.9	4.0	29.00	17.00	2.5	1.4	33.0	63.1	51.55	9.56
30	109.6	4.0	28.00	17.00	2.4	1.4	31.8	64.4	49.84	9.55
45	110.1	4.2	28.00	17.00	2.4	1.5	31.6	64.5	50.44	9.44
60	110.1	4.2	28.00	17.50	2.3	1.4	32.4	63.9	52.81	9.28
75	110.3	4.2	28.00	17.00	2.4	1.4	34.2	62.0	50.97	9.34
90	110.3	4.3	29.00	17.00	2.4	1.4	33.9	62.3	54.63	9.02
105	110.3	4.1	29.00	17.00	2.3	1.4	35.0	61.3	45.72	10.78
120	110.3	4.0	28.00	17.00	2.6	1.4	34.5	61.5	49.07	9.70
135	110.3	4.0	29.00	16.50	2.4	1.4	33.4	62.8	53.39	8.96
150	110.4	4.1	29.00	17.00	2.3	1.5	34.4	61.8	53.39	9.23
165	110.6	4.2	30.00	17.00	2.3	1.4	34.4	61.9	52.53	9.71
180	110.6	4.1	29.00	16.75	2.3	1.4	33.5	62.8	53.49	9.08

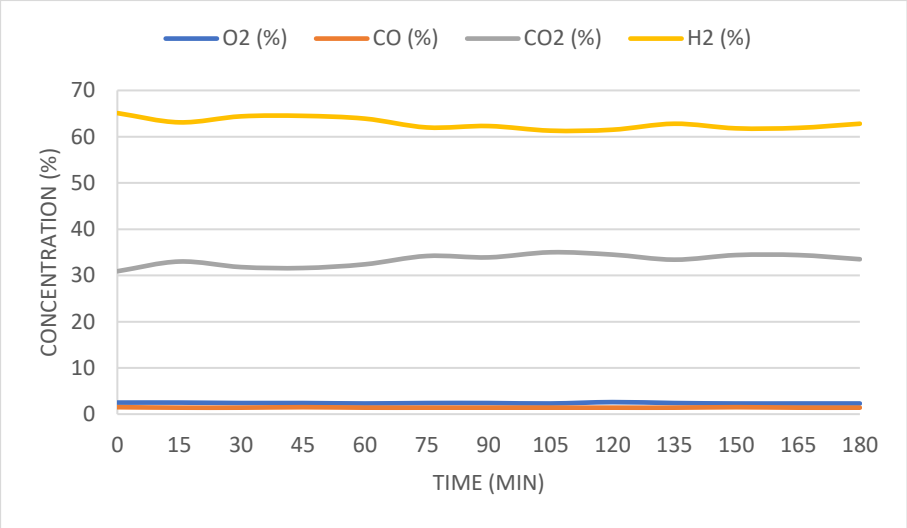

Figure 3-6: Gas outlet composition over the duration of the test, 1M KOH, at 4 bar(g) and 110 ºC;

Among the data obtained the key important parameters to note are:

- 1.4 % of oxygen in the outlet;
- 34.1 % of carbon dioxide;
- 62.2 % of hydrogen;
- 53.14 l/h of produced gas with an energetic cost of 9.34 Wh/l.

3.2.1.7. 1M KOH, at 5 bar(g) and 90 ºC

Table 3-8: Conditions and collected results, 1M KOH, at 5 bar(g) and 90 ºC;

Time (min)	T (°C)	P (bar(g))	V (V)	I (A)	O_2 (%)	CO (%)	CO_2 (%)	H_2 (%)	F (l/h)	W/F (Wh/l)
0	90.9	4.6	33.00	15.00	5.0	2.2	22.2	70.6	47.91	10.33
15	88.9	4.5	33.00	15.00	3.5	2.2	28.0	66.3	46.65	10.61
30	90.8	4.9	33.00	15.00	3.2	2.2	28.5	66.1	48.26	10.26
45	89.9	5.2	33.00	15.00	3.0	2.1	30.4	64.5	43.76	11.31
60	90.0	4.1	33.00	15.00	3.1	2.1	31.9	62.9	41.80	11.84
75	89.3	4.7	33.00	15.00	3.1	2.1	30.5	64.3	43.22	11.45
90	90.4	4.9	33.00	14.90	3.0	2.1	29.7	65.2	41.99	11.71
105	89.5	5.2	33.00	15.00	2.7	2.0	30.9	64.4	46.15	10.73
120	89.9	4.8	33.00	15.00	3.0	2.0	30.9	64.1	45.17	10.96
135	91.1	5.3	33.00	15.00	2.9	2.0	29.4	65.7	42.54	11.64
150	89.9	4.6	33.00	15.00	2.8	2.0	30.9	64.3	48.26	10.26
165	90.0	4.6	33.00	15.00	3.0	2.0	30.7	64.3	46.37	10.67
180	91.1	4.9	33.00	15.00	3.0	2.1	29.3	65.6	48.34	10.24

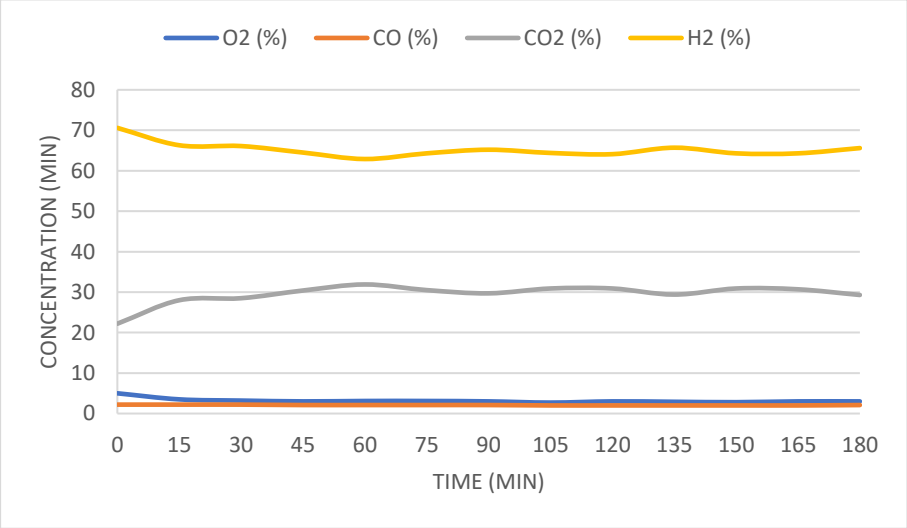

Figure 3-7: Gas outlet composition over the duration of the test, 1M KOH, at 5 bar(g) and 90 ºC;

Among the data obtained the key important parameters to note are:

- 2.9 % of oxygen in the outlet;
- 30.3 % of carbon dioxide;
- 64.7 % of hydrogen;
- 47.66 l/h of produced gas with an energetic cost of 10.39 Wh/l.

3.2.1.8. 1M KOH, at 5 bar(g) and 100 ºC

Table 3-9: Conditions and collected results, 1M KOH, at 5 bar(g) and 100 ºC;

Time (min)	T (°C)	P (bar(g))	V (V)	I (A)	O_2 (%)	CO (%)	CO_2 (%)	H_2 (%)	F (l/h)	W/F (Wh/l)
0	100.2	5.2	30.00	15.00	2.7	2.2	29.1	66.0	42.55	10.58
15	100.6	4.5	30.00	15.00	2.8	2.0	32.8	62.4	43.29	10.40
30	100.7	5.6	30.00	15.00	2.7	2.1	31.6	63.6	39.26	11.46
45	100.7	4.8	30.00	15.00	2.8	2.0	32.3	62.9	48.19	9.34
60	101.0	4.3	30.00	15.00	2.3	2.0	32.7	63.0	48.82	9.22
75	101.4	4.8	30.00	15.00	2.1	2.1	31.1	64.7	44.21	10.18
90	101.3	5.2	30.00	15.00	2.2	2.1	31.4	64.3	39.91	11.28
105	100.1	5.1	30.00	15.00	2.2	2.0	33.2	62.6	40.42	11.13
120	99.7	5.1	30.00	15.00	2.2	2.0	31.7	64.1	40.77	11.04
135	98.8	4.9	30.00	15.00	2.1	2.0	32.0	63.9	37.28	12.07
150	98.8	5.5	30.00	15.00	2.1	2.0	33.2	62.7	38.34	11.74
165	99.6	4.5	30.00	15.00	1.9	2.0	30.7	65.4	45.19	9.96
180	100.9	4.8	30.00	15.00	2.0	2.0	31.1	64.9	46.31	9.72

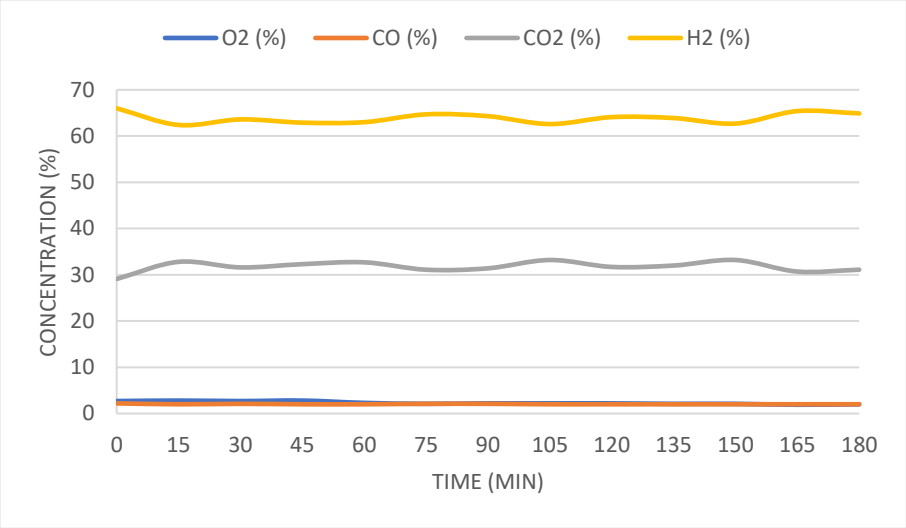

Figure 3-8: Gas outlet composition over the duration of the test, 1M KOH, at 5 bar(g) and 100 ºC;

Among the data obtained the key important parameters to note are:

- 2.0 % of oxygen in the outlet;
- 31.7 % of carbon dioxide;
- 64.3 % of hydrogen;
- 43.28 l/h of produced gas with an energetic cost of 10.47 Wh/l.

3.2.1.9. 1M KOH. at 5 bar(g) and 110 ºC

Table 3-10: Conditions and collected results, 1M KOH, at 5 bar(g) and 110 ºC;

Time (min)	T (°C)	P (bar(g))	V (V)	I (A)	O_2 (%)	CO (%)	CO_2 (%)	H_2 (%)	F (l/h)	W/F (Wh/l)
0	109.7	4.8	30.00	15.00	2.3	1.9	30.9	64.9	50.30	8.95
15	109.7	5.3	30.00	15.00	2.1	1.9	30.3	65.7	56.40	7.98
30	109.5	5.0	31.00	17.00	2.1	1.8	31.6	64.5	45.88	11.49
45	109.5	4.8	31.00	17.00	2.2	1.8	31.3	64.7	50.37	10.46
60	109.6	5.0	31.00	17.00	2.0	1.8	30.8	65.4	50.02	10.54
75	109.6	4.6	31.00	17.00	2.0	1.9	31.2	64.9	50.21	10.50
90	109.7	5.1	31.00	17.00	1.9	1.8	31.4	64.9	51.09	10.32
105	109.7	5.1	31.00	17.00	2.0	1.8	31.0	65.2	51.60	10.21
120	110.2	5.2	31.00	17.00	1.9	1.9	31.0	65.2	51.11	10.31
135	109.9	5.0	31.00	17.00	1.9	1.8	31.3	65.0	51.06	10.32
150	109.7	4.9	31.00	17.00	1.9	1.8	31.3	65.0	50.42	10.45
165	109.3	5.0	31.00	17.50	1.9	1.8	30.3	66.0	54.88	9.89
180	109.7	5.3	31.00	17.50	1.8	1.9	29.9	66.4	50.59	10.72

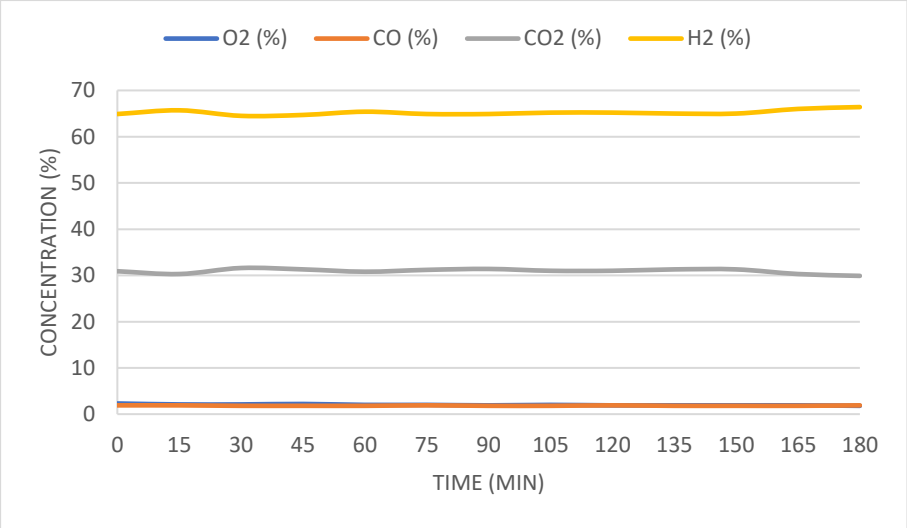

Figure 3-9: Gas outlet composition over the duration of the test, 1M KOH, at 5 bar(g) and 110 ºC;

Among the data obtained the key important parameters to note are:

- 2.0 % of oxygen in the outlet;
- 30.5 % of carbon dioxide;
- 65.8 % of hydrogen;
- 51.96 l/h of produced gas with an energetic cost of 10.35 Wh/l.

3.2.2. KOH electrolyte performance analysis

Considering the objective of producing syngas to later introduce a Sabatier system for methane production, the typical syngas composition used in the Sabatier process is adjusted to achieve as close as possible the stoichiometric ratio of CO_2:H_2 for the production of CH_4, which is 1:4 (although this varies slightly depending on factors such as the catalyst operational conditions, and desired methane yield). Furthermore, the presence of oxygen causes the catalyst deactivation, so ideally its concentration should be as low as possible to minimize the need for frequent catalyst replacement.

Regarding this first set of results, the increase in temperature within the established range caused consistent decrease in O_2 concentration in the produced gas outlet independent of pressure of the process. Additionally, temperatures above 90 ºC are observed to promote higher CO_2 concentrations, with all pressures except for 3 bar(g) (likely due graphite disc wear down, a phenomenon that will be discussed further down the line) showing peak concentration at 100 ºC. As consequence of the increase in CO_2 production, H_2 concentration in the outlet lowers, thus rising CO_2:H_2 ratio.

When looking at the correlation between process temperature and energy spent per unit of flow, the tests show better performances (in other words higher flow rates and less energy expenditure) when using higher temperatures. Once again, the 3 bar(g) group are an exception due to all signs pointing to the stack performance being hindered by accumulated wear in the graphite disks inside.

In relation to the effect of pressure, once again O_2 concentrations reveal a significant reduction when increasing pressure inside the system. On the other hand, as opposite to temperature, CO_2 concentrations also decrease at higher pressures and consequentially H_2 concentration increase leading to a lower CO_2:H_2 ratio. In terms of its effect on the exiting gas flow, while there was some variation, it couldn't be clearly linked to the change in pressure (with further data being needed).

For a clearer analysis and comparison of tests, Table 3-11 displays each test O_2 concentration, CO_2:H_2 ratio, produced flow as well as energy spent per unit of gas flow produced:

Table 3-11: Compiled results of each test using KOH electrolyte solution and respectives CO_2:H_2 ratios;

Test Conditions	O_2 (%)	CO (%)	CO_2 (%)	H_2 (%)	F (l/h)	W/F (Wh/l)	CO2:H2 Ratio
1M KOH; 3 bar(g); 90 ºC	6.4	2.0	31.7	59.9	45.71	12.28	1:1.89
1M KOH; 3 bar(g); 100 ºC	5.4	2.0	39.5	53.0	35.06	13.98	1:1.34
1M KOH; 3 bar(g); 110 ºC	5.1	2.0	40.1	52.8	34.62	13.98	1:1.32
1M KOH; 4 bar(g); 90 ºC	3.5	2.0	31.3	63.3	47.52	10.24	1:2.02
1M KOH; 4 bar(g); 100 ºC	2.4	1.6	35.1	60.9	50.36	8.89	1:1.74
1M KOH; 4 bar(g); 110 ºC	2.3	1.4	34.1	62.2	53.14	9.34	1:1.82
1M KOH; 5 bar(g); 90 ºC	2.9	2.0	30.3	64.7	47.66	10.39	1:2.14
1M KOH; 5 bar(g); 100 ºC	2.0	2.0	31.7	64.3	43.28	10.47	1:2.03
1M KOH; 5 bar(g); 110 ºC	1.9	1.8	30.5	65.8	51.96	10.35	1:2.16

Among this first set of tests, the one executed at 5 bar(g) and 110 ºC exhibited both the lowest O_2 concentration and the closest CO_2:H_2 ratio to the desired 1:4 with 1.9 % and 1:2.16 respectively.

Although the 1M KOH solution offers good results in terms of "direct performance" when used as electrolyte, a few additional negative factors keep it from being the ideal choice, namely:

- Faster degradation of the graphite disks inside the stack, requiring more frequent maintenance to substitute them (to avoid a decline in performance) and consequentially increasing the costs associated with the process;
- Over the course of multiple tests, its circulation caused noticeable wear and, in some cases, even significant damage to the equipment such as junctions, elbows and valves and even the Teflon used to seal the stack. As a result, the frequency of leaks increased, multiple parts were damaged and had to be replaced, and more frequent maintenance was required to assure the stack was kept safely sealed;
- During the execution of each test, there was more difficulty in controlling and maintain the required conditions, with this problem aggravated when testing for higher pressures.

3.2.3. Tests and results, $NaOH$ electrolyte

3.2.3.1. 1M $NaOH$, at 3 bar(g) and 90 ºC

Table 3-12: Conditions and collected results, 1M NaOH, at 3 bar(g) and 90 ºC;

Time (min)	T (°C)	P (bar(g))	V (V)	I (A)	O_2 (%)	CO (%)	CO_2 (%)	H_2 (%)	F (l/h)	W/F (Wh/l)
0	91.3	3.2	41.76	19.71	13.3	2.0	13.2	71.5	81.26	10.13
15	92.0	3.1	41.74	21.37	13.3	2.0	20.1	64.6	92.54	9.64
30	92.9	3.0	41.75	20.01	12.5	2.0	21.6	63.9	95.41	8.76
45	89.6	2.9	37.1	15.03	11.2	2.0	23.9	62.9	57.69	9.67
60	89.8	3.4	37.12	15.55	10.0	2.0	24.6	63.4	67.71	8.52
75	89.6	3.3	37.11	15.64	9.9	2.0	26.4	61.7	68.18	8.51
90	89.4	3.0	37.11	15.13	9.6	2.0	27.5	60.9	67.29	8.34
105	90.1	3.0	37.12	14.99	9.7	2.0	27.5	60.8	66.87	8.32
120	88.6	2.9	37.11	14.49	9.8	2.0	26.4	61.8	65.10	8.26
135	89.6	3.0	37.12	14.86	9.7	2.0	26.9	61.4	64.02	8.62
150	89.6	3.0	37.11	14.81	9.6	2.0	26.9	61.5	61.16	8.99
165	89.7	3.0	37.11	14.41	9.6	2.0	27.2	61.2	60.30	8.87
180	88.9	3.0	37.12	14.45	9.6	2.0	27.0	61.4	64.29	8.34

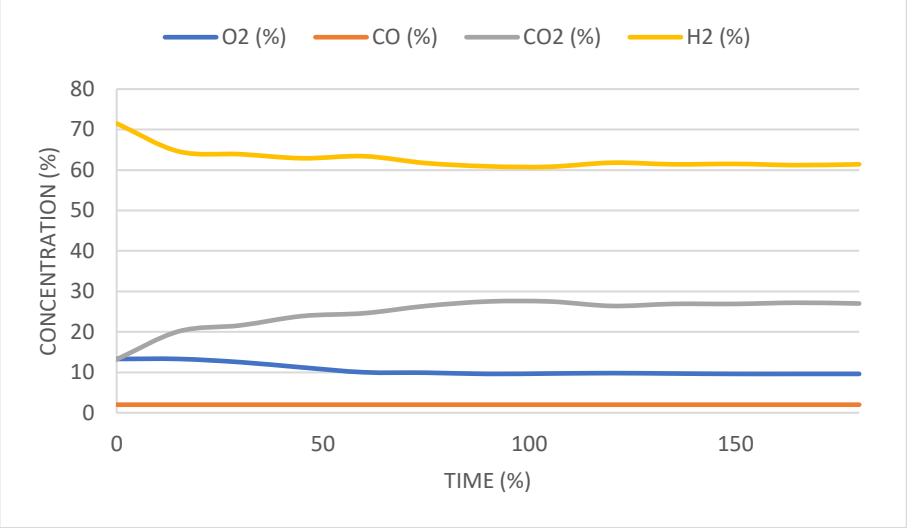

Figure 3-10: Gas outlet composition over the duration of the test, 1M NaOH, at 3 bar(g) and 90 ºC;

Among the data obtained the key important parameters to note are:

- 9.6 % of oxygen in the outlet;
- 27.0 % of carbon dioxide;
- 61.4 % of hydrogen;
- 61.91 l/h of produced gas with an energetic cost of 8.73 Wh/l.

3.2.3.2. *1M NaOH, at 3 bar(g) and 100 ºC*

Table 3-13: Conditions and collected results, 1M NaOH, at 3 bar(g) and 100 ºC;

Time (min)	T (°C)	P (bar(g))	V (V)	I (A)	O_2 (%)	CO (%)	CO_2 (%)	H_2 (%)	F (l/h)	W/F (Wh/l)
0	100.4	2.9	33.79	14.88	9.3	2.0	8.5	80.2	51.63	9.74
15	100.9	2.9	33.76	15.05	7.5	2.0	19.3	71.2	56.49	9.00
30	100.0	3.0	33.71	14.97	6.5	2.0	26.6	64.9	58.13	8.68
45	100.1	3.1	33.72	15.03	6.0	2.0	30.2	61.8	59.24	8.55
60	100.4	3.0	33.71	15.30	5.4	2.0	32.1	60.5	56.10	9.19
75	100.4	3.1	33.73	14.79	5.2	2.0	33.0	59.8	56.19	8.88
90	100.4	3.0	33.74	14.44	5.2	2.0	34.5	58.3	61.43	7.93
105	100.3	3.0	33.75	14.27	5.0	2.0	33.5	59.5	56.16	8.58
120	100.2	3.0	33.74	14.43	4.8	2.0	34.4	58.8	56.46	8.62
135	100.5	3.0	33.75	14.30	4.9	2.0	35.3	57.8	54.93	8.79
150	100.5	3.0	33.75	14.21	4.7	2.0	35.2	58.1	54.05	8.87
165	101.0	3.1	33.75	14.00	4.7	2.0	34.6	58.7	50.97	9.27
180	100.6	3.0	33.76	13.70	4.6	2.0	34.4	59.0	51.80	8.93

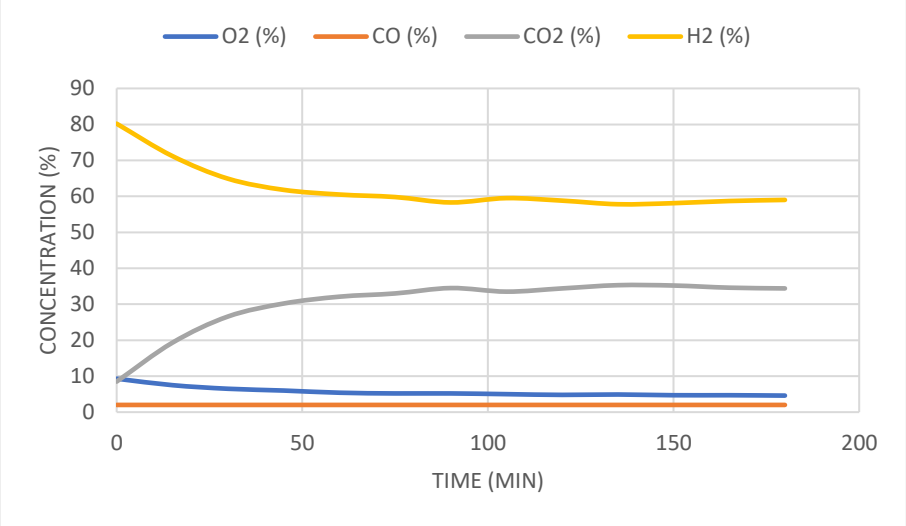

Figure 3-11: Gas outlet composition over the duration of the test, 1M NaOH, at 3 bar(g) and 100 ºC;

Among the data obtained the key important parameters to note are:

- 4.7 % of oxygen in the outlet;
- 34.7 % of carbon dioxide;
- 58.6 % of hydrogen;
- 52.27 l/h of produced gas with an energetic cost of 9.02 Wh/l.

3.2.3.3. 1M NaOH, at 3 bar(g) and 110 ºC

Table 3-14: Conditions and collected results, 1M NaOH, at 3 bar(g) and 110 ºC;

Time (min)	T (°C)	P (bar(g))	V (V)	I (A)	O_2 (%)	CO (%)	CO_2 (%)	H_2 (%)	F (l/h)	W/F (Wh/l)
0	109.0	2.7	32.88	15.99	9.8	2.0	25.3	62.9	56.66	9.28
15	109.1	3.0	32.69	15.98	5.9	2.0	29.7	62.4	58.98	8.86
30	110.6	3.3	32.69	16.54	5.1	2.0	33.7	59.2	61.93	8.73
45	109.5	3.3	32.80	16.18	4.7	2.0	33.7	59.6	59.67	8.89
60	110.3	3.4	32.90	15.94	4.5	2.0	34.3	59.2	59.08	8.88
75	109.5	3.3	32.79	15.55	4.3	2.0	35.0	58.7	59.37	8.59
90	110.1	3.4	32.80	16.06	4.2	2.0	34.9	58.9	59.77	8.81
105	110.7	3.4	32.77	16.11	4.0	2.0	35.5	58.5	58.00	9.10
120	110.1	3.3	32.81	15.64	3.9	2.0	37.1	57.0	57.69	8.89
135	110.4	3.2	32.62	15.65	3.8	2.0	36.0	58.2	57.17	8.93
150	110.4	3.2	32.80	15.67	3.8	2.0	35.9	58.3	55.36	9.28
165	110.6	3.2	32.80	15.57	3.7	2.0	34.8	59.5	52.35	9.76
180	110.5	3.2	32.80	15.24	3.7	2.0	35.5	58.8	55.05	9.08

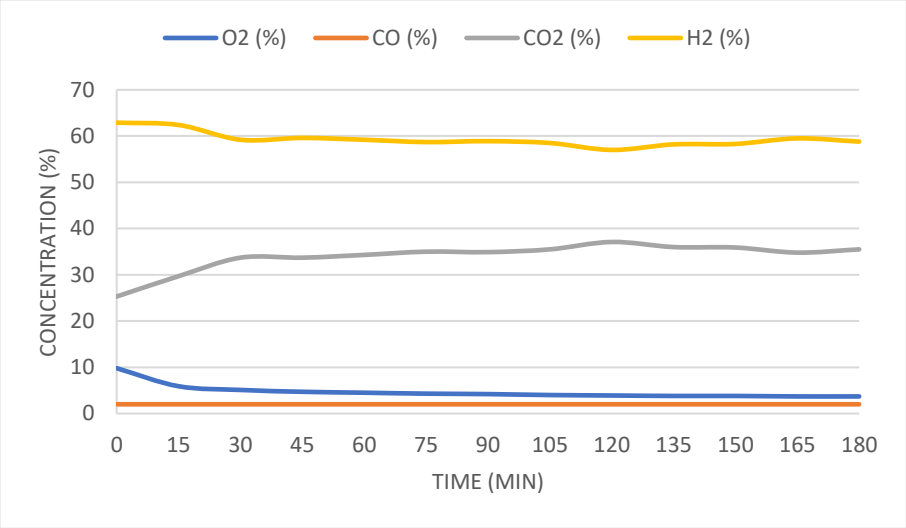

Figure 3-12: Gas outlet composition over the duration of the test, 1M NaOH, at 3 bar(g) and 110 ºC;

Among the data obtained the key important parameters to note are:

- 3.7 % of oxygen in the outlet;
- 35.4 % of carbon dioxide;
- 58.9 % of hydrogen;
- 54.25 l/h of produced gas with an energetic cost of 9.37 Wh/l.

3.2.3.4. 1M NaOH, at 4 bar(g) and 90 ºC

Table 3-15: Conditions and collected results, 1M NaOH, at 4 bar(g) and 90 ºC;

Time (min)	T (°C)	P (bar(g))	V (V)	I (A)	O_2 (%)	CO (%)	CO_2 (%)	H_2 (%)	F (l/h)	W/F (Wh/l)
0	91.9	3.9	34.00	15.50	9.3	1.8	16.5	72.4	51.92	10.15
15	89.9	4.5	34.00	15.00	7.7	1.8	20.9	69.6	58.70	8.69
30	91.6	4.2	34.00	15.00	7.0	1.8	24.5	66.7	52.33	9.75
45	90.2	3.9	34.00	15.00	6.5	1.8	25.5	66.2	51.16	9.97
60	91.2	3.8	36.00	15.00	6.5	1.8	26.1	65.6	47.02	11.49
75	91.1	4.1	36.00	15.00	6.2	1.8	25.7	66.3	52.99	10.19
90	90.9	4.1	34.00	15.00	6.1	1.8	26.1	66.0	50.42	10.12
105	90.5	4.1	34.00	15.00	6.0	1.8	26.2	66.0	48.21	10.58
120	90.6	4.1	34.00	15.00	5.9	1.8	26.4	65.9	52.66	9.69
135	90.6	4.3	34.00	15.00	5.9	1.8	26.6	65.7	53.47	9.54
150	91.3	4.3	36.00	15.00	5.9	1.8	26.8	65.5	54.85	9.85
165	90.9	4.3	36.00	15.00	5.9	1.8	26.7	65.6	54.96	9.83
180	90.8	4.1	34.00	14.50	5.8	1.8	26.7	65.7	54.41	9.06

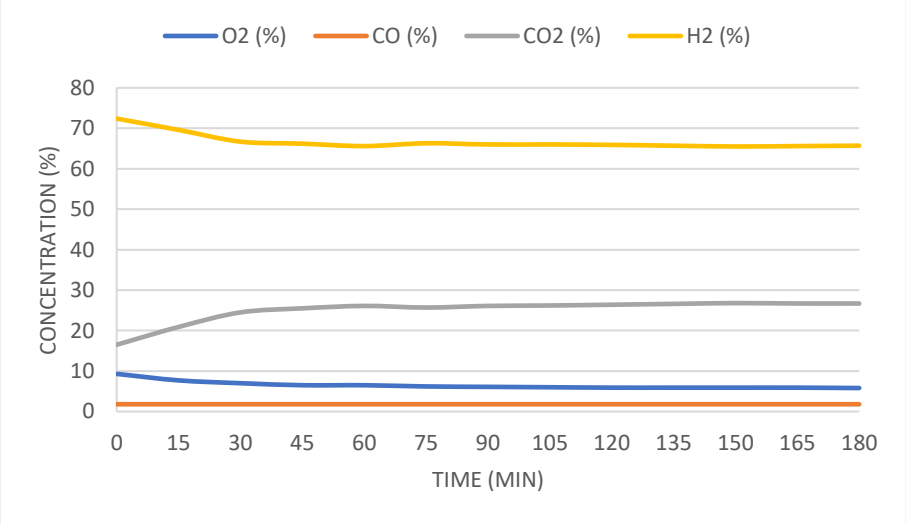

Figure 3-13: Gas outlet composition over the duration of the test, 1M NaOH, at 4 bar(g) and 90 ºC;

Among the data obtained the key important parameters to note are:

- 5.9 % of oxygen in the outlet;
- 26.7 % of carbon dioxide;
- 65.6 % of hydrogen;
- 54.74 l/h of produced gas with an energetic cost of 9.58 Wh/l.

3.2.3.5. *1M NaOH, at 4 bar(g) and 100 ºC*

Table 3-16: Conditions and collected results, 1M NaOH, at 4 bar(g) and 100 ºC;

Time (min)	T (°C)	P (bar(g))	V (V)	I (A)	O_2 (%)	CO (%)	CO_2 (%)	H_2 (%)	F (l/h)	W/F (Wh/l)
0	100.0	4.1	32.00	15.00	5.3	1.8	24.3	68.6	49.27	9.74
15	99.6	4.1	32.00	15.00	4.7	1.8	25.7	67.8	48.26	9.95
30	99.8	4.2	33.00	15.00	4.5	1.8	24.7	69.0	45.80	10.81
45	99.7	4.1	32.00	15.50	4.7	1.8	26.4	67.1	45.82	10.82
60	100.2	4.1	34.00	15.00	5.1	1.8	26.1	67.0	46.65	10.93
75	100.0	4.1	33.00	15.00	4.4	1.8	25.7	68.1	44.96	11.01
90	101.6	4.2	33.00	15.00	4.2	1.8	25.6	68.4	45.84	10.80
105	100.2	4.1	33.00	15.00	4.2	1.8	25.8	68.2	46.49	10.65
120	101.5	4.1	33.00	15.00	4.1	1.8	25.7	68.4	46.41	10.67
135	100.9	4.1	33.00	14.50	4.2	1.8	25.5	68.5	45.67	10.48
150	100.5	4.0	32.00	14.50	4.1	1.8	25.1	69.0	48.71	9.52
165	100.8	4.2	34.00	15.00	4.2	1.8	26.0	68.0	45.86	11.12
180	101.2	4.2	34.00	15.00	4.1	1.8	25.0	69.1	45.96	11.10

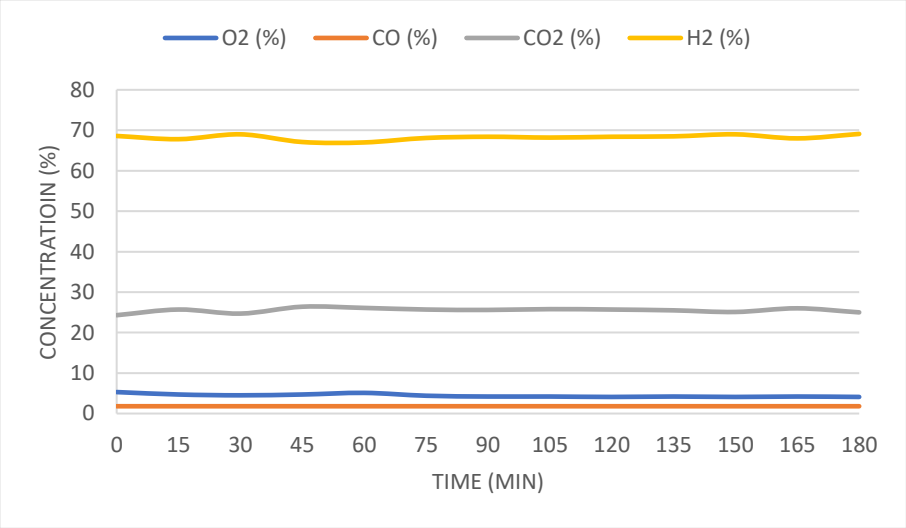

Figure 3-14: Gas outlet composition over the duration of the test, 1M NaOH, at 4 bar(g) and 100 ºC;

Among the data obtained the key important parameters to note are:

- 4.1 % of oxygen in the outlet;
- 25.4 % of carbon dioxide;
- 68.7 % of hydrogen;
- 46.84 l/h of produced gas with an energetic cost of 10.58 Wh/l.

3.2.3.6. *1M NaOH, at 4 bar(g) and 110 ºC*

Table 3-17: Conditions and collected results, 1M NaOH, at 4 bar(g) and 110 ºC;

Time (min)	T (°C)	P (bar(g))	V (V)	I (A)	O_2 (%)	CO (%)	CO_2 (%)	H_2 (%)	F (l/h)	W/F (Wh/l)
0	109.9	4.1	36.00	18.00	4.4	1.8	24.4	69.4	57.11	11.35
15	109.8	3.8	33.00	18.00	4.0	1.8	25.5	68.7	52.50	11.31
30	111.5	4.0	32.00	17.00	3.9	1.8	25.2	69.1	52.02	10.46
45	110.1	4.0	34.00	16.00	3.8	1.8	25.3	69.1	47.47	11.46
60	109.8	3.9	34.00	16.00	3.8	1.8	25.7	68.7	44.37	12.26
75	109.6	4.0	32.00	16.00	3.6	1.8	25.4	69.2	45.44	11.27
90	110.5	4.3	33.00	17.00	3.6	1.8	25.6	69.0	48.96	11.46
105	110.8	4.0	32.00	16.00	3.6	1.8	26.1	68.5	46.15	11.09
120	110.5	3.9	32.00	16.00	3.5	1.8	26.0	68.7	46.33	11.05
135	110.3	3.9	32.00	16.00	3.5	1.8	26.4	68.3	45.90	11.15
150	110.2	4.0	32.00	16.00	3.5	1.8	26.3	68.4	45.30	11.30
165	109.9	4.0	32.00	16.00	3.5	1.8	26.0	68.7	45.28	11.31
180	109.9	4.0	32.00	16.00	3.5	1.8	26.3	68.4	44.26	11.57

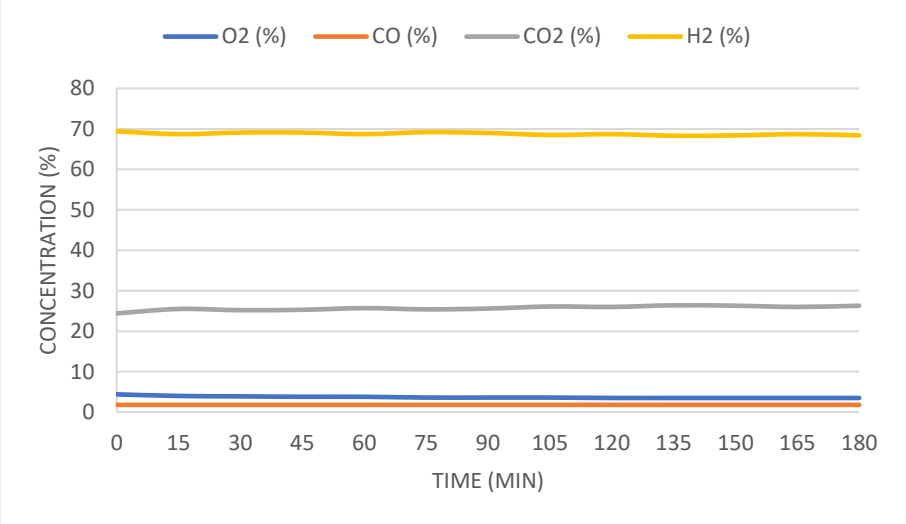

Figure 3-15: Gas outlet composition over the duration of the test, 1M NaOH, at 4 bar(g) and 110 ºC;

Among the data obtained the key important parameters to note are:

- 3.5 % of oxygen in the outlet;
- 26.2 % of carbon dioxide;
- 68.5 % of hydrogen;
- 44.95 l/h of produced gas with an energetic cost of 11.39 Wh/l.

3.2.3.7. *1M NaOH, at 5 bar(g) and 90 ºC*

Table 3-18: Conditions and collected results, 1M NaOH, at 5 bar(g) and 90 ºC

Time (min)	T (°C)	P (bar(g))	V (V)	I (A)	O_2 (%)	CO (%)	CO_2 (%)	H_2 (%)	F (l/h)	W/F (Wh/l)
0	89.8	5.2	39.97	14.94	10.8	2.0	25.6	61.5	65.41	9.13
15	89.1	5.3	39.97	14.89	10.7	2.0	25.9	61.4	63.28	9.41
30	90.6	5.4	39.97	15.62	10.4	2.0	26.2	61.4	67.23	9.29
45	90.6	5.1	39.97	15.32	10.3	2.0	26.4	61.2	67.12	9.12
60	90.3	5.2	39.96	15.20	10.5	2.0	26.2	61.3	66.49	9.14
75	90.6	5.4	39.96	16.02	10.7	2.0	25.8	61.5	71.55	8.95
90	90.0	4.8	39.25	14.94	10.3	2.0	26.1	61.6	67.80	8.65
105	89.8	5.5	38.95	15.22	10.4	2.0	26.3	61.3	68.72	8.63
120	90.4	4.7	38.96	15.12	11.9	1.9	26.3	59.9	62.78	9.38
135	89.8	4.8	38.96	14.75	11.5	2.0	26.2	60.2	53.07	10.83
150	90.6	5.0	38.95	14.75	10.8	2.0	26.2	61.0	72.05	7.97
165	89.4	5.2	38.93	14.86	11.0	2.0	26.2	60.7	69.78	8.29
180	89.8	5.6	38.93	15.26	10.9	2.1	26.2	60.8	70.18	8.47

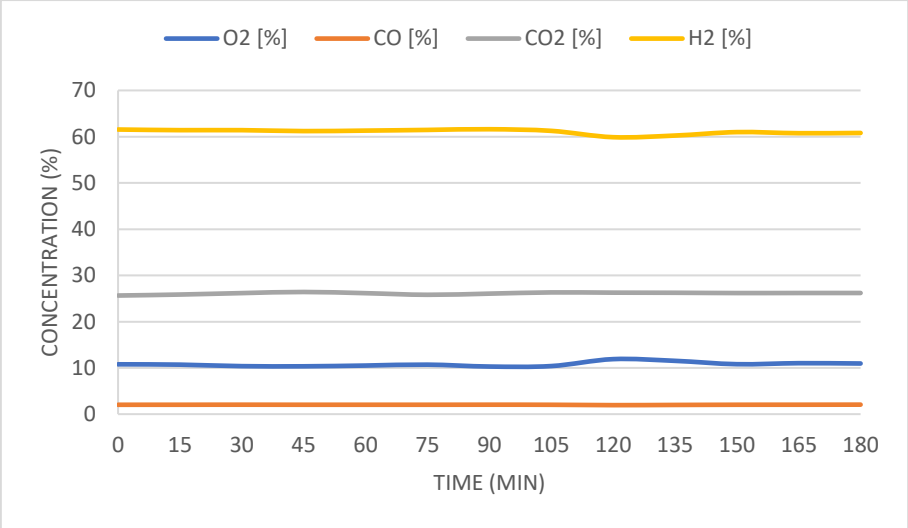

Figure 3-16: Gas outlet composition over the duration of the test, 1M NaOH, at 5 bar(g) and 90 ºC;

Among the data obtained the key important parameters to note are:

- 10.9 % of oxygen in the outlet;
- 26.2 % of carbon dioxide;
- 60.8 % of hydrogen;
- 70.67 l/h of produced gas with an energetic cost of 8.24 Wh/l.

3.2.3.8. *1M NaOH, at 5 bar(g) and 100 ºC*

Table 3-19: Conditions and collected results, 1M NaOH, at 5 bar(g) and 100 ºC;

Time (min)	T (°C)	P (bar(g))	V (V)	I (A)	O_2 (%)	CO (%)	CO_2 (%)	H_2 (%)	F (l/h)	W/F (Wh/l)
0	101.9	5.3	37.78	15.12	9.7	2.2	20.4	67.8	80.48	7.10
15	102.5	5.0	37.79	13.99	7.5	2.1	29.9	60.5	40.13	13.17
30	102.0	5.0	37.78	14.42	7.4	2.1	30.9	59.6	62.46	8.72
45	102.4	5.1	37.76	14.58	7.3	2.2	30.3	60.2	60.79	9.06
60	102.5	5.2	37.77	14.26	7.3	2.2	30.1	60.4	58.65	9.18
75	102.3	5.1	37.77	14.44	7.5	2.2	30.0	60.3	60.23	9.06
90	101.7	5.0	37.76	13.80	7.6	2.2	30.0	60.2	60.88	8.56
105	100.8	4.9	37.74	14.46	8.1	2.1	29.6	60.2	58.24	9.37
120	100.9	5.0	38.13	14.21	8.5	2.1	29.6	59.8	62.65	8.65
135	101.7	5.3	38.60	13.10	8.5	2.1	30.2	59.2	59.53	8.49
150	101.1	5.3	39.35	13.01	8.4	2.1	29.8	59.7	57.34	8.93
165	100.7	5.0	39.30	14.64	9.0	2.1	29.1	59.9	57.04	10.09
180	102.4	5.2	39.46	9.91	9.0	2.0	30.0	59.0	57.20	6.84

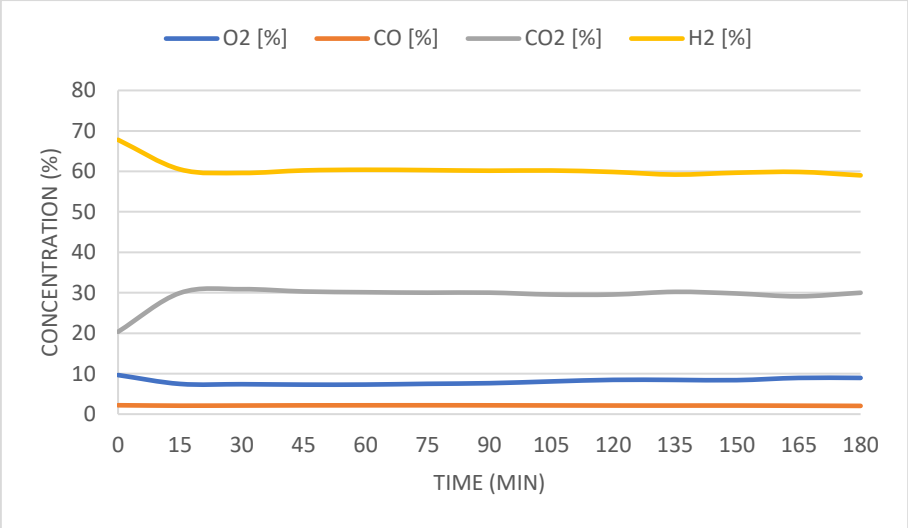

Figure 3-17: Gas outlet composition over the duration of the test, 1M NaOH, at 5 bar(g) and 100 ºC;

Among the data obtained the key important parameters to note are:

- 8.8 % of oxygen in the outlet;
- 29.6 % of carbon dioxide;
- 59.5 % of hydrogen;
- 57.19 l/h of produced gas with an energetic cost of 8.62 Wh/l.

3.2.3.9. *1M NaOH, at 5 bar(g) and 110 ºC*

Table 3-20: Conditions and collected results, 1M NaOH, at 5 bar(g) and 110 ºC;

Time (min)	T (°C)	P (bar(g))	V (V)	I (A)	O_2 (%)	CO (%)	CO_2 (%)	H_2 (%)	F (l/h)	Wh/l
0	111.9	6.1	35.85	14.50	10.0	2.3	13.2	74.4	51.18	10.16
15	111.8	5.4	35.85	14.05	7.5	2.2	26.7	63.6	55.71	9.04
30	110.6	4.9	35.85	13.93	6.6	2.1	31.6	59.7	55.66	8.97
45	111.6	5.1	35.85	14.03	6.5	2.1	30.5	60.9	56.53	8.90
60	110.5	5.3	35.85	13.88	6.2	2.2	31.4	60.2	58.35	8.53
75	110.3	4.9	35.86	13.76	5.3	2.2	31.3	61.2	65.41	7.54
90	111.4	5.5	35.87	13.72	7.6	2.1	31.7	58.7	59.67	8.25
105	111.1	5.3	35.87	13.48	6.5	2.1	31.5	59.9	58.66	8.24
120	112.2	5.2	35.87	13.38	6.1	2.1	32.0	59.8	58.59	8.19
135	111.0	5.2	35.87	13.51	6.3	2.1	31.3	60.2	63.39	7.65
150	112.2	5.4	35.86	13.87	6.3	2.1	31.7	59.9	63.83	7.79
165	110.9	3.8	35.87	13.26	5.4	2.1	33.8	58.7	61.80	7.70
180	110.7	5.4	35.86	13.80	8.3	2.1	30.0	59.7	59.73	8.28

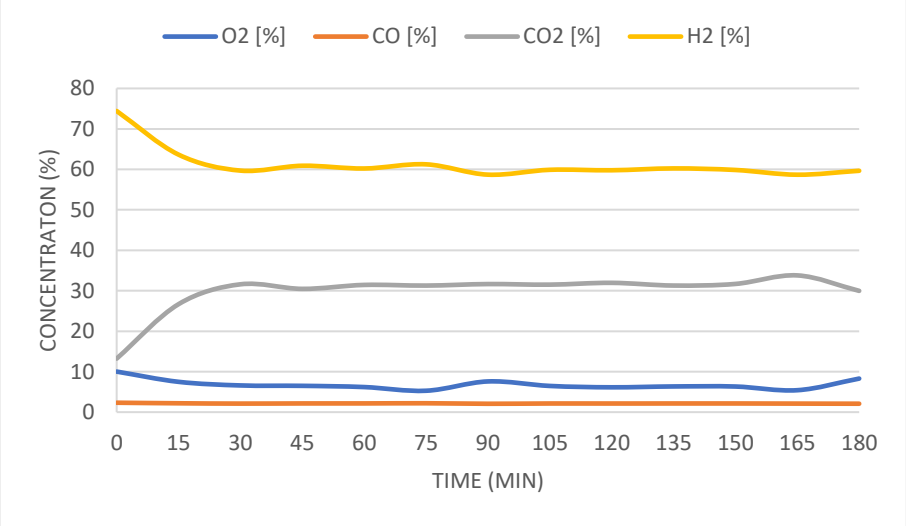

Figure 3-18: gas outlet composition over the duration of the test, 1M NaOH, at 5 bar(g) and 110 ºC;

Among the data obtained the key important parameters to note are:

- 6.7 % of oxygen in the outlet;
- 31.8 % of carbon dioxide;
- 59.4 % of hydrogen;
- 61.79 l/h of produced gas with an energetic cost of 7.92 Wh/l.

3.2.4. NaOH electrolyte performance analysis

Similarly, to the tests using KOH, O_2 concentrations have been shown to decrease at higher temperatures, with the lowest values in all cases being reported at 110 ºC. Regarding CO_2 and H_2, in general, with the particular exception of the test done at 4 bar(g), 90 ºC which exhibits the highest concentration at its pressure, CO_2 concentrations increase with temperature in most cases H_2 decreasing as a result.

While the highest gas flow and lowest energy cost were achieved at 90 ºC, the high percentages of O_2 at this temperature implies strongly a lower rate of carbon oxidation and by consequence a lower production of CO_2. For these reasons, while not offering the best performance of energy/gas produced, higher temperatures are preferable due to a more advantageous composition of the gas outlet (namely a lower O_2 content).

Although it is difficult to compare directly the production of O_2 at 5 bar(g) seeing as they were performed using a different set of sensors due to necessity, using the remaining tests it is still possible to see that, at 4 bar(g), the produced gas outlet presented a lower O_2 concentration in comparison to 3 bar(g). Furthermore, in pressures of 4 bar(g), CO_2 percentages are the lowest leading to CO_2:H_2 ratio closer to the desired value. This either implies a higher production of H_2 or most likely lower CO_2 production. All this data implies that increasing the pressure above 3 bar(g) favors the process in both lowering O_2 concentrations an achieving a better CO_2:H_2 ratio.

Table 3-21 compiles each test O_2 concentration, CO_2:H_2 ratio, produced flow as well as the energy spent per unit of gas flow produced:

Table 3-21: Compiled results of each test using NaOH electrolyte solution and respective CO_2:H_2 ratios;

Test Conditions	O_2 (%)	CO (%)	CO_2 (%)	H_2 (%)	F (l/h)	W/F (Wh/l)	CO_2:H_2 Ratio
1M NaOH; 3 bar(g); 90 ºC	9.6	2.0	27.0	61.4	61.91	8.73	1:2.27
1M NaOH; 3 bar(g); 100 ºC	4.7	2.0	34.7	58.6	52.27	9.02	1:1.69
1M NaOH; 3 bar(g); 110 ºC	3.7	2.0	35.4	58.9	54.25	9.37	1:1.66
1M NaOH; 4 bar(g); 90 ºC	5.9	1.8	26.7	65.6	54.74	9.58	1:2.45
1M NaOH; 4 bar(g); 100 ºC	4.1	1.8	25.4	68.7	46.84	10.58	1:2.71
1M NaOH; 4 bar(g); 110 ºC	3.5	1.8	26.2	68.5	44.95	11.39	1:2.61
1M NaOH; 5 bar(g); 90 ºC	10.9	2.0	26.2	60.8	70.67	8.24	1:2.32
1M NaOH; 5 bar(g); 100 ºC	8.8	2.1	29.6	59.5	57.19	8.62	1:2.01
1M NaOH; 5 bar(g); 110 ºC	6.7	2.1	31.8	59.4	61.79	7.92	1:1.87

From this group of tests, the conditions that resulted in the lowest O_2 content were 4 bar(g) and 110 ºC with 3.5 % in the gas outlet, although results at 5 bar(g)s are inconclusive due to the use of a different set of sensors. On the other hand, at 4 bar(g), 100 ºC CO_2:H_2 ratio was the closest to the 1:4 ideal for methanation.

Besides its direct effects on performance, the use of NaOH as the electrolyte is advantageous for multiple reasons. In comparison to KOH, NaOH is less" aggressive" and less corrosive, causing less strain on the system and increasing the graphite disks lifespan. As a result, it requires less maintenance and decreases the costs associated with the process. On top of that, after working on each test with both electrolytes, little by little it became clear that when using NaOH it was easier to control and maintain the process under the desired condition, even at higher pressures that in the case of KOH which had showed to be harder to work with. Although the reasons for this phenomenon are uncertain, it may be a result of KOH smaller particle size or possible formation of unknown salt byproducts.

3.2.5. KOH and NaOH electrolyte comparison

For the comparison of each electrolyte performance, and considering the objective of producing syngas to be later used in the production of methane, the following factors need to be taken in consideration:

- Gas outlet O_2 content;
- CO_2:H_2 ratio;
- Flow produced/ energy spent per unit gas flow;
- Strain put on the system/ease to work.

3.2.5.1. Gas outlet O_2 content:

To better compare the O_2 content generated by the two different electrolyte solutions, Figure 3-19 organizes each pair of tests (NaOH and KOH) based on their operational conditions:

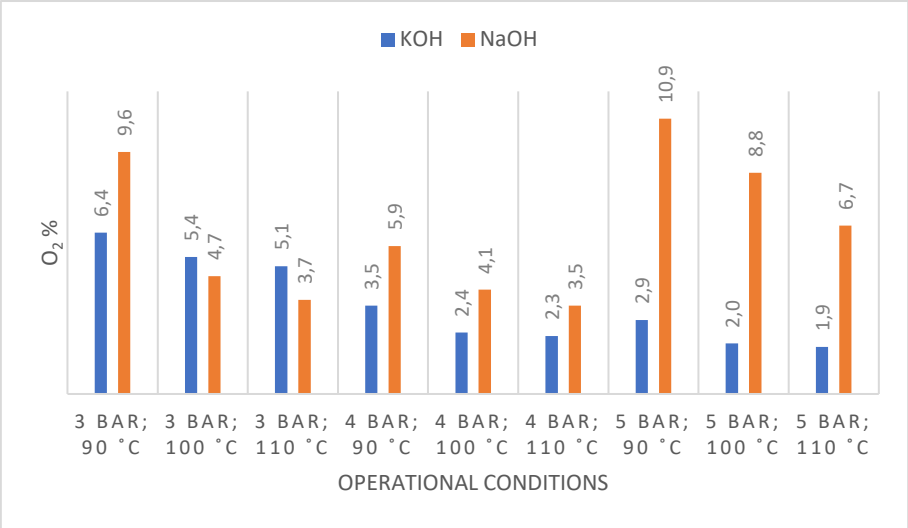

Figure 3-19: NaOH and KOH tests O_2 content comparison;

(As previously referred, since the NaOH tests at 5 bar(g) were executed using a different set of sensors, their values of O_2 content in the gas outlet vary significantly from the rest and as such this was taken into consideration when comparing its results with the ones obtained using KOH.)

With the exception of the test at 3 bar(g) with temperatures of 100 and 110 ºC, the direct comparison at the same conditions shows significantly lower O_2 concentration when using the 1M KOH electrolyte solution with the lowest value appearing in the test done at 5 bar(g) and 100 ºC. As such, in terms of lowering O_2 production, KOH as the advantage.

As a way to facilitate the comparison, Figure 3-20 display each test's CO_2:H_2 ratio paired based on their operational conditions:

Figure 3-20: NaOH and KOH tests CO_2:H_2 ratio comparison;

Excluding the tests at 5 bar(g) and 100 and 110 ºC (which could be a result of using a different set of sensors) in most cases the use of a NaOH electrolyte solution led to lower CO_2:H_2 ratios. While still far from the ideal 1:4 (or 4 moles of H_2 for each one of CO_2) when opposed to KOH, NaOH produces syngas better suited to be used as feedstock in methanation.

3.2.5.2. Flow produced/ Energy spent per unit gas flow:

Since the continual wear of the graphite disks inside the stack undermines the direct comparison of energy expenditure between tests, a comparison of produced gas flow was conjugated to better evaluate each electrolyte performance. Figure 3-21 and Figure 3-22 show flow productions and energy expenditures respectively for all tests organized by their operational conditions.

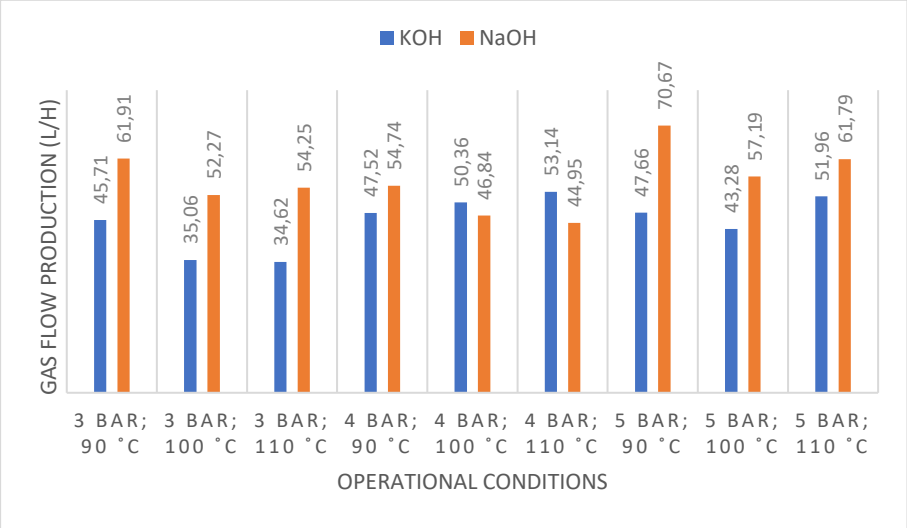

Figure 3-21: NaOH and KOH tests produced gas flow comparison;

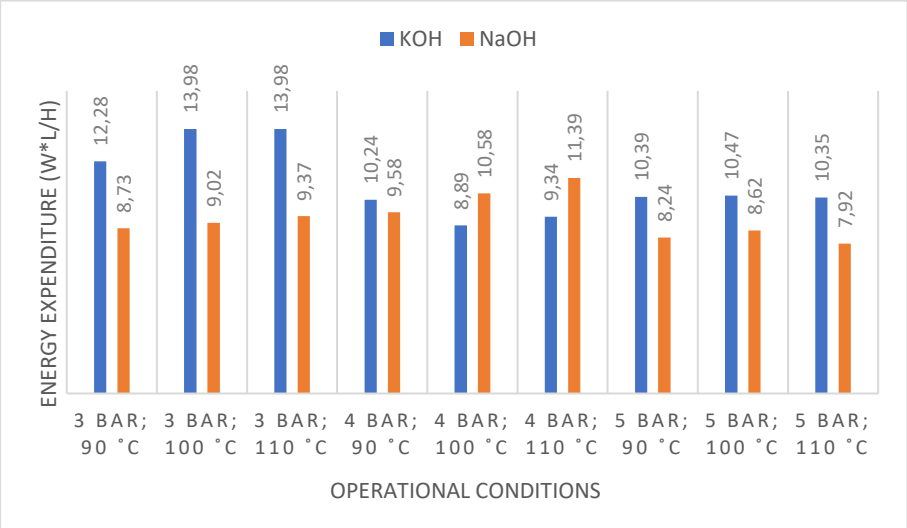

Figure 3-22: NaOH and KOH tests energy expenditure comparison;

Focusing on the flow produced, in general, with the exception of tests at 4 bar(g) with 100 and 110 ºC, the use of NaOH electrolyte resulted in a considerably higher syngas production with the greatest difference appearing at 3 bar(g) and 110 ºC with a 56.71 % increase. On the other hand, the analysis in terms of energy expenditure reveals once again the NaOH electrolyte as the favored one due to noticeable decrease in energy consumption when opposed to KOH. Once again, the outliers were at 4 bar(g) with 100 and 110 ºC, possibly as a result of significant graphite disks wear during the execution of the NaOH tests.

3.2.5.3. Strain put on the system/ease to work:

Although it was not possible to quantify or necessarily display in the form of measurable data, through carrying out each test, the two electrolyte solutions presented noticeable differences in terms of "ease to work with", strain and resultant damage placed on the system and other particularities that while not directly connected with direct performance may have a major impact on the applicability of the electrolytes when on a larger or industrial scale.

As it was formerly mentioned, although KOH showed promising results when it comes to reducing O_2 percentage in the gas outlet, throughout all the experimental work, it proved itself harder to work with in comparison to NaOH, mainly in terms of strain placed on the system (resulting in damaged that required the fix or substitution of important components) and the reported acceleration of the wear down experienced in the graphite disks. Once again, while this doesn´t affect directly the performance of the system, it has further ramifications that degrade indirectly its applicability beyond a prototypal scale, seen as the increase in the need for maintenance results in lower operation time and an obvious increase in operational costs. For these reasons, due to being easier to work with, NaOH is the preferable one.

3.2.5.4. Choice New parameters for the subsequent set of tests:

The first set of tests and analysis of the results provided groundwork for the selection of a narrower range of parameters based on the conditions that offered the best performance to be used for the second set. This liquified biomass samples were introduced by diluting in the electrolyte and serve as a secondary source of carbon. In similarity to the first set, the main objective was the production of synthesis gas intended for future use in green methane production.

This new range of conditions included, only the use of NaOH electrolyte (with the same concentration as the previous set of tests), chosen due to being easier to work with and offering a better performance in terms of $CO_2 : H_2$ ratio and gas production/energy expenditure solution, and a new range for pressure and temperature of 4-5 bar(g) and 100-110 ºC respectively, also selected due to in the first set reducing O_2 content and favoring $CO_2 : H_2$ ratio.

3.3. Tests performed with the addition of liquified biomass

A second set of tests was conducted with the already specified new range of conditions, now with the addition of liquified biomass to test its viability as an alternative source of carbon for syngas production. In total, as previous referred in the reagent's description. two different biomass samples were used. One produced and supplied by Instituto Superior Técnico from pieces of acacia. and the other supplied by Secil. labelled Energreen (with uncleared Composition). Furthermore. two different biomass concentrations were tested, specifically, 2.5 and 5 % (m/m). meaning a total of 16 tests using liquified biomass.

The Table 3-22 below shows the specific parameters established for each test in this second set:

Table 3-22:Test conditions with addition of liquified biomass;

Test	Liquified Biomass sample	Conc. (%)	Relative Pressure (bar(g))	Temperature (ºC)
19	Acacia	2.5	4	100
20	Acacia	2.5	4	110
21	Acacia	2.5	5	100
22	Acacia	2.5	5	110
23	Acacia	5	4	100
24	Acacia	5	4	110
25	Acacia	5	5	100
26	Acacia	5	5	110
27	Energreen	2.5	4	100
28	Energreen	2.5	4	110
29	Energreen	2.5	5	100
30	Energreen	2.5	5	110
31	Energreen	5	4	100
32	Energreen	5	4	110
33	Energreen	5	5	100
34	Energreen	5	5	110

3.4. Tests and results

3.4.1. Acacia Biomass

3.4.1.1. 2.5 % Acacia biomass at 4 bar and 100 ºC

Table 3-23: Conditions and collected results, 2.5 % Acacia biomass, at 4 bar and 100 ºC;

Time (min)	T (°C)	P (bar)	V (V)	I (A)	O_2 (%)	CO (%)	CO_2 (%)	H_2 (%)	F (l/h)	W/F (Wh/l)
0	100.0	4.3	33.20	14.73	3.3	2.0	31.5	63.2	64.79	7.55
15	100.3	4.6	33.19	14.88	3.5	2.0	35.0	59.5	65.49	7.54
30	98.8	4.6	33.21	14.20	3.5	2.0	34.0	60.5	69.19	6.82
45	98.7	4.6	33.19	14.28	3.5	2.0	34.0	60.5	65.06	7.28
60	100.5	4.1	33.19	14.46	3.6	2.0	35.0	59.4	65.65	7.31
75	98.9	3.9	33.20	13.93	3.7	2.0	33.7	60.6	66.63	6.94
90	99.4	4.0	33.18	14.24	3.8	2.0	34.0	60.2	63.57	7.43
105	99.3	4.0	33.18	14.43	3.9	2.0	34.6	59.5	68.01	7.04
120	99.5	4.0	33.18	14.06	3.8	2.0	34.8	59.4	67.16	6.95
135	100.6	4.1	33.17	14.57	3.8	2.0	34.2	60.0	65.41	7.39
150	98.9	4.0	33.18	14.26	3.9	2.0	34.3	59.8	66.83	7.08
165	98.3	4.0	33.18	14.34	3.9	2.0	34.7	59.4	68.05	6.99
180	98.4	4.0	33.18	14.47	3.9	2.0	34.6	59.5	67.71	7.09

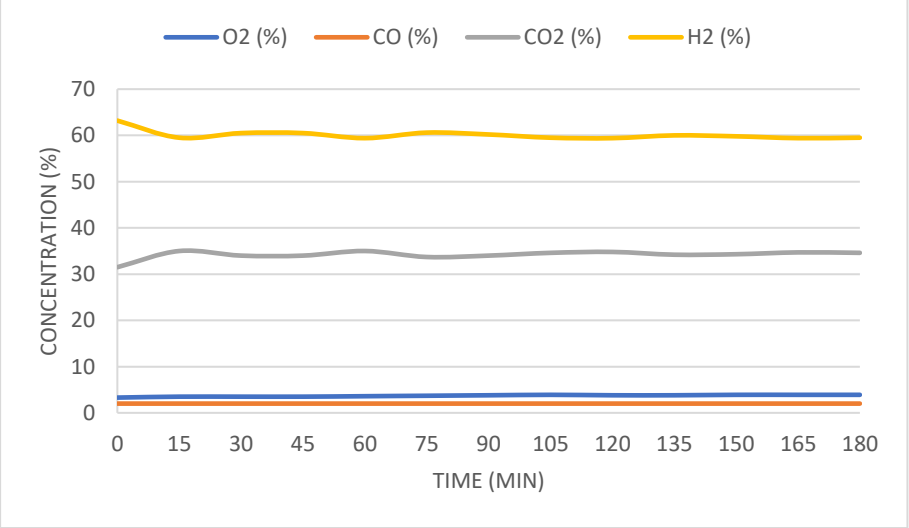

Figure 3-23: Gas outlet composition over the duration of the test, 2.5 % Acacia biomass, at 4 bar and 100 ºC;

Among the data obtained the key important parameters to note are:

- 3.9 % of oxygen in the outlet;
- 34.5 % of carbon dioxide;
- 59.6 % of hydrogen;
- 67.53 l/h of produced gas with an energetic cost of 7.05 Wh/l.

3.4.1.2. 2.5 % Acacia biomass at 4 bar and 110 ºC

Table 3-24: Conditions and collected results, 2.5 % Acacia biomass, at 4 bar and 110 ºC;

Time (min)	T (°C)	P (bar)	V (V)	I (A)	O_2 (%)	CO (%)	CO_2 (%)	H_2 (%)	F (l/h)	W/F (Wh/l)
0	107.9	4.3	30.62	14.97	2.4	2.0	41.1	54.5	70.77	6.48
15	110.1	4.4	30.61	15.31	2.3	2.0	40.5	55.2	71.67	6.54
30	109.5	4.3	30.61	14.86	2.3	2.0	40.7	55.0	68.48	6.64
45	111.3	4.3	30.61	14.98	2.3	2.0	41.4	54.3	68.10	6.73
60	110.5	4.2	30.60	14.60	2.3	2.0	41.2	54.5	68.27	6.54
75	111.6	4.2	30.59	14.40	2.3	2.0	42.5	53.2	67.88	6.49
90	110.6	4.3	30.61	14.45	2.3	2.0	42.4	53.3	69.36	6.38
105	109.7	4.4	30.63	13.87	2.3	2.0	42.1	53.6	63.01	6.74
120	110.8	4.1	30.61	14.10	2.2	2.0	43.7	52.1	66.67	6.47
135	108.9	4.0	30.60	13.74	2.2	2.0	42.6	53.2	62.32	6.75
150	110.8	4.2	30.60	13.80	2.2	2.0	42.8	53.0	64.83	6.51
165	111.4	4.4	30.60	13.92	2.1	2.0	42.3	53.6	61.12	6.97
180	110.6	4.5	30.60	13.63	2.1	2.0	42.7	53.2	62.83	6.64

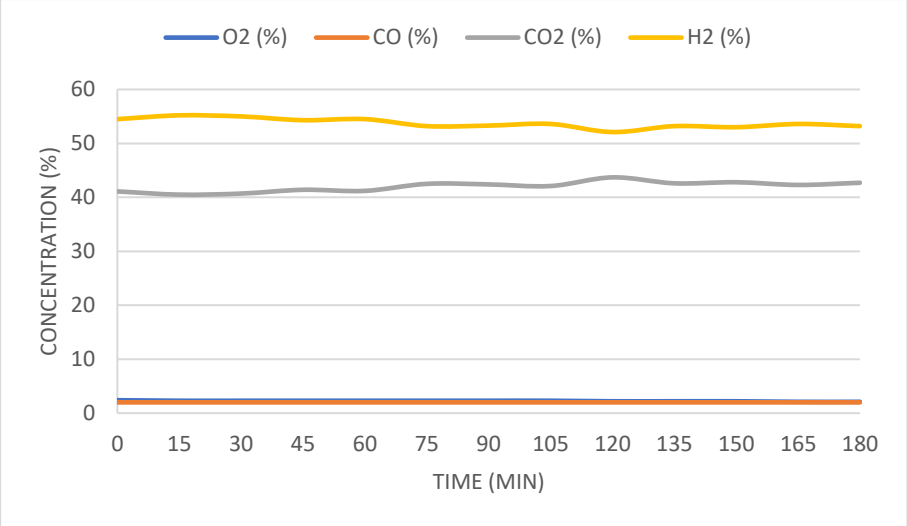

Figure 3-24: Gas outlet composition over the duration of the test, 2.5 % Acacia biomass, at 4 bar and 110 ºC;

Among the data obtained the key important parameters to note are:

- 2.1 % of oxygen in the outlet;
- 42.6 % of carbon dioxide;
- 53.3 % of hydrogen;
- 62.92 l/h of produced gas with an energetic cost of 6.71 Wh/l.

3.4.1.3. 2.5 % Acacia biomass at 5 bar and 100 ºC

Table 3-25: Conditions and collected results, 2.5 % Acacia biomass, at 5 bar and 100 ºC;

Time (min)	T (°C)	P (bar)	V (V)	I (A)	O_2 (%)	CO (%)	CO_2 (%)	H_2 (%)	F (l/h)	W/F (Wh/l)
0	101.0	5.3	33.05	14.89	4.6	2.0	36.8	56.6	62.57	7.86
15	99.8	5.3	33.05	14.51	4.4	2.0	39.5	54.1	64.36	7.45
30	100.3	5.3	33.05	14.37	4.3	2.0	40.7	53.0	64.67	7.34
45	100.0	5.4	33.07	14.14	4.2	2.0	41.9	51.9	63.79	7.33
60	100.9	5.1	33.07	14.25	4.2	2.0	42.8	51.0	64.67	7.29
75	99.9	5.0	33.05	14.08	4.1	2.0	43.2	50.7	66.22	7.03
90	99.7	4.9	33.07	13.57	4.0	2.0	43.2	50.8	64.02	7.01
105	99.9	4.9	33.07	13.65	4.0	2.0	43.5	50.5	61.96	7.29
120	99.8	4.8	33.07	13.54	3.9	2.0	43.1	51.0	61.26	7.31
135	100.1	4.8	33.05	13.37	3.8	2.0	44.9	49.3	60.13	7.35
150	99.8	4.8	33.04	13.26	3.8	2.0	45.5	48.7	62.00	7.07
165	100.4	4.8	33.03	13.54	3.8	2.0	45.4	48.8	59.60	7.50
180	98.9	4.7	33.05	12.91	3.7	2.0	45.2	49.1	57.42	7.43

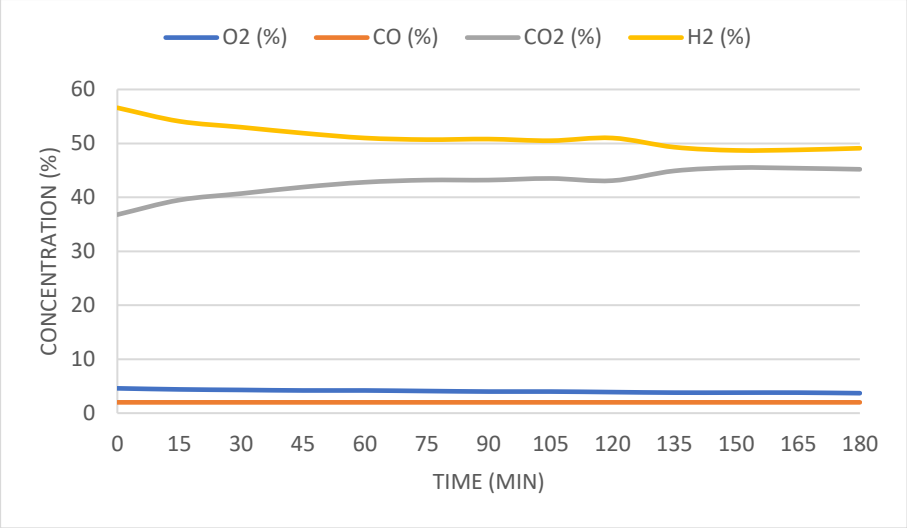

Figure 3-25: Gas outlet composition over the duration of the test, 2.5 % Acacia biomass, at 5 bar and 100 ºC;

Among the data obtained the key important parameters to note are:

- 3.8 % of oxygen in the outlet;
- 45.4 % of carbon dioxide;
- 48.9 % of hydrogen;
- 59.67 l/h of produced gas with an energetic cost of 7.33 Wh/l.

3.4.1.4. 2.5 % Acacia biomass at 5 bar and 110 ºC

Table 3-26: Conditions and collected results, 2.5 % Acacia biomass, at 5 bar and 110 ºC;

Time (min)	T (°C)	P (bar)	V (V)	I (A)	O_2 (%)	CO (%)	CO_2 (%)	H_2 (%)	F (l/h)	W/F (Wh/l)
0	111.9	4.8	31.74	16.78	12.9	2.0	26.5	58.6	69.32	7.68
15	111.1	5.3	31.74	15.80	9.9	2.0	44.7	43.4	72.78	6.89
30	108.6	4.3	30.82	13.46	6.4	2.0	54.9	36.7	65.26	6.36
45	111.4	4.8	32.08	15.50	5.4	2.0	55.5	37.1	73.87	6.73
60	112.0	5.6	32.07	15.89	4.9	2.0	54.6	38.5	72.48	7.03
75	110.3	5.1	32.08	15.19	4.5	2.0	54.8	38.7	72.73	6.70
90	109.1	5.0	32.09	14.83	4.2	2.0	53.2	40.6	68.57	6.94
105	112.4	5.4	32.07	15.65	3.9	2.0	54.1	40.0	71.90	6.98
120	111.8	5.4	32.08	14.97	3.7	2.0	53.6	40.7	73.62	6.52
135	110.2	5.2	32.09	14.55	3.6	2.0	54.5	39.9	66.18	7.06
150	110.0	5.3	32.08	14.12	3.5	2.0	54.0	40.5	66.06	6.86
165	109.5	5.5	32.09	13.99	3.4	2.0	52.4	42.2	62.72	7.16
180	109.5	5.6	32.09	13.84	3.4	2.0	53.9	40.7	59.15	7.51

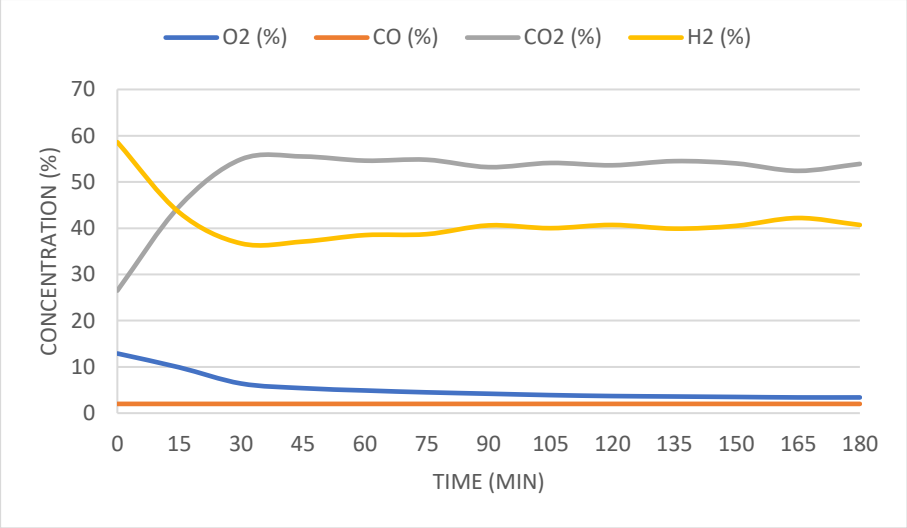

Figure 3-26: Gas outlet composition over the duration of the test, 2.5 % Acacia biomass, at 5 bar and 110 ºC;

Among the data obtained the key important parameters to note are:

- 3.4 of oxygen in the outlet;
- 53.4 % of carbon dioxide;
- 41.1 % of hydrogen;
- 62.64 l/h of produced gas with an energetic cost of 7.17 Wh/l.

3.4.1.5. 5 % Acacia at 4 bar and 100 ºC

Table 3-27: Conditions and collected results, 5 % Acacia biomass, at 4 bar and 100 ºC;

Time (min)	T (°C)	P (bar)	V (V)	I (A)	O_2 (%)	CO (%)	CO_2 (%)	H_2 (%)	F (l/h)	W/F (Wh/l)
0	100.9	4.6	34.52	13.69	4.4	2.0	35.5	58.1	58.89	8.03
15	100.8	4.6	34.93	13.67	3.8	2.0	53.1	41.1	60.98	7.83
30	103.1	4.4	36.56	15.96	3.6	2.0	54.8	39.6	75.10	7.77
45	104.5	4.2	36.56	15.92	3.6	2.0	54.8	39.6	76.87	7.57
60	105.7	3.1	36.57	15.68	3.5	2.0	54.8	39.7	78.49	7.31
75	106.3	3.8	36.57	15.99	3.5	2.0	54.8	39.7	71.62	8.16
90	107.1	3.9	36.57	15.62	3.4	2.0	54.9	39.7	71.95	7.94
105	103.8	4.0	35.68	14.78	3.3	2.0	54.8	39.9	70.77	7.45
120	105.9	4.3	35.68	14.51	3.2	2.0	55.0	39.8	64.59	8.02
135	105.6	4.6	35.67	14.17	3.3	2.0	55.1	39.6	66.22	7.63
150	105.1	3.1	35.68	14.15	3.4	2.0	54.8	39.8	65.41	7.72
165	105.3	3.8	35.67	14.22	3.3	2.0	54.8	39.9	62.07	8.17
180	105.2	4.3	35.68	13.92	3.3	2.0	55.2	39.5	62.14	7.99

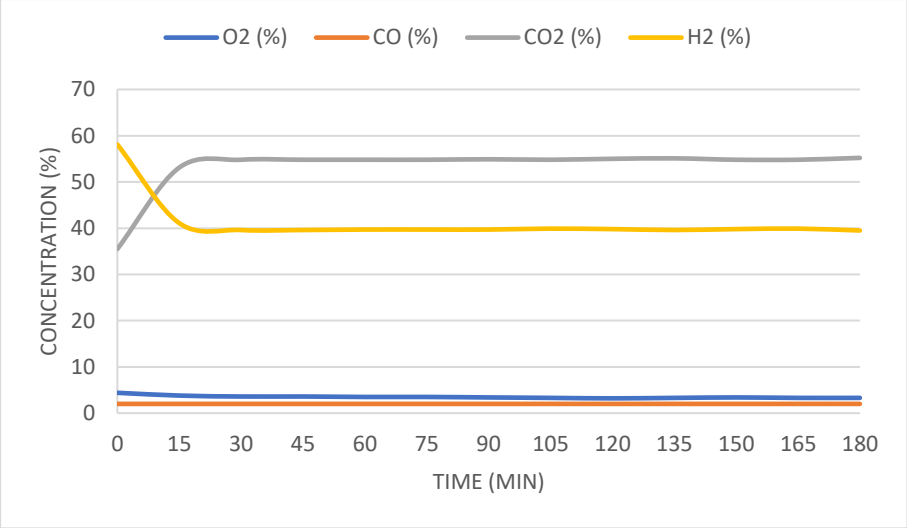

Figure 3-27: Gas outlet composition over the duration of the test, 5 % Acacia biomass, at 4 bar and 100 ºC;

Among the data obtained the key important parameters to note are:

- 3.3 % of oxygen in the outlet;
- 39.7 % of carbon dioxide;
- 54.9 % of hydrogen;
- 63.21 l/h of produced gas with an energetic cost of 7.96 Wh/l.

3.4.1.6. 5 % Acacia at 4 bar and 110 ºC

Table 3-28: Conditions and collected results, 5 % Acacia biomass, at 4 bar and 110 ºC;

Time (min)	T (°C)	P (bar)	V (V)	I (A)	O_2 (%)	CO (%)	CO_2 (%)	H_2 (%)	F (l/h)	W/F (Wh/l)
0	110.0	3.9	34.80	13.89	4.6	2.0	53.5	39.9	65.61	7.37
15	109.9	3.8	34.79	13.62	3.9	2.0	55.2	38.9	61.05	7.76
30	110.2	4.0	34.81	12.59	3.5	2.0	55.2	39.3	59.11	7.41
45	108.0	4.2	34.81	12.96	3.4	2.0	55.1	39.5	63.91	7.06
60	109.6	3.2	36.82	14.62	3.4	2.0	55.5	39.1	75.26	7.15
75	110.6	4.2	36.82	14.48	3.2	2.0	55.6	39.2	72.05	7.40
90	110.4	4.1	36.81	14.71	3.2	2.0	55.1	39.7	75.37	7.18
105	111.0	4.3	36.81	14.65	3.1	2.0	55.1	39.8	77.75	6.94
120	109.7	4.4	36.81	14.95	3.1	2.0	55.0	39.9	77.03	7.14
135	111.1	4.0	36.80	15.45	3.1	2.0	55.1	39.8	69.99	8.12
150	111.6	4.3	36.81	15.67	3.1	2.0	55.0	39.9	71.95	8.02
165	112.0	4.5	36.83	15.43	3.1	2.0	55.1	39.8	70.73	8.03
180	112.0	4.8	36.62	15.49	3.1	2.0	55.0	39.9	71.38	7.95

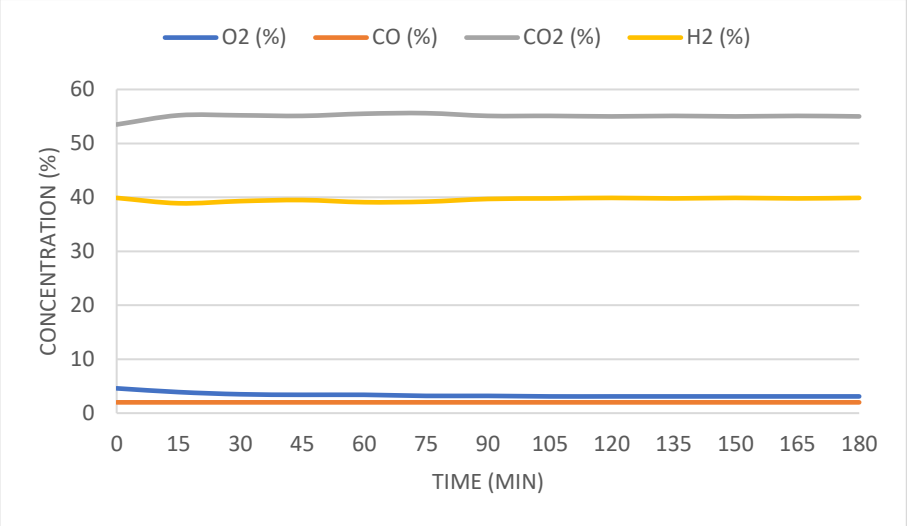

Figure 3-28: Gas outlet composition over the duration of the test, 5 % Acacia biomass, at 4 bar and 110 ºC;

Among the data obtained the key important parameters to note are:

- 3.1 % of oxygen in the outlet;
- 55.0 % of carbon dioxide;
- 39.9 % of hydrogen;
- 71.35 l/h of produced gas with an energetic cost of 8.00 Wh/l.

3.4.1.7. 5 % Acacia biomass at 5 bar and 100 ºC

Table 3-29: Conditions and collected results, 5 % Acacia biomass, at 5 bar and 100 ºC;

Time (min)	T (°C)	P (bar)	V (V)	I (A)	O_2 (%)	CO (%)	CO_2 (%)	H_2 (%)	F (l/h)	W/F (Wh/l)
0	103.2	4.7	37.75	15.24	5.7	2.0	28.4	63.9	59.57	9.66
15	103.1	5.4	36.61	13.78	3.8	2.0	46.7	47.5	54.88	9.19
30	102.9	5.3	36.61	13.64	3.3	2.0	52.6	42.1	62.68	7.97
45	102.7	4.8	36.62	13.42	3.2	2.0	54.9	39.9	58.10	8.46
60	99.5	4.9	38.13	14.38	3.4	2.0	52.8	41.8	59.37	9.23
75	99.7	5.4	38.11	15.36	3.5	2.0	52.9	41.6	64.17	9.12
90	97.8	5.1	36.81	13.63	3.4	2.0	54.5	40.1	58.44	8.58
105	97.9	5.5	37.78	14.65	3.7	2.0	53.0	41.3	65.22	8.49
120	102.8	5.3	37.75	15.70	3.5	2.0	54.8	39.7	69.99	8.47
135	100.0	5.1	37.77	15.18	3.8	2.0	54.5	39.7	67.16	8.54
150	99.6	5.0	37.77	14.74	3.9	2.0	54.1	40.0	62.94	8.85
165	99.5	5.1	38.45	15.26	4.1	2.0	53.4	40.5	66.34	8.84
180	99.3	4.9	38.00	14.57	4.1	2.0	54.0	39.9	62.46	8.86

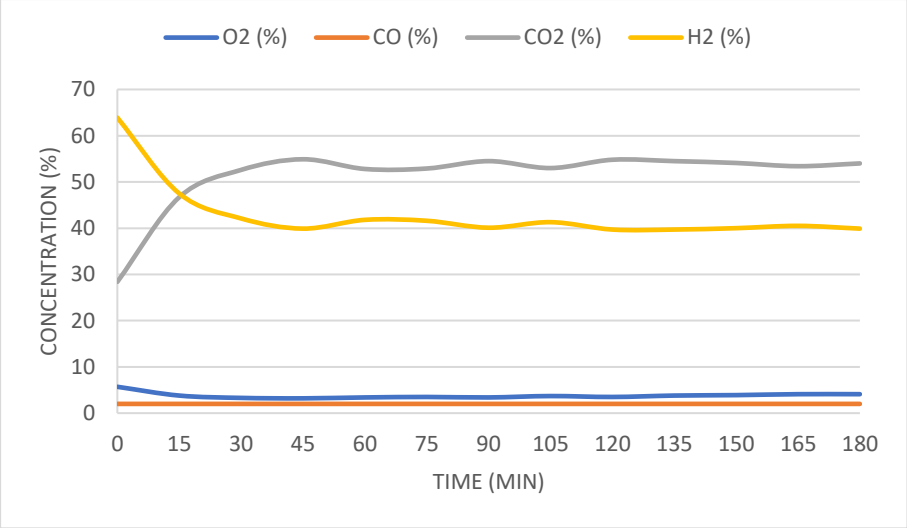

Figure 3-29: Gas outlet composition over the duration of the test, 5 % Acacia biomass, at 5 bar and 100 ºC;

Among the data obtained the key important parameters to note are:

- 4.0 % of oxygen in the outlet;
- 53.8 % of carbon dioxide;
- 40.1 % of hydrogen;
- 63.91 l/h of produced gas with an energetic cost of 8.85 Wh/l.

3.4.1.8. 5 % Acacia biomass at 5 bar and 110 ºC

Table 3-30: Conditions and collected results, 5 % Acacia biomass, at 5 bar and 110 ºC;

Time (min)	T (°C)	P (bar)	V (V)	I (A)	O_2 (%)	CO (%)	CO_2 (%)	H_2 (%)	F (l/h)	W/F (Wh/l)
0	109.5	4.8	37.71	15.33	6.8	2.0	15.5	75.7	65.93	8.77
15	111.3	4.6	37.69	14.80	3.6	2.0	38.7	55.7	58.95	9.46
30	112.1	4.9	39.25	15.80	3.3	2.0	42.9	51.8	68.05	9.11
45	111.9	5.2	39.23	16.16	3.3	2.0	43.2	51.5	67.84	9.34
60	111.5	5.2	39.24	16.07	3.3	2.0	43.5	51.2	70.54	8.94
75	111.3	5.0	39.20	16.51	3.3	2.0	43.2	51.5	72.24	8.96
90	112.7	5.1	39.16	17.32	3.4	2.0	42.9	51.7	76.16	8.91
105	111.6	4.6	37.23	15.12	3.2	2.0	45.5	49.3	58.60	9.61
120	110.1	5.1	37.23	14.84	3.2	2.0	44.0	50.8	63.12	8.75
135	112.4	5.3	37.22	14.96	3.2	2.0	44.5	50.3	63.08	8.83
150	111.1	5.0	37.22	14.68	3.2	2.0	44.0	50.8	62.97	8.68
165	111.6	4.9	37.20	14.73	3.2	2.0	44.7	50.1	59.15	9.26
180	111.0	4.8	37.16	13.89	3.2	2.0	44.8	50.0	59.08	8.74

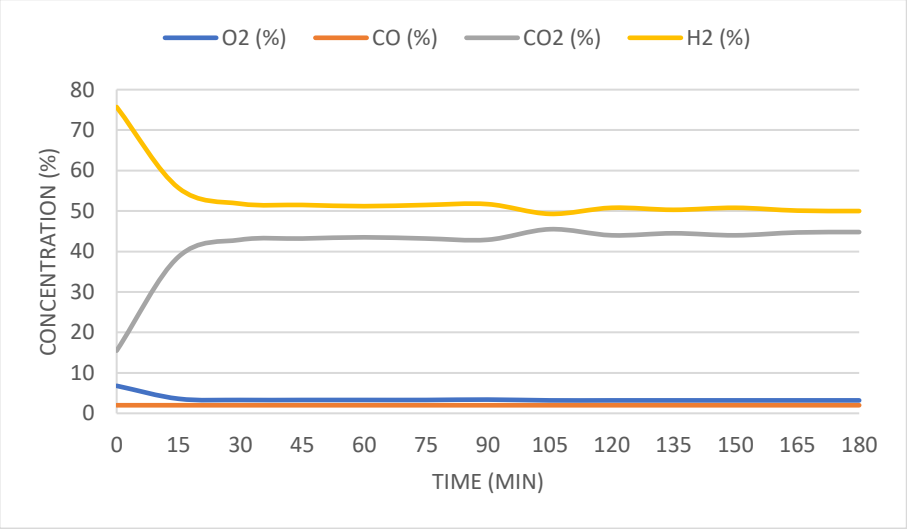

Figure 3-30: Gas outlet composition over the duration of the test, 5 % Acacia biomass, at 5 bar and 110 ºC;

Among the data obtained the key important parameters to note are:

- 3.2 % of oxygen in the outlet;
- 44.5 % of carbon dioxide;
- 50.3 % of hydrogen;
- 60.40 l/h of produced gas with an energetic cost of 8.89 Wh/l.

3.4.2. Liquified Acacia performance

A compilation of the final results of each test using liquified Acacia biomass (average of the three last collections in stationary state) is showed in Table 3-31 to facilitate the discussion of results

Table 3-31: Compiled results of each test with the addition of liquified Acacia biomass and respective CO2:H2 ratios;

Test Conditions	O_2 (%)	CO (%)	CO_2 (%)	H_2 (%)	F (l/h)	W/F (Wh/l)	CO_2:H_2 Ratio
4 bars 100 ºC 1M NaOH 2.5 %Acacia	3.9	2.0	34.5	59.6	67.53	7.05	1.72
4 bars 110 ºC 1M NaOH 2.5 %Acacia	2.1	2.0	42.6	53.3	62.92	6.71	1.25
5 bars 100 ºC 1M NaOH 2.5 %Acacia	3.8	2.0	45.4	48.9	59.67	7.33	1.08
5 bars 110 ºC 1M NaOH 2.5 %Acacia	3.4	2.0	53.4	41.1	62.64	7.17	0.77
4 bars 100 ºC 1M NaOH 5 %Acacia	3.3	2.0	54.9	39.7	63.21	7.96	0.72
4 bars 110 ºC 1M NaOH 5 %Acacia	3.1	2.0	55.0	39.9	71.35	8.00	0.72
5 bars 100 ºC 1M NaOH 5 %Acacia	4.0	2.0	53.8	40.1	63.91	8.85	0.75
5 bars 110 ºC 1M NaOH 5 %Acacia	3.2	2.0	44.5	50.3	60.40	8.89	1.13

To better evaluate how the addition of liquified biomass affects performance, each test results were compared directly to their counter parts with no biomass addition. Furthermore, produced gas flow and energy expenditure were considered together to avoid the influence that graphite disk wear may have on the analysis.

As Figure 3-31 displays, the addition of liquified biomass shows promising results in reducing the O_2 content in the gas outlet, with the lowest concentration being obtained with the addition of 2.5 % of liquified Acacia biomass at 4 bar(g), 110 ºC.

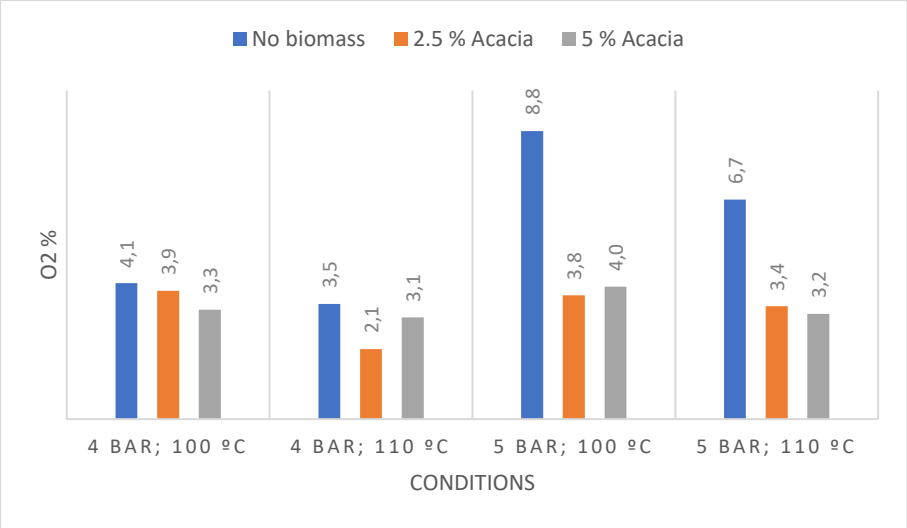

Figure 3-31: Gas outlet O_2 content comparison for the Acacia biomass;

Between the two tested concentrations, it is still inconclusive which one offers the better performance in reducing O_2 concentration with only the tests at 4 bar(g) presenting

striking differences with 0.6 and 1.0 % respectably. On the other hand, at 5 bar(g) the percentages obtained for both biomass dilutions were relatively closed to each other (with a difference of 0.2 % in both cases), although just as at 4 bar(g)s the increase in temperature caused a reduction in O_2 concentration for both biomass dilutions.

Through the comparison of units of H_2 per 1 unit of CO_2 (where the CO_2: H_2 ratio corresponds to 1: units of H_2 per unit of CO_2) presented in Figure 3-32 it is possible to conclude that the addition of biomass increase the production of CO_2. This was expected considering the simultaneous decrease in O_2 content in the produced syngas which is consumed to produce CO_2.

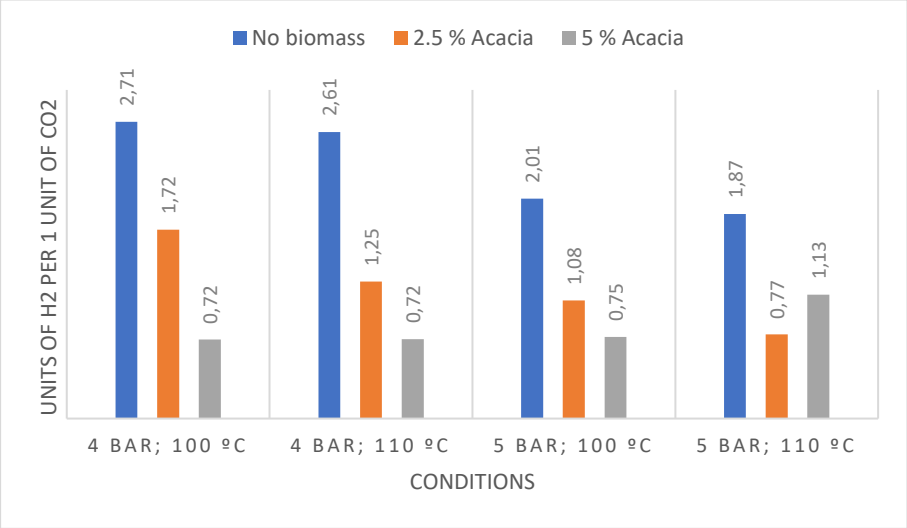

Figure 3-32: Units of H_2 per 1 unit of CO_2/CO_2: H_2 ratios, content comparison for the Acacia biomass;

While the increase in CO_2 production induces a less desirable ratio, it is still acceptable as a necessary consequence of reducing O_2 content. The removal of excess CO_2 or even, possibly, addition of more H_2 is significantly easier in comparison to removing O_2 content within the syngas mixture. In other words, although CO_2: H_2 ratios may appear less optimal with the addition of liquified biomass, they're counterbalanced by the associated lower O_2 fraction (Han et al., 2014).

Figure 3-33 presents both gas flow production (a) and energy expenditure (b) of each test to facilitate direct comparison.

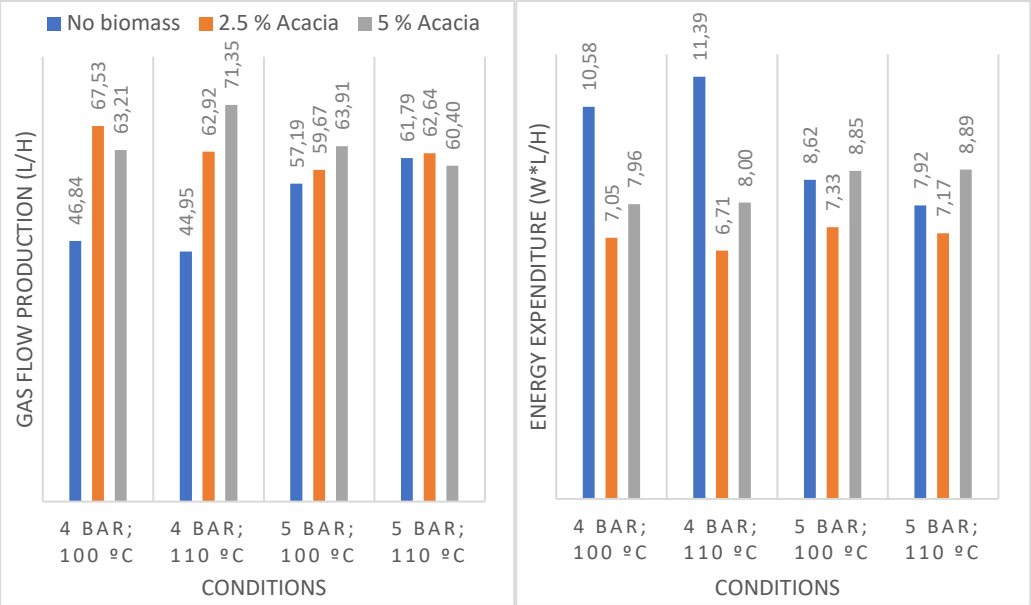

Figure 3-33: Gas flow production(a) and energy expenditure(b) comparison for the Acacia biomass;

In most cases, with the only exception being at 5 bar(g), 110 ºC (in which only the 5 % mixture performed below the test without addition), the use of liquified biomass induced the production of higher syngas flows. Additionally, even when taking into account different degrees of wear in the graphite disks throughout the tests, the 2.5 % solution had consistently the lowest energy expenditure while producing higher flowrates in comparison to the tests without the addition of biomass.

Overall, despite the less preferable CO_2: H_2 ratios (that can be adjusted postproduction as previously referred), the addition of liquified biomass improved performance by lowering the syngas O_2 content, increasing production flowrate, and, in the case of the 2.5 % solution, also lowering the energy expenditure. Between the two tested concentrations, arguably the 2.5 % mixture offered the best performance by having consistently the lowest energy expenditure while producing a more optimal CO_2: H_2 ratios than the same tests with 5 % liquified biomass.

3.4.3. Energreen Biomass

3.4.3.1. 2.5 % Energreen biomass at 4 bar and 100 ºC

Table 3-32: Conditions and collected results, 2.5 % Energreen biomass, at 4 bar and 100 ºC;

Time (min)	T (°C)	P (bar)	V (V)	I (A)	O_2 (%)	CO (%)	CO_2 (%)	H_2 (%)	F (l/h)	W/F (Wh/l)
0	95.9	4.2	39.93	13.30	7.3	2.0	40.0	50.7	45.82	11.59
15	102.4	4.3	41.35	15.77	6.8	2.0	42.5	48.7	68.70	9.49
30	102.4	3.6	38.95	13.73	6.1	2.0	45.7	46.2	59.41	9.00
45	102.8	3.4	40.31	14.61	6.1	2.0	45.3	46.6	64.52	9.13
60	103.7	3.1	40.32	15.21	6.0	2.0	45.4	46.6	67.37	9.10
75	102.5	3.4	40.76	14.54	5.8	2.0	43.3	48.9	60.47	9.80
90	98.8	3.7	40.78	13.92	6.2	2.0	42.4	49.4	57.75	9.83
105	99.1	3.5	41.83	14.79	6.9	2.0	41.8	49.3	62.39	9.92
120	100.0	4.4	41.82	14.96	6.2	2.0	41.0	50.8	60.71	10.31
135	100.3	4.0	41.82	14.92	6.1	2.0	41.8	50.1	61.50	10.15
150	98.8	4.1	41.83	14.69	6.3	2.0	39.3	52.4	60.23	10.20
165	99.0	4.0	41.83	14.77	6.2	2.0	41.1	50.7	57.29	10.78
180	99.2	3.9	41.84	14.22	6.1	2.0	41.5	50.4	52.97	11.23

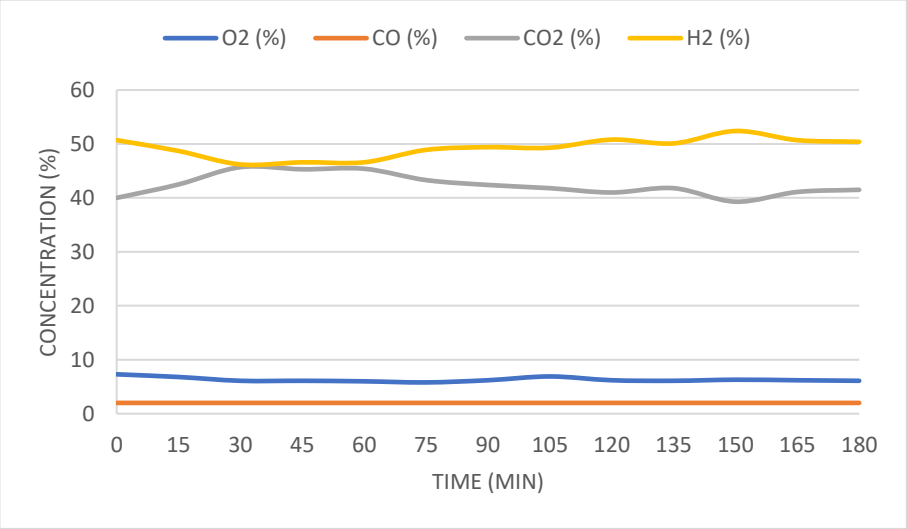

Figure 3-34: Gas outlet composition over the duration of the test, 2.5 % Energreen biomass, at 4 bar and 100 ºC;

Among the data obtained the key important parameters to note are:

- 6.2 % of oxygen in the outlet;
- 40.6 % of carbon dioxide;
- 51.2 % of Hydrogen;
- 56.83 l/h of produced gas with an energetic cost of 10.74 Wh/l.

3.4.3.2. 2.5% Energreen biomass at 4 bar and 110 ºC

Table 3-33: Conditions and collected results, 2.5 % Energreen biomass, at 4 bar and 110 ºC;

Time (min)	T (°C)	P (bar)	V (V)	I (A)	O_2 (%)	CO (%)	CO_2 (%)	H_2 (%)	F (l/h)	W/F (Wh/l)
0	109.6	3.6	31.54	16.36	4.5	2.0	43.2	50.3	87.66	5.89
15	110.1	4.0	30.90	15.21	4.3	2.0	43.8	49.9	75.95	6.19
30	110.2	4.1	30.90	14.89	4.1	2.0	44.8	49.1	73.52	6.26
45	109.9	4.1	30.91	14.60	3.9	2.0	45.0	49.1	73.37	6.15
60	109.7	4.1	30.91	14.21	3.9	2.0	44.8	49.3	72.53	6.06
75	109.6	4.1	30.91	13.97	3.7	2.0	44.7	49.6	69.54	6.21
90	109.8	4.1	30.91	13.87	3.6	2.0	45.2	49.2	68.83	6.23
105	110.2	4.2	30.91	13.93	3.6	2.0	45.6	48.8	68.14	6.32
120	110.4	4.2	30.91	13.97	3.4	2.0	46.6	48.0	66.50	6.49
135	110.1	4.3	30.91	13.69	3.4	2.0	47.3	47.3	65.41	6.47
150	109.4	4.1	30.92	13.29	3.3	2.0	46.1	48.6	65.85	6.24
165	110.5	4.2	30.92	13.35	3.2	2.0	45.8	49.0	67.00	6.16
180	110.9	4.2	30.92	13.30	3.2	2.0	46.2	48.6	64.79	6.35

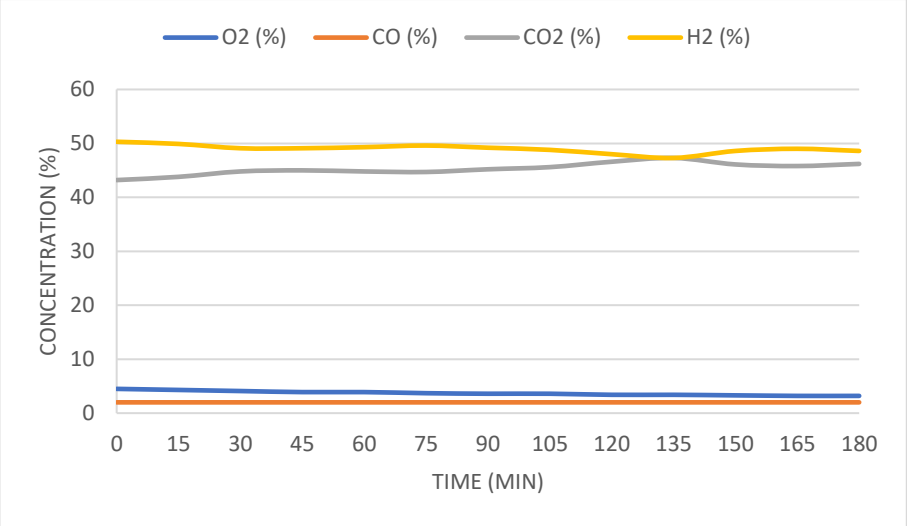

Figure 3-35: Gas outlet composition over the duration of the test, 2.5 % Energreen biomass, at 4 bar and 110 ºC;

Among the data obtained the key important parameters to note are:

- 3.2 % of oxygen in the outlet;
- 46.0 % of carbon dioxide;
- 48.7 % of hydrogen;
- 65.88 l/h of produced gas with an energetic cost of 6.25 Wh/l.

3.4.3.3. 2.5 % Energreen biomass at 5 bar and 100 ºC

Table 3-34: Conditions and collected results, 2.5 % Energreen biomass, at 5 bar and 100 ºC;

Time (min)	T (°C)	P (bar)	V (V)	I (A)	O_2 (%)	CO (%)	CO_2 (%)	H_2 (%)	F (l/h)	W/F (Wh/l)
0	100.5	5.0	32.65	14.69	5.3	2.0	37.8	54.9	71.52	6.71
15	100.6	5.0	32.65	14.50	5.0	2.0	36.7	56.3	75.42	6.28
30	100.6	5.0	32.65	14.56	5.0	2.0	36.4	56.6	74.59	6.37
45	100.5	5.0	32.65	14.44	5.0	2.0	37.3	55.7	75.47	6.25
60	100.2	5.0	32.65	14.42	5.0	2.0	37.4	55.6	76.70	6.14
75	100.9	5.0	32.64	14.28	5.0	2.0	37.3	55.7	73.82	6.31
90	100.6	4.9	32.64	14.07	5.0	2.0	38.6	54.4	73.42	6.26
105	100.6	5.0	32.64	14.90	4.9	2.0	38.7	54.4	72.83	6.68
120	100.9	5.0	32.64	14.29	4.9	2.0	38.8	54.3	73.47	6.35
135	100.1	4.9	32.65	14.19	4.9	2.0	39.0	54.1	73.22	6.33
150	100.4	4.9	32.64	14.38	4.9	2.0	38.6	54.5	73.87	6.35
165	101.1	5.0	32.65	14.15	4.7	2.0	39.8	53.5	72.39	6.38
180	100.6	4.9	32.65	13.71	4.8	2.0	38.9	54.3	70.59	6.34

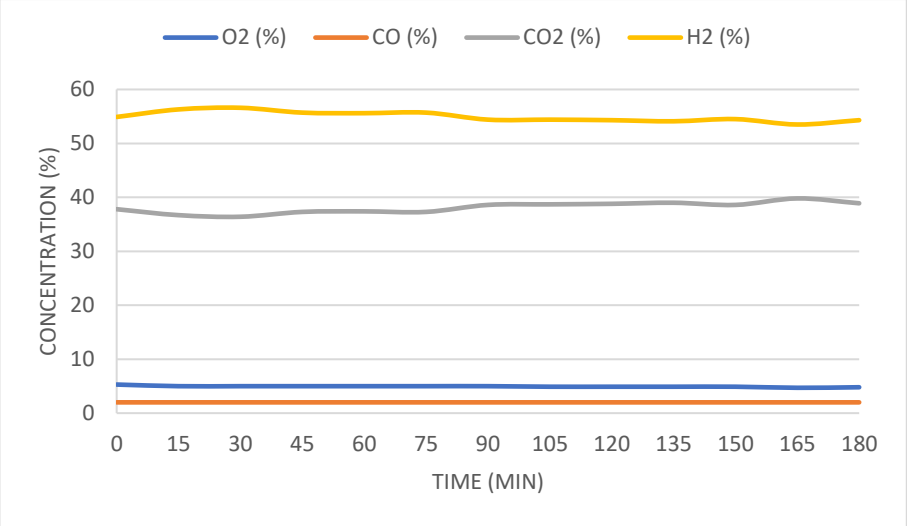

Figure 3-36: Gas outlet composition over the duration of the test, 2.5 % Energreen biomass, at 5 bar and 100 ºC;

Among the data obtained the key important parameters to note are:

- 4.8 % of oxygen in the outlet;
- 39.1 % of carbon dioxide;
- 54.1 % of hydrogen;
- 72.28 l/h of produced gas with an energetic cost of 6.36 Wh/l.

3.4.3.4. 2.5 % Energreen at 5 bar and 110 ºC

Table 3-35: Conditions and collected results, 2.5 % Energreen biomass, at 5 bar and 110 ºC;

Time (min)	T (°C)	P (bar)	V (V)	I (A)	O_2 (%)	CO (%)	CO_2 (%)	H_2 (%)	F (l/h)	W/F (Wh/l)
0	109.5	4.9	32.25	16.18	3.9	2.0	43.0	51.1	81.82	6.38
15	109.8	4.2	31.04	14.00	3.6	2.0	45.8	48.6	69.99	6.21
30	109.6	4.0	31.04	13.69	3.4	2.0	45.6	49.0	66.96	6.35
45	110.3	4.0	31.04	13.76	3.3	2.0	45.4	49.3	66.83	6.39
60	110.7	5.3	32.00	14.33	3.3	2.0	43.2	51.5	69.68	6.58
75	110.9	5.4	31.99	14.57	3.2	2.0	46.5	48.3	72.58	6.42
90	110.8	5.3	32.00	14.25	3.2	2.0	46.6	48.2	68.79	6.63
105	110.3	5.2	32.01	14.14	3.2	2.0	46.7	48.1	66.42	6.81
120	110.3	5.1	32.01	13.64	3.1	2.0	46.4	48.5	66.91	6.52
135	110.7	5.1	32.01	13.57	3.1	2.0	45.9	49.0	65.81	6.60
150	110.8	5.1	32.02	13.53	3.0	2.0	46.9	48.1	65.10	6.65
165	109.9	5.0	32.02	13.06	3.0	2.0	46.6	48.4	61.78	6.77
180	110.9	5.0	32.02	13.25	3.0	2.0	46.6	48.4	63.08	6.73

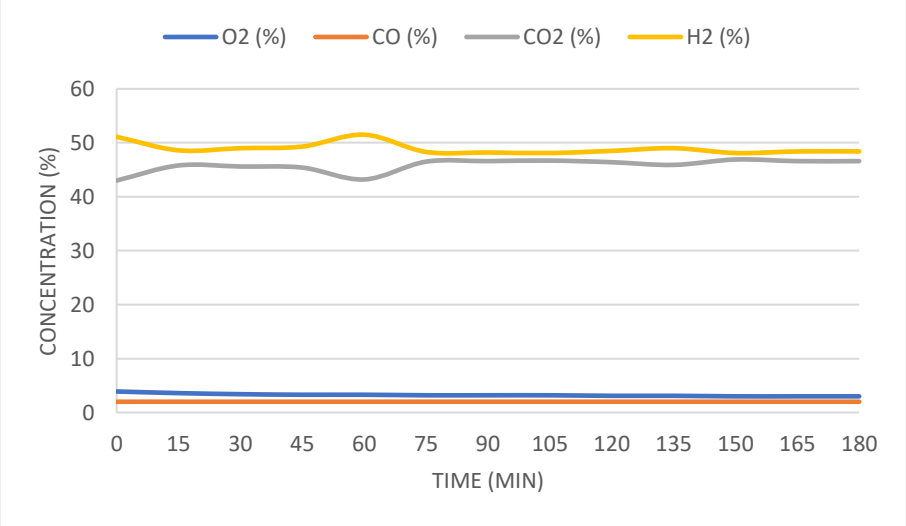

Figure 3-37: Gas outlet composition over the duration of the test, 2.5 % Energreen biomass, at 5 bar and 110 ºC;

Among the data obtained the key important parameters to note are:

- 3 % of oxygen in the outlet;
- 46.7 % of carbon dioxide;
- 48.3 % of hydrogen;
- 63.32 l/h of produced gas with an energetic cost of 6.72 Wh/l.

3.4.3.5. 5 % Energreen biomass at 4 bar and 100 ºC

Table 3-36: Conditions and collected results, 5 % Energreen biomass, at 4 bar and 100 ºC;

Time (min)	T (°C)	P (bar)	V (V)	I (A)	O_2 (%)	CO (%)	CO_2 (%)	H_2 (%)	F (l/h)	W/F (Wh/l)
0	100.9	3.9	35.25	14.27	4.3	2.0	37.3	56.4	65.06	13.00
15	101.0	3.6	35.25	14.22	4.1	2.0	39.0	54.9	69.45	7.22
30	100.9	4.1	35.25	13.94	4.0	2.0	38.5	55.5	69.10	7.11
45	100.8	4.0	35.24	13.92	4.0	2.0	40.2	53.8	66.71	7.35
60	101.4	3.8	35.25	14.35	4.1	2.0	41.2	52.7	68.14	7.42
75	100.9	3.7	35.25	13.86	4.0	2.0	41.1	52.9	68.27	7.16
90	101.7	3.6	35.25	14.19	4.1	2.0	40.7	53.2	67.58	7.40
105	101.1	3.6	35.24	14.08	4.1	2.0	40.2	53.7	67.92	7.30
120	101.1	3.5	35.25	14.05	4.1	2.0	40.8	53.1	66.10	7.49
135	101.0	3.5	35.25	14.14	4.1	2.0	41.2	52.7	66.38	7.51
150	100.6	4.6	35.25	14.18	4.1	2.0	40.1	53.8	68.35	7.31
165	101.1	4.4	35.25	13.86	4.1	2.0	40.8	53.1	65.77	7.43
180	102.3	4.4	35.24	14.22	4.1	2.0	40.9	53.0	68.92	7.27

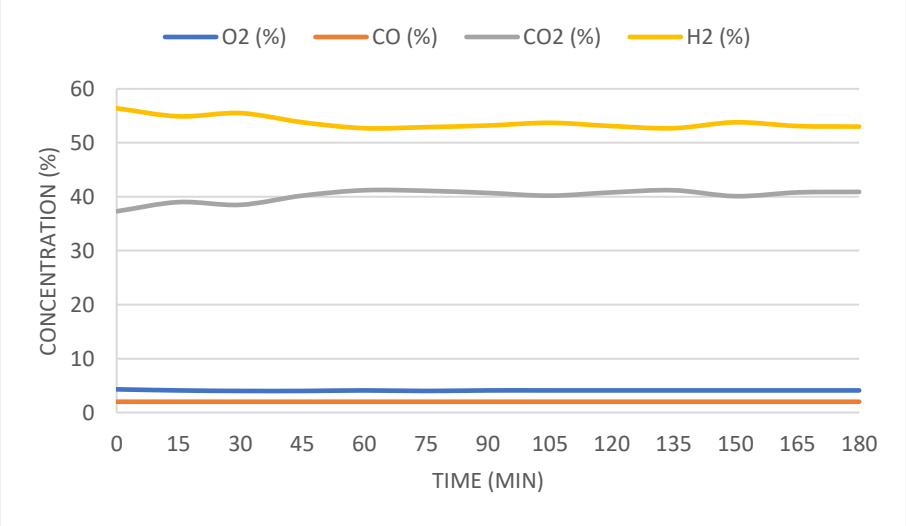

Figure 3-38: Gas outlet composition over the duration of the test, 5 % Energreen biomass, at 4 bar and 100 ºC;

Among the data obtained the key important parameters to note are:

- 4.1 % of oxygen in the outlet;
- 40.6 % of carbon dioxide;
- 53.3 % of hydrogen;
- 67.68 l/h of produced gas with an energetic cost of 7.34 Wh/l.

3.4.3.6. 5 % Energreen biomass at 4 bar and 110 ºC

Table 3-37: Conditions and collected results, 5 % Energreen biomass, at 4 bar and 110 ºC;

Time (min)	T (°C)	P (bar)	V (V)	I (A)	O_2 (%)	CO (%)	CO_2 (%)	H_2 (%)	F (l/h)	W/F (Wh/l)
0	109.2	3.7	35.00	15.29	4.1	2.0	34.8	59.1	74.90	7.15
15	109.9	3.9	35.01	15.15	3.9	2.0	34.0	60.1	72.58	7.31
30	109.6	4.0	35.03	15.21	3.7	2.0	34.9	59.4	71.43	7.46
45	110.0	4.2	35.03	14.61	3.6	2.0	36.6	57.8	69.86	7.33
60	110.0	4.1	35.02	14.29	3.4	2.0	35.1	59.5	69.41	7.21
75	110.0	4.1	35.01	14.06	3.5	2.0	34.5	60.0	66.26	7.43
90	110.3	4.1	35.01	14.33	3.4	2.0	35.1	59.5	63.49	7.90
105	110.0	4.3	35.72	14.41	3.4	2.0	35.2	59.4	69.14	7.44
120	110.8	4.3	35.71	14.93	3.5	2.0	34.3	60.2	69.72	7.65
135	110.3	4.3	35.72	14.39	3.3	2.0	34.7	60.0	67.71	7.59
150	109.6	4.2	35.72	14.40	3.4	2.0	35.1	59.5	67.80	7.59
165	109.9	4.1	35.72	14.44	3.5	2.0	35.7	58.8	67.80	7.61
180	111.2	4.0	35.72	14.27	3.3	2.0	34.1	60.6	65.89	7.74

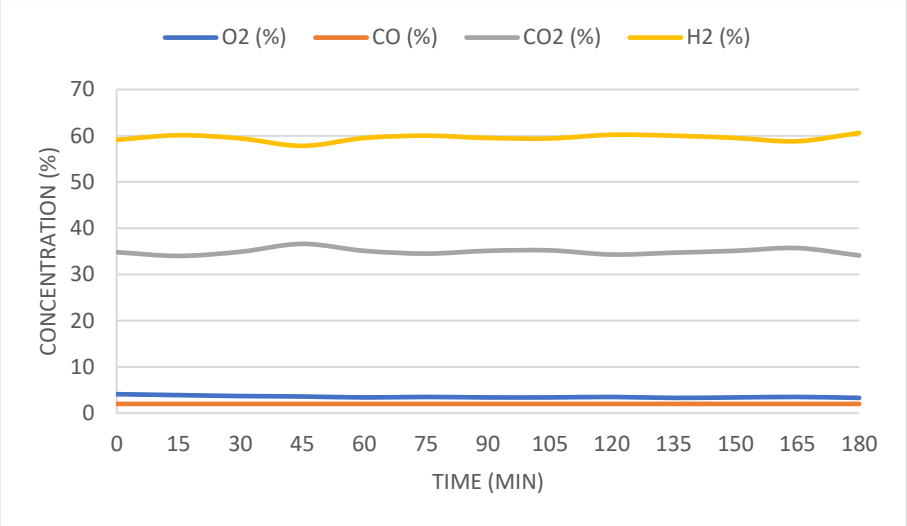

Figure 3-39: Gas outlet composition over the duration of the test, 5 % Energreen biomass, at 4 bar and 110 ºC;

Among the data obtained the key important parameters to note are:

- 3.4 % of oxygen in the outlet;
- 35.0 % of carbon dioxide;
- 59.6 % of hydrogen;
- 67.19 l/h of produced gas with an energetic cost of 7.64 Wh/l.

3.4.3.7. 5 % Energreen biomass at 5 bar and 100 ºC

Table 3-38: Conditions and collected results, 5 % Energreen biomass, at 5 bar and 100 ºC;

Time (min)	T (°C)	P (bar)	V (V)	I (A)	O_2 (%)	CO (%)	CO_2 (%)	H_2 (%)	F (l/h)	W/F (Wh/l)
0	100.6	4.7	36.66	14.92	4.9	2.0	34.2	58.9	71.15	7.69
15	100.5	4.4	36.67	14.75	4.5	2.0	33.8	59.7	67.08	8.06
30	100.4	5.1	36.67	14.84	4.3	2.0	33.7	60.0	66.91	8.13
45	100.4	5.1	36.67	14.90	4.2	2.0	35.6	58.2	67.37	8.11
60	100.7	5.0	36.67	14.68	4.1	2.0	36.2	57.7	66.46	8.10
75	100.7	4.7	36.67	14.76	4.1	2.0	35.6	58.3	67.04	8.07
90	101.0	5.0	36.66	14.76	4.2	2.0	35.9	57.9	64.21	8.43
105	100.7	5.0	36.68	14.44	4.0	2.0	35.4	58.6	65.02	8.15
120	100.4	4.9	36.67	14.38	4.1	2.0	36.2	57.7	65.18	8.09
135	100.8	4.9	36.68	14.19	4.1	2.0	35.8	58.1	64.25	8.10
150	101.0	4.9	36.68	14.22	4.2	2.0	37.3	56.5	63.19	8.25
165	101.3	4.9	36.68	14.27	4.2	2.0	36.3	57.5	61.75	8.48
180	101.0	4.7	36.68	13.97	4.1	2.0	35.8	58.1	62.10	8.25

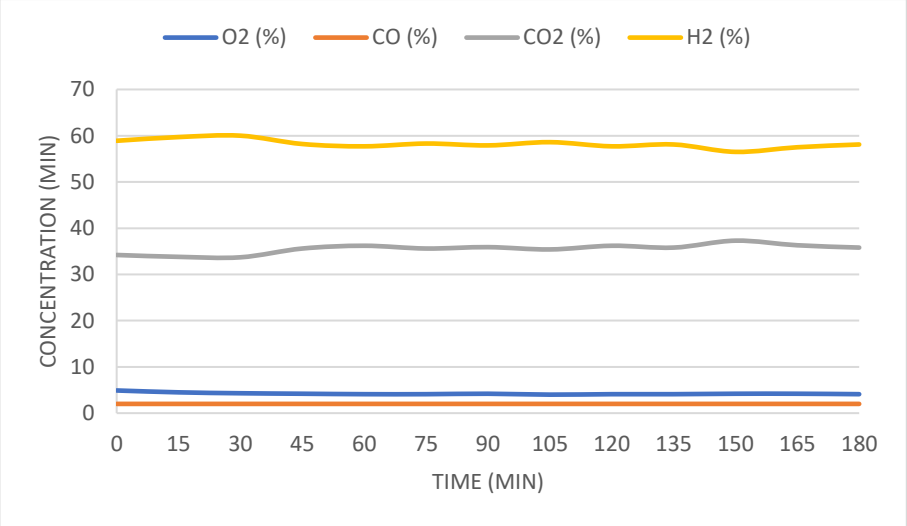

Figure 3-40: Gas outlet composition over the duration of the test, 5 % Energreen biomass, at 5 bar and 100 ºC;

Among the data obtained the key important parameters to note are:

- 4.2 % of oxygen in the outlet;
- 36.5 % of carbon dioxide;
- 57.4 % of hydrogen;
- 62.35 l/h of produced gas with an energetic cost of 8.33 Wh/l.

3.4.3.8. 5% Energreen biomass at 5 bar and 110 ºC

Table 3-39: Conditions and collected results, 5 % Energreen biomass, at 5 bar and 110 ºC;

Time (min)	T (°C)	P (bar)	V (V)	I (A)	O_2 (%)	CO (%)	CO_2 (%)	H_2 (%)	F (l/h)	W/F (Wh/l)
0	110.0	4.7	34.17	14.81	3.5	2.0	37.6	56.9	66.67	7.59
15	109.8	5.2	34.14	14.29	3.2	2.0	38.5	56.3	63.60	7.67
30	110.3	5.1	34.14	14.68	3.0	2.0	39.8	55.2	65.97	7.60
45	110.7	4.9	34.12	14.24	2.9	2.0	38.2	56.9	64.63	7.52
60	110.3	5.0	34.16	14.42	3.0	2.0	39.8	55.2	63.75	7.73
75	111.0	5.0	34.16	14.31	2.9	2.0	40.5	54.6	62.18	7.86
90	110.3	4.8	34.12	14.18	2.9	2.0	40.8	54.3	62.86	7.70
105	111.5	4.8	34.11	14.36	2.9	2.0	40.4	54.7	62.83	7.80
120	112.0	4.8	34.21	14.2	2.8	2.0	40.1	55.1	62.43	7.78
135	111.3	4.5	34.22	13.97	2.8	2.0	38.3	56.9	62.68	7.63
150	111.5	4.6	34.94	14.89	2.8	2.0	38.8	56.4	64.83	8.03
165	112.1	4.7	35.44	15.28	2.9	2.0	38.1	57.0	67.67	8.00
180	112.0	4.9	35.44	15.04	2.9	2.0	38.1	57.0	66.58	8.01

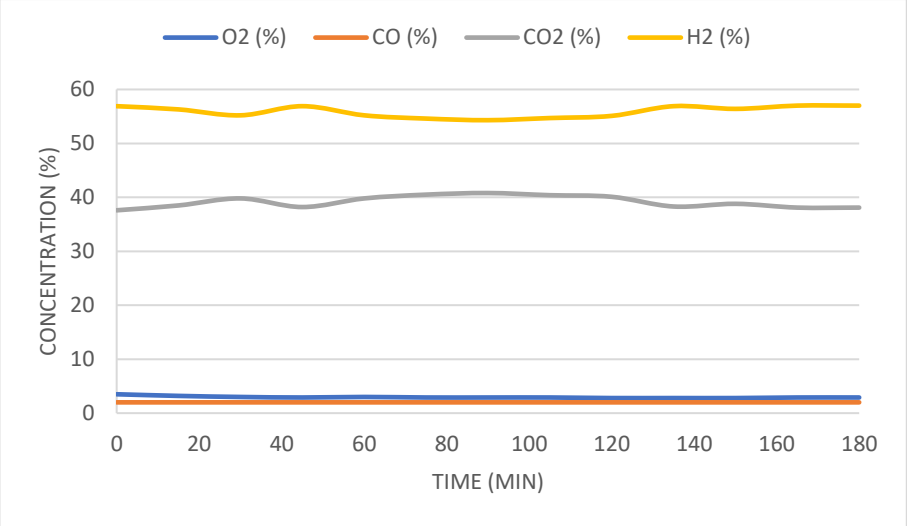

Figure 3-41: Gas outlet composition over the duration of the test, 5 % Energreen biomass, at 5 bar and 110 ºC;

Among the data obtained the key important parameters to note are:

- 2.9 % of oxygen in the outlet;
- 38.3 % of carbon dioxide;
- 56.8 % of hydrogen;
- 66.36 l/h of produced gas with an energetic cost of 8.01 Wh/l.

3.4.4. Energreen performance

Similarly to the previous analysis, Table 3-40 presents a compilation of the final results of each test using liquified Energreen biomass.

Table 3-40: Compiled results of each test with the addition of liquified Energreen biomass and respective CO_2:H_2 ratios;

Test Conditions	O2 (%)	CO (%)	CO2 (%)	H2 (%)	F (l/h)	W/F (Wh/l)	CO2:H2 Ratio
4 bars 100 ºC 1M NaOH 2.5 %Energreen	6.2	2.0	40.6	51.2	56.83	10.74	1.26
4 bars 110 ºC 1M NaOH 2.5 %Energreen	3.2	2.0	46.0	48.7	65.88	6.25	1.06
5 bars 100 ºC 1M NaOH 2.5 %Energreen	4.8	2.0	39.1	54.1	72.28	6.36	1.38
5 bars 110 ºC 1M NaOH 2.5 %Energreen	3.0	2.0	46.7	48.3	63.32	6.72	1.03
4 bars 100 ºC 1M NaOH 5 %Energreen	4.1	2.0	40.6	53.3	67.68	7.34	1.31
4 bars 110 ºC 1M NaOH 5 %Energreen	3.4	2.0	35.0	59.6	67.16	7.64	1.71
5 bars 100 ºC 1M NaOH 5 %Energreen	4.2	2.0	36.5	57.4	62.35	8.33	1.57
5 bars 110 ºC 1M NaOH 5 %Energreen	2.9	2.0	38.3	56.8	66.36	8.01	1.48

As Figure 3-42 displays, in general and similarly to the Acacia tests, the addition of Evergreen lowered the O_2 concentrations in the syngas produced. The only exception to this was the test at 4 bar(g), 100 ºC with 2.5 % liquified biomass, likely a consequence of heavy erosion in the graphite disks. The two subsequent tests exhibited the same problem but at a larger scale resulting in the need for their repetition.

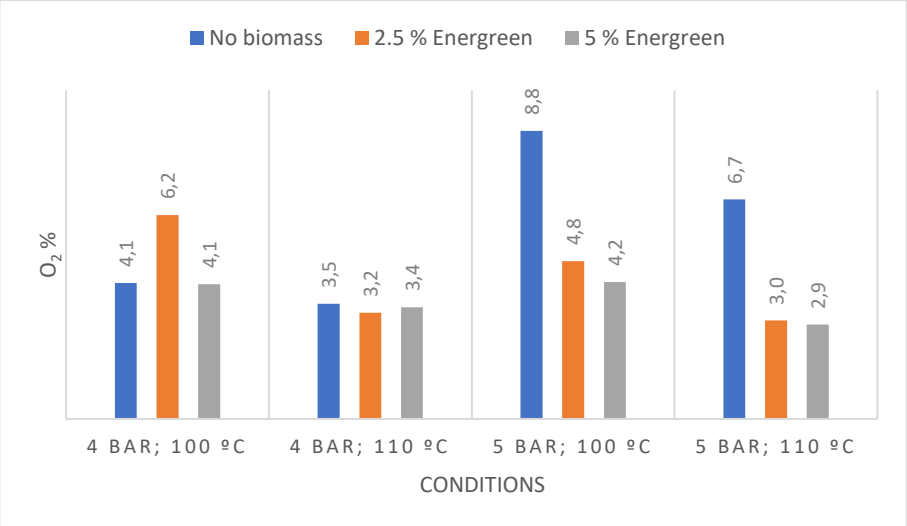

Figure 3-42: Gas outlet O_2 content comparison for the Energreen biomass;

In both concentrations there is a decrease in O_2 when rising pressure and temperature, although the latter induces a more noticeable decline. Beyond that, the 5 % group had, for the most part, the lowest values with the only exclusion being at 4 bar(g), 110 ºC where is slightly higher than the 2.5 % test (only a 0.2 difference).

In terms of CO_2: H_2 ratio, as Figure 3-43 shows, just as it was observed in the Acacia tests, the addition of Energreen significantly decreased the number of units of H_2 per 1 unit of CO_2, meaning a less ideal ratio.

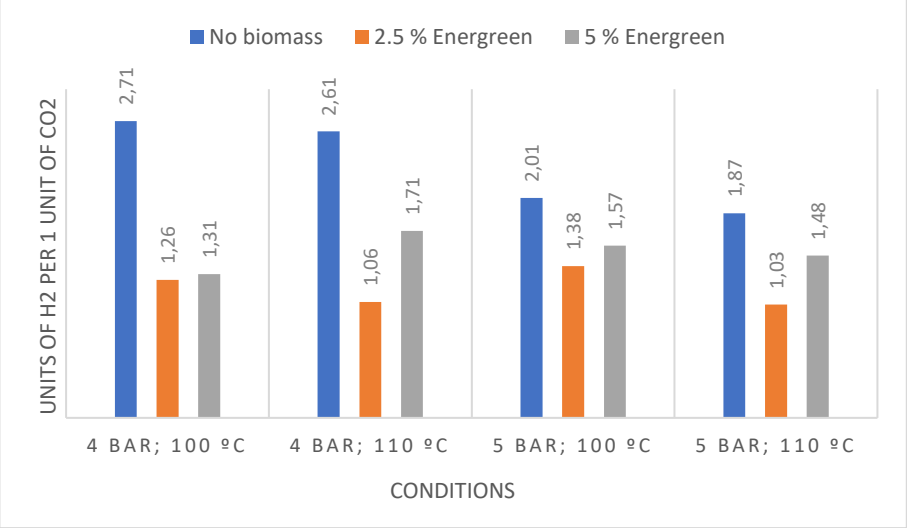

Figure 3-43: Units of H_2 per 1 unit of CO_2 /CO_2: /H_2ratios comparison for the Energreen biomass;

According to the results, the two Energreen concentrations exhibited different behaviors in relation to test conditions. In the case of the 2.5 % group, despite no significant changes brought by the change in pressure (with only a 0.12 and 0.3 difference for 100 and 110 ºC respectively), the rise in temperature produced syngas mixtures richer in CO_2 (possibly resulting from this change favoring carbon oxidation and consequent CO_2 production). The 5 %, on the other hand, did not display consistent behavior for both pressure and temperature changes.

Unlike the Acacia counterpart (where the 2.5 % performed better in terms of CO_2: H_2ratio), in the Energreen tests the 5 % group got more optimal values in all cases with the peak being achieved at 4 bar(g), 110 ºC with a 1:1.71 ratio. Once again, while still less optimal compared with electrolyte only, it is counterbalanced by the associated decrease in O_2 content and the possibility for post-production adjustments to composition.

Figure 3-44 presents both gas flow production (a) and energy expenditure (b) of each test to facilitate direct comparison and evaluate the effects of the Energreen addition.

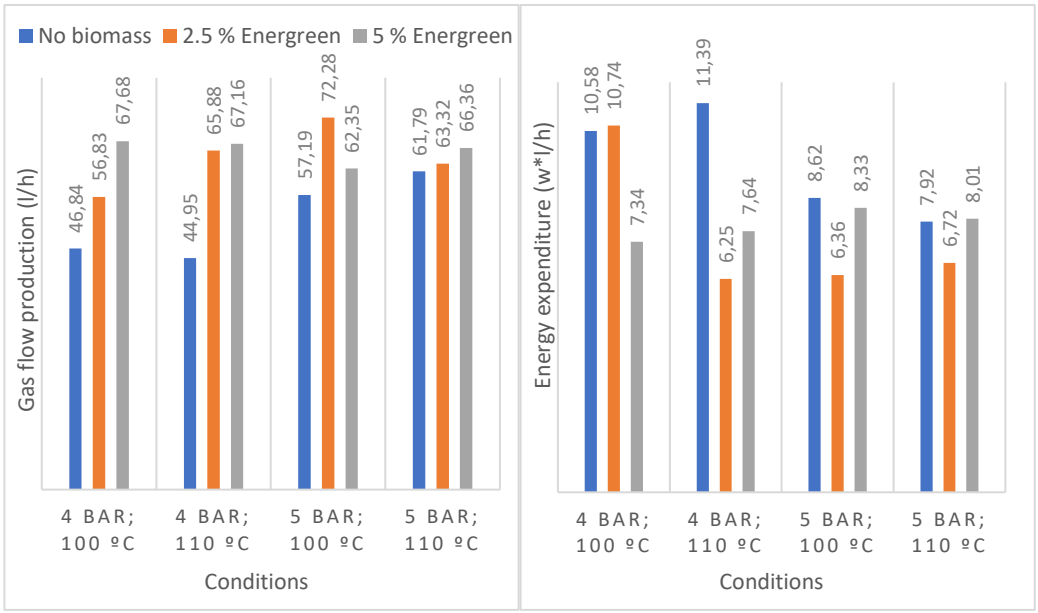

Figure 3-44: Gas flow production(a) and energy expenditure(b) comparison for the Energreen biomass;

As expected, the added Energreen boosted syngas production leading to higher flow values when comparing to the tests without biomass. Furthermore, with the exception of the test at 4 bar(g), 100 ºC with 2.5 % liquified biomass (previously pointed out as a possible result of graphite disk erosion), all Energreen tests showed lower levels of energy expenditure. The 2.5 % group had the lowest consumptions with the lowest reported being 6.25 Wl/h at 4 bar(g), 110 ºC.

Much like the case with Acacia, altogether when comparing performances between tests without addition any biomass and the two groups with of Energreen, the later were observed to have the advantage in all factors excluding CO_2:H_2 ratio. Unlike the Acacia tests though, it is not as clear which of the two concentrations offers the best performance with 2.5 % producing syngas at a lower energy cost and being close to 5 % in terms of O_2 content but producing a less ideal CO_2:H_2 ratio. The choice between the two is dependent on establishing the priority between process efficiency and the produced composition.

3.4.5. Liquified Biomass Comparisons

After the individual performance analysis of both Acacia and Evergreen groups, the following step is to compare their results and better establish the strong and weak points for each type of biomass. This comparison was done by grouping both biomasses at 2.5 and 5 % (w/w) by test conditions for a more efficient result analysis.

Regarding the syngas O_2 content, as Figure 3-45 showcases, with exception of the 5 bar(g), 110 ºC group, the Acacia tests have the lowest results with the lowest appearing at 4 bar(g), 110 ºC with a value of 2.1 %.

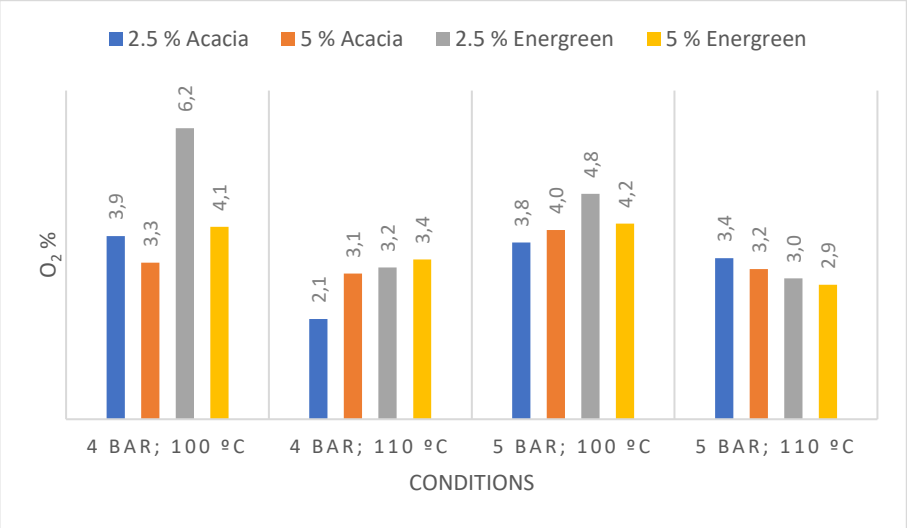

Figure 3-45: Gas outlet O2 content direct comparison between Acacia and Energreen;

Although further research would be needed to prove it or not, data in Figure 3-45 leads to the conclusion that while Acacia produces lower O_2 contents at the previously specified conditions, Energreen's performance may be favored by higher pressures. If the set of tests included pressures above the 5 bar(g) (Not possible with the current setup), Energreen's resultant O_2 fraction would possibly continue to decrease.

By the analysis of Figure 3-46, it is inferred that Energreen offers a clear advantage in terms of syngas CO_2: H_2 ratio at all conditions except for 4 bar(g), 100 ºC. where Acacia had the highest result (and the highest over all the tests).

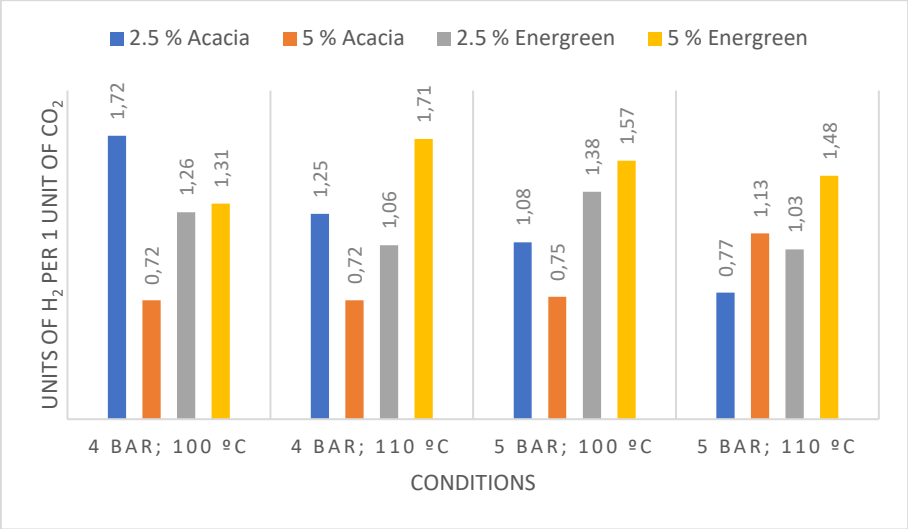

Figure 3-46: Units of H_2 per 1 unit of CO_2 (or 1/(CO_2 /H_2)) direct comparison between Acacia and Energreen;

This data in conjunction with the corresponding O_2 contents displayed in Figure 3-45 implies an increase in CO_2 production when increasing both temperature and pressure. Additionally, this phenomenon is more noticeable with Acacia, resulting in a sharper CO_2: H_2 ratio decrease, (although 5 %, 5 bar(g), 110 ºC seems to be an outlier, most likely due to starting signs of wear in the graphite disks). On the other hand, Energreen, while showing a similar behavior, has a less steep decline with the increase in temperature causing more significant changes.

In terms of flow of produced gas alone, by looking at the data at Figure 3-47, it is not possible to clearly determine which of the two types of biomasses produces more syngas.

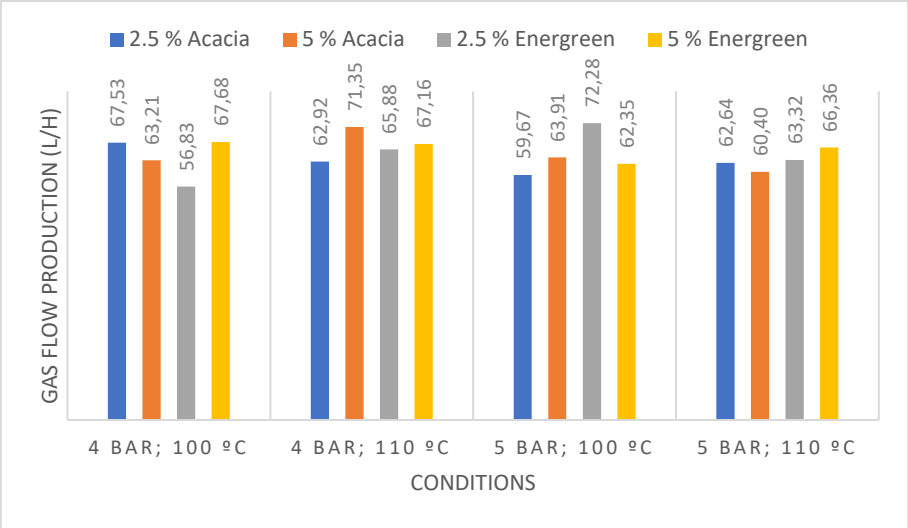

Figure 3-47: Gas flow production direct comparison between Acacia and Energreen;

While flow values are not consistent, due to the influence of other factors such as the current applied or wear in the graphite disks, the flow alone doesn't necessarily dictate which of the two offers the best performance. To complement it, Figure 3-48 shows the correspondent energy expenditures.

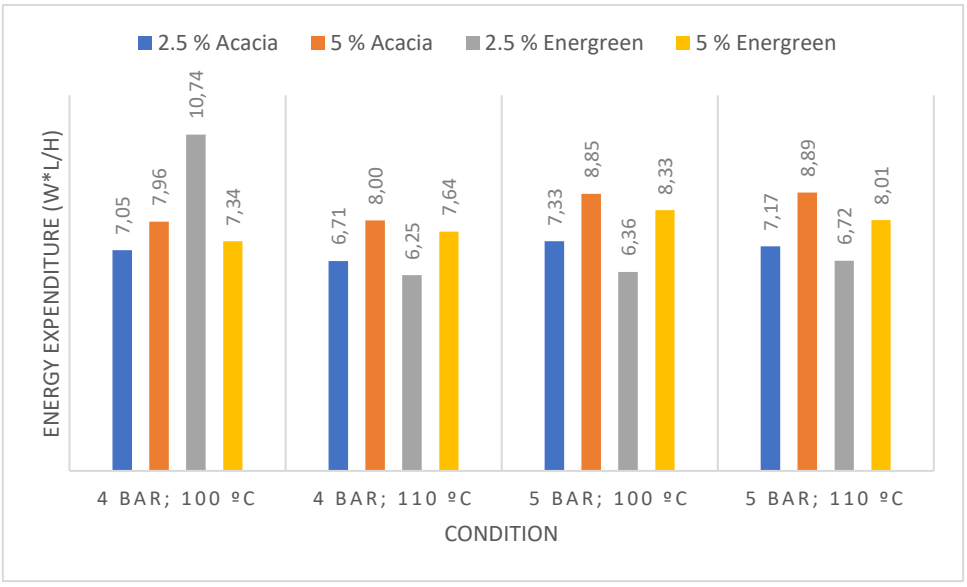

Figure 3-48: Energy expenditure direct comparison between Acacia and Energreen;

Ignoring the case of the 2.5 % Energreen at 5 bar(g), 110 ºC due to the effects wear off in graphite disks, overall, the pattern at each set of conditions is fairly consistent with both 2.5 % groups presenting the less expenditure in comparison to 5 %. In all cases Energreen presented the lowest consumption for both concentrations with the highest flow corresponding to the second lowest consumption. Knowing this, it can be concluded that Energreen offers better performance in terms of energy consumption per flow produced.

Altogether, when considering the conditions range in study, it is not possible to appoint objectively which of the two is the best as a carbon source. Still, it was possible to identify the strong and weak points of each one:

- In general, Acacia produces less O_2 content, mainly as a result of an increase in CO_2 production which logically leads to a less desirable CO_2/H_2 ratio. Nevertheless, this ratio may be fixed postproduction, making it an acceptable consequence of producing a syngas with less O_2;
- Energreen on the other hand, shows signs of only decreasing O_2 contents at pressures higher than the tested range, although further research would be needed to prove it. It also produced a more optimal CO_2/H_2 ratio (at the cost of less O_2 consumption), and most importantly, has showed the best relation between energy consumed and gas production.

Overall, the data collected shows that Acacia is the better choice when prioritizing the production of a syngas mixture with lower O_2 content. Although this carries the consequence of producing a less desirable CO_2/H_2 ratio, it is still acceptable due to the post-production processes of adding hydrogen or removing the excess CO_2 being easier and more affordable than the removal of excess O_2. Energreen on the other hand, while being less efficient at reducing O_2 content, produces a more desirable ratio. Furthermore, if the priority is energy cost reduction, Energreen has the advantage, allowing to produce syngas while consuming less electric energy.

4. Graphite disk wear down and observed consequences

Throughout all experimental work, one important factor to consider when analyzing results was the degree of wear off in the graphite disks inside the stack. As the process goes on, the carbon constituting the disks is consumed, either directly as a result of the reaction with O_2 or by being simply carried out by the circulating fluid. Consequentially, the surface of each disk is gradually eroded, leading eventually to holes and reduction of surface area that will hinder performance.

In spite of the fact that an entire set of experimental tests focusing on this topic would be needed to fully evaluate it (which was not possible under the scope of this work), a short comparison was done between two tests at the same conditions but opposite degrees of wear. The first was a test where the effects of wear in the disks was enough to completely reject the results and call for their substitution, and the second was the following test with new disks, devoid of any wear. The objective of this short study was a surface level analysis of the signs and consequences of wear in the graphite disks and estimate roughly the expected lifespan of each set of disks.

The following Figure 4-1, show on the left a new disk followed on the right by a completely worn out one.

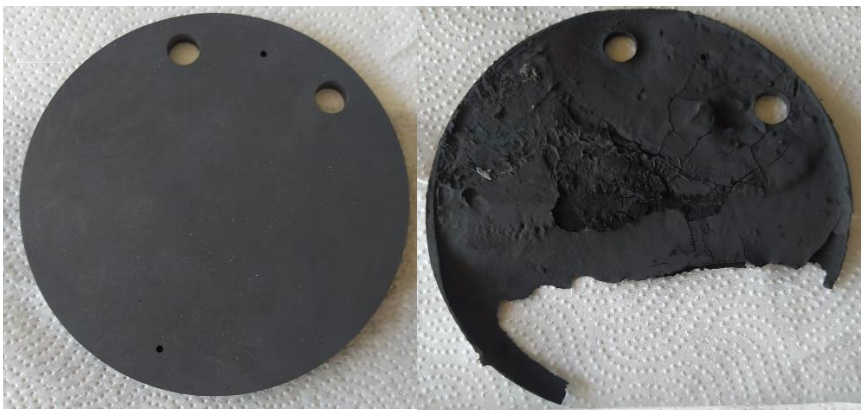

Figure 4-1:Direct comparison between a new disk (left) and a completely worn-out one (right);

The specific disk showed on the right of Figure 4-1 was the first counting from the top, having suffered the most damage. While not all disks suffered erosion to this extent, in general, after a total estimated operation time of around 30 hours (or 8 tests of 3 hours plus around 25 % additional time spent operating outside of the allotted time for the tests, for warming or cooling the system, all of the 11 disks inside the stack displayed considerable loss in mass with a consequent increase in the distance between disks of each cell, and appearance of holes that generate less desirable electrolyte flow patterns.

To better understand the degree of wear in the disks, Table 4-1 showcases the data collected on one of the occasions where the disks had to be replaced. Each disk was weighted alone post being removed from the stack and compared with their weight registered pre installation.

Table 4-1:Registered wear off in the disks and percentual loss of mass;

Disk weight (g)		**Mass loss (%)**
New	**Worn-out**	
90.76	50.65	44.19
91.67	45.02	50.89
91.50	45.00	50.82
91.01	36.73	59.64
91.22	39.44	56.76
91.01	37.43	58.87
91.05	43.09	52.67
91.08	35.25	61.30
91.84	43.58	52.55
90.32	32.08	64.48
91.46	37.91	58.55
Average		
91.17	40.56	55.52

With the exception of the topmost one (that still lost a considerable 44.19 %), all disks lost more than half of his original weight. As further data will show, the performance of the stack is compromised when working with this degree of wear in the disks. This means that they can no longer be used in tests with their remaining graphite being wasted unless any alternative uses are found.

The following test with 2.5 % Energreen at 5 bar(g), 100 ºC offers a brief analysis of the effect the wear on the graphite disks has on the system performance and how it affects the syngas produced. At the time, it was rejected due to clear signs of heavy wear, thus offering the best counterpart to a repeated test using new disks (which corresponds to the one previously showed for experimental work results).

4.1. Test with worn out disks-2.5 % Energreen biomass at 5 bar and 100 ºC

Table 4-2: Conditions and collected results for the rejected test;

Time (min)	T (°C)	P (bar)	V (V)	I (A)	O_2 (%)	CO (%)	CO_2 (%)	H_2 (%)	F (l/h)	Wh/l
0	100.9	4.7	37.06	15.26	5.8	2.0	34.1	58.1	42.55	13.29
15	102.0	5.5	37.06	15.19	5.3	2.0	37.9	54.8	44.78	12.57
30	102.3	4.5	36.74	14.89	5.0	2.0	41.7	51.3	50.54	10.82
45	102.1	4.6	36.74	14.96	5.0	2.0	41.2	51.8	47.62	11.54
60	102.0	5.3	36.75	14.53	5.0	2.0	41.4	51.6	41.35	12.91
75	101.9	5.2	36.75	14.51	5.0	2.0	41.9	51.1	41.84	12.74
90	101.7	4.2	36.75	14.19	5.0	2.0	44.8	48.2	44.83	11.63
105	103.0	5.5	37.74	15.34	5.1	2.0	41.7	51.2	45.69	12.67
120	102.8	5.0	36.72	14.43	5.0	2.0	44.2	48.8	43.11	12.29
135	102.9	5.1	36.72	14.57	5.0	2.0	45.9	47.1	42.72	12.52
150	103.1	5.2	36.72	14.80	5.0	2.0	45.2	47.8	41.21	13.19
165	103.4	5.4	36.72	14.85	5.0	2.0	44.9	48.1	42.54	12.82
180	104.0	5.3	36.71	15.15	5.0	2.0	46.6	46.4	43.57	12.77

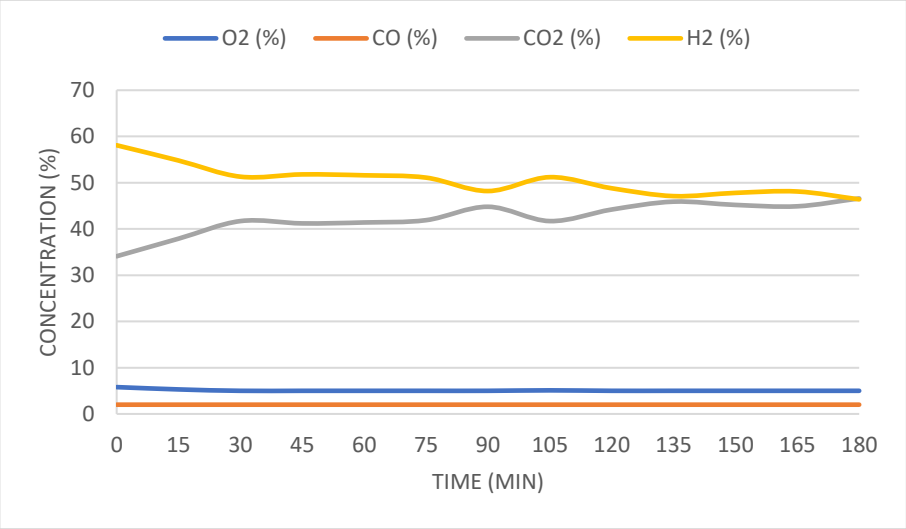

Figure 4-2: Gas outlet composition over the duration of the rejected test;

Among the data obtained the key important parameters to note are:

- 5 % of oxygen in the outlet;
- 45.6 % of carbon dioxide;
- 47.4 % of Hydrogen;
- 42.44 l/h of produced gas with an energetic cost of 12.92 Wh/l.

4.2. Result Comparison

By comparing the results of the rejected test with the one obtained after changing the disks it is possible to detect some key differences likely to be a result of the considerable wear in the disks.

As the surface of the disks suffers erosion, the distance between each disk increases, and holes may form, leading to alternative routes for fluid circulation and a reduction of the time spent by the electrolyte in each cell. Consequently, there is a decrease in the electrolyzer efficiency. This can be observed by comparing H_2 contents as showed in Figure 4-3.

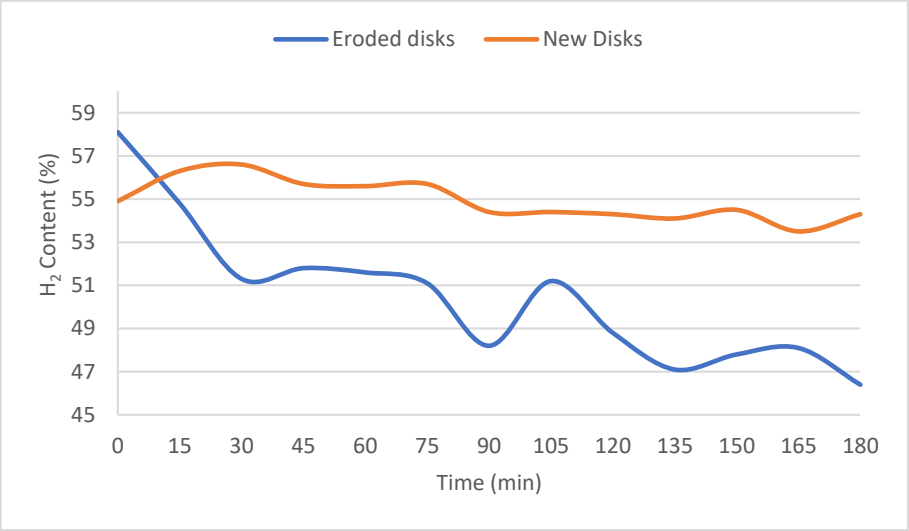

Figure 4-3: Effects of graphite disk erosion on H_2 production;

As expected and shown in Figure 4-3, worn out disks produce syngas with less H_2 content. In addition, the eroded disks test had a less stable behavior, proved by the inability to achieve stationary state, even after 3 hours.

Although the CO_2 percentage is higher in the eroded test, this does not correlate necessarily to an increase in its production. In fact, as the reduction in syngas flow imply, this likely a result of the decrease in H_2 production. A more detailed study, focused on this topic, would be needed to better determine the case and how wear in disks affects CO_2 production.

Regarding its effects on gas production and energy expenditure, as predicated, more eroded disks have more difficulty producing syngas. This is confirmed by Figure 4-4 and Figure 4-5 where the eroded test got consistently lower flows of production at much higher energy costs.

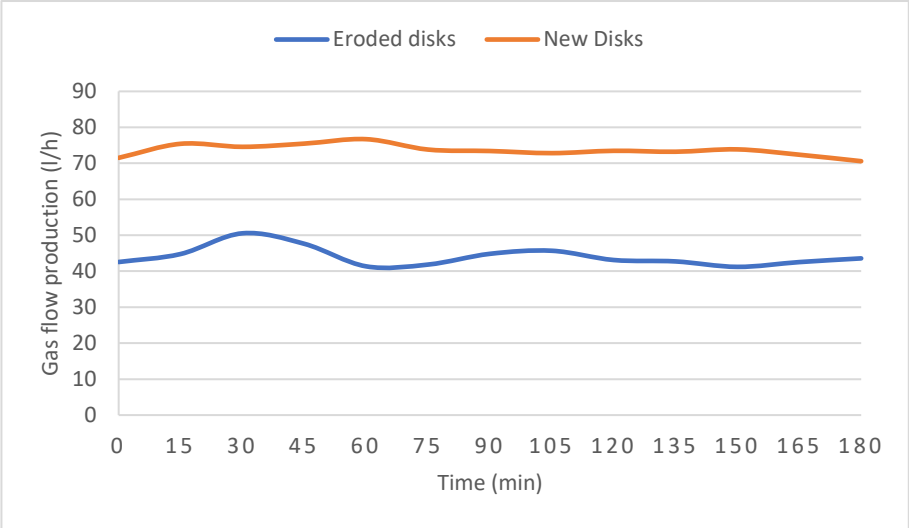

Figure 4-4: Effects of graphite disk erosion on syngas production;

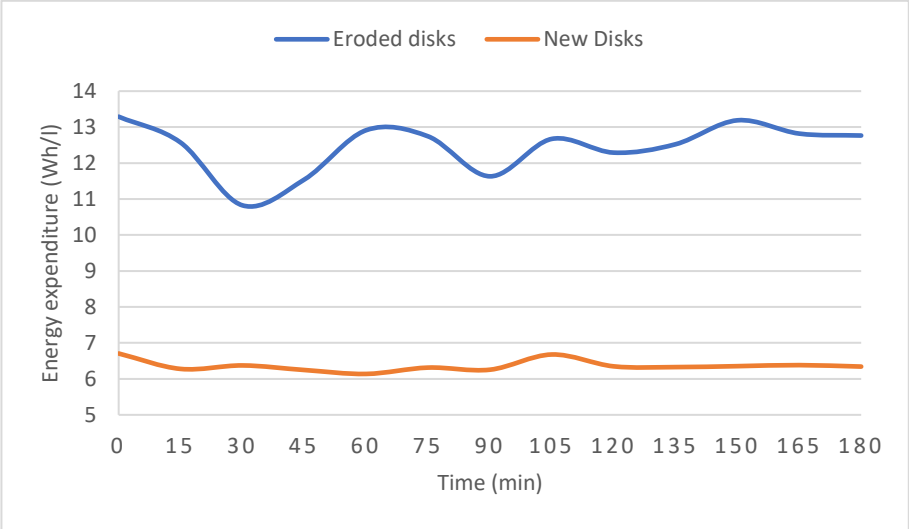

Figure 4-5: Effects of graphite disk erosion on energy expenditure;

All in all, in its current iteration, the graphite disks inside the stack act both as middle step and obstacle for its industrial application as an alternative method for syngas production. With only an estimated lifespan of 30 hours of operation, the disks greatly compromise the viability of the process by requiring frequent maintenance stops and increasing consumable costs.

Additionally, while syngas composition had stayed fairly unaffected until the point when wear in the disks is no longer within the acceptable range for testing, the amount of gas produced and correspondent energy expenditure gradually decline in efficiency, creating a whole new variable to take in account when analyzing performance. This was noticeable throughout experimental work and later analysis of results, where the degree in wear had to be considered before comparing flows/energy consumptions of different tests done at different

points in time. For these reasons it is imperative that future versions of the prototype aim to remove the graphite disks by relying only on biomass as a carbon source for co-electrolysis.

5. Conclusions and perspectives for future work

This chapter will feature the main conclusions obtained throughout all the experimental work, followed by some perspectives for future work and development of the prototype plant.

This study was carried out with the objective of optimizing the operation and promote the development of a pilot co-electrolysis plant to produce syngas using liquified biomass obtained from forest residues as a second source of carbon for the electrochemical reaction. The syngas produced is to be used, in the future, as a feedstock for methane production. As such, the experimental work aimed at analyzing and comparing the effects of different sets of conditions, and later, the addition of two different biomass samples at two concentrations, on the outputs of the process, like the composition and energy cost of the syngas produced.

In terms of the main criteria to evaluate the composition of the gas outlet and, considering its use as feedstock in methane production, the syngas produced aims to:

- Have oxygen content as low as possible (to minimize the risk of catalyst deactivation during methanation);
- A CO_2: H_2 ratio ideally close to the one associated with the conversion of CO_2 into methane (1:4);
- A good relation between the flow of gas produced and the energy consumed to produce it.

The experimental work was divided into two main parts. The first focused on operating the system without adding any liquified biomass (relying only on the carbon present in the graphite electrodes) and testing a more ample range of conditions (3, 4, and 5 bar(g) and 90, 100, and 110 ºC) with two different electrolyte solutions (a 1M KOH solution and NaOH with the same concentration).

From the data obtained in this first part, the conclusions found are the following:

- Increasing the system temperature originates both a decrease in O_2 content and an increase in CO_2concentration. Most likely, this is a result of a higher rate of carbon oxidation;
- Similarly, higher pressures and temperatures also lead to the same effect, thus beneficiating the process;
- While it is difficult to examine the implications of pressure and temperature on the amount of gas produced (due to factors such the degree in wear of the electrodes), energy expenditure (electric energy supplied to the stack/the flow produced) offers a better basis for comparison between tests;

- Although the correlation between temperature and energy consumption is not certain due to inconsistent behavior, in the case pressure, both electrolytes displayed less energy consumption above 3 bar(g). In the case of KOH the lowest expenditures appeared consistently at 4 bar(g), and in NaOH at 5 bar(g);
- The KOH electrolyte produced a gas outlet with lower O_2 content (with the lowest value being 1.9 % at 5 bar(g) and 110 ºC) and less desirable $CO_2:H_2$ ratios, implying a higher rate of carbon oxidation in comparison with NaOH.
- When using the NaOH electrolyte, the $CO_2:H_2$ ratios of the gas outlet were closer to the desired 1:4, although this implies lower rates of CO_2 production;
- In terms of the amount of gas produced and energy expenditure, NaOH had consistently the best performance, producing more syngas while consuming less energy;
- Even though KOH has multiple advantages, it proved itself significantly harder to work with. It placed a heavier strain on the system in comparison to NaOH, even damaging equipment and having a faster rate of erosion in the graphite electrode disks.

The results obtained from this were later used in the second part to select a smaller set of conditions, establish a baseline of the operation of the prototype and to later compare with the tests using biomass.

Regarding the second part of the experimental work, this one was focused on testing and evaluating the performance of the system when adding some amount of liquified biomass to serve as a secondary carbon source. Two different samples were tested, one sourced from forest residues of acacia wood (thus labelled “Acacia”) and another of unknown composition, supplied by Secil, labeled as “Energreen”.

As for the new range of conditions, the NaOH solution was chosen as the electrolyte, due to its advantages in reducing energy costs and being easier to work with in general, and new ranges of pressure (4, and 5 bar(g)), and temperature (100, and 110 ºC) were selected.

From the data obtained in this second part, the following could be concluded:

- In both samples, the additions of liquified biomass boosted CO_2 production leading to a significant increase in its content within the gas outlet, consequently lowering the $CO_2:H_2$ ratio. Consequently, O_2 concentrations also lowered;
- Acacia shows favored results regarding the production of a syngas mixture while lowering its O_2 content. Best results at 4 bar(g) at 110 ºC with 2.5%;

- Energreen produced a more optimal $CO_2:H_2$ ratio (at the cost of lower O_2 consumption), and most importantly, has showed the best relation between energy consumed and gas production. Best results at 4 bar(g) at 110 ºC with 2.5 %.
- Regarding optimal conditions, and considering each biomass strong points, coincidentally both have their best performance at 4 bar(g) at 110 ºC with 2.5 %, with Acacia having the lowest O_2 content associated with the lowest expenditure, and Energreen also having the lowest expenditure;
- Although, $CO_2:H_2$ ratios are farther from the ideal value (1:4) when compared to the tests without biomass, this is secondary to the decreasing of O_2 concentrations. Either way, this can be resolved by a later addition of H_2 or alternatively by the partial removal of its CO_2 (being easier compared to removing the O_2).

Besides the optimization tests, a brief study on the erosion of the graphite disks its effects was done by comparing two tests, at the same conditions, with opposite degrees or wear in the electrodes (one with disks eroded to the point where the results had to be rejected and another with a brand-new set). As expected, performance becomes gradually more hindered by the erosion of the disks, with the most noticeable consequence being the production of less syngas at the cost of more energy needed to produce it. Overall, with a limited estimated lifespan of around 30 hours, the graphite electrodes as they are in the current iteration, are a liability to prototype applicability and scale up, by increasing the costs and time associated for maintenance and being a non-renewable source of carbon in an otherwise green alternative for syngas production.

In conclusion, as the data obtained from testing shows, liquified biomass obtained from lignocellulosic forest residues shows a lot of potential as a possible carbon source in co-electrolysis to produce syngas. Although the current prototype iteration still relies on graphite disk electrodes inside the stack to act as a primary source, the addition of biomass improves the process. As such, future iterations should research a possible upgrade by removing the graphite entirely to rely only on the liquified biomass.

Perspectives for future work

As previously mentioned, this research, and all experimental work throughout it, was executed on a 1 kW prototype plant. For this reason and the limitation imposed by this type of study, further testing and development is still needed, with this work merely offering a landmark to help further research in how it should proceed, and which direction should it be focused. Based on the analysis of this current study the advised perspectives are as follows:

- Repeat the tests with KOH at 5 bar(g) group and the 4 bar(g), 100 ºC with 2.5 % Energreen test, as these were done with a significant degree of wear in the electrodes. Repeating these tests would allow for a better analysis of results;
- Redo some tests, now using the new and more precise set of sensors, that unfortunately were only available for the tests with NaOH at 5 bar(g) and had a later malfunction due to excess humidity in the gas outlet. Although they were fixed before finishing experimental work, it was deliberated to continue to use the old set to avoid inconsistencies within the results obtained. (The NaOH at 5 bar(g) were kept due to not being possible to repeat and as way to showcase more precise values for the composition of the syngas);
- A more profound study needs to be done on the gradual erosion of the graphite electrodes in order to find a way to directly compare results without this being an obstacle;
- Implement new and better ways to remove moisture in the gas outlet. The addition of biomass caused a rise in the humidity of the syngas produced, which may damage the sensors if no completely removed. Even after modifying the process by inserting an additional condensation circuit, some humidity is still left;
- The outer shell of the stack should be replaced for a new one able to withstand higher relative pressures (ideally 10 bar(g)) and better adapted to suit this type of process. Originally, there were plans for a set of tests at 6 bar(g) but unfortunately, accumulated damages, caused partially by the used of KOH, left the system unable to function at this pressure without severe leaks and risk of accident;
- Seen as the graphite disks act as unrenewable source of carbon and create multiple problems for the scale up and sustainability of the system, future iteration of the prototype should try to substitute them for steel electrodes and use graphite directly added to the electrolyte and eventually only the liquified biomass as the primary carbon source. Nevertheless, the importance of the disks shouldn’t be undermined as an intermediary set for the final system.

- With regard to the biomass used, although it was not possible to characterise it in detail at the time of this study, a parallel study (by the same colleagues who supplied us with Acacia) is being carried out on this subject;
- In addition to the costs directly associated with the co-electrolysis process, the pre-processing of the biomass to produce the bio-oil should also be considered. As such, further research focused on the economics should also estimate this part.

Publications of the research results

As part of Project Clean Forest, a section of the research results obtained in this thesis were published in the following:

- In Forum de Engenheira Química e Biológica-ISEL (IFEQB) , 2022 and 23, both in the form of posters;
- In the 1st International Conference on Challenges in Engineering, Medical, Economics and Education: Research & Solutions (CEMEERS-23), where the research was the topic of an oral presentation, with an article was published in conjunction;
- In International Chemical and Biological Engineering Conference (CHEMPOR) of 2023, in the form of a poster presentation.

6. Bibliography

Akkala, S. R., Jeremias, M., Kaviti, A. K., & Sikarwar, V. S. (2023). Biomass conversion by gasification process. *Reference Module in Earth Systems and Environmental Sciences*. https://doi.org/10.1016/B978-0-323-93940-9.00017-7

Anion exchange membrane water electrolysis: How it works - Enapter. (n.d.). Retrieved January 2, 2023, from https://www.enapter.com/newsroom/aem-water-electrolysis-how-it-works

B.P. Statistical Review. (2022). *bp Statistical Review of World Energy globally consistent data on world energy markets . The review is one of the most widely respected The Statistical of publications World Energy analyses and Review energy used from by the prior The Review academia , ha. june*.

Barcena, A. (1992). An Overview of the Oceans in Agenda 21 of the 1992 United Nations Conference on Environment and Development. *Marine Pollution Bulletin*, *25*(1–4), 107–111. https://doi.org/10.1016/0025-326X(92)90197-E

Bolt, A., Dincer, I., & Agelin-Chaab, M. (2020). A critical review of synthetic natural gas production techniques and technologies. *Journal of Natural Gas Science and Engineering*, *84*. https://doi.org/10.1016/J.JNGSE.2020.103670

Bolt, H. M. (2022). Methane. *Reference Module in Biomedical Sciences*. https://doi.org/10.1016/B978-0-12-824315-2.00224-4

Cai, W., Gao, L., Luo, Y., Li, X., Zheng, X., Zhang, X., Cheng, X., Jia, F., Purich, A., Santoso, A., Du, Y., Holland, D. M., Shi, J. R., Xiang, B., & Xie, S. P. (2023). Southern Ocean warming and its climatic impacts. In *Science Bulletin* (Vol. 68, Issue 9, pp. 946–960). https://doi.org/10.1016/j.scib.2023.03.049

Calam, A., Aydoğan, B., & Halis, S. (2020). The comparison of combustion, engine performance and emission characteristics of ethanol, methanol, fusel oil, butanol, isopropanol and naphtha with n-heptane blends on HCCI engine. *Fuel*, *266*, 117071. https://doi.org/10.1016/J.FUEL.2020.117071

Chen, W., Lin, T., Dai, Y., An, Y., Yu, F., Zhong, L., Li, S., & Sun, Y. (2018). Recent advances in the investigation of nanoeffects of Fischer-Tropsch catalysts. *Catalysis Today*, *311*, 8–22. https://doi.org/10.1016/J.CATTOD.2017.09.019

Clean Forest | Instituto Superior de Engenharia de Lisboa. (n.d.). Retrieved July 18, 2023, from https://www.isel.pt/investigacao-e-inovacao/ecossistema-de-inovacao/projetos/2019/clean-forest

Climate Change - United Nations Sustainable Development. (n.d.). Retrieved December 20, 2022, from https://www.un.org/sustainabledevelopment/climate-change/

Data.GISS: GISS Surface Temperature Analysis (v4): Global Maps. (n.d.). Retrieved December 18, 2022, from https://data.giss.nasa.gov/gistemp/maps/index_v4.html

Dessie, W., Luo, X., He, F., Liao, Y., Duns, G. J., & Qin, Z. (2023). Lignin valorization: A crucial step towards full utilization of biomass, zero waste and circular bioeconomy. *Biocatalysis and Agricultural Biotechnology*, *51*, 102777. https://doi.org/10.1016/J.BCAB.2023.102777

Dittrich, L., Nohl, M., Jaekel, E. E., Foit, S., Haart, B., & Eicchel, R.-A. (2019). High-Temperature Co-Electrolysis: A Versatile Method to Sustainably Produce Tailored Syngas Compositions. *Journal of The Electrochemical Society*, *13*. https://doi.org/10.1149/2.0581913jes

Franz, R., Uslamin, E. A., & Pidko, E. A. (2021). Challenges for the utilization of methane as a chemical feedstock. *Mendeleev Communications*, *31*(5), 584–592. https://doi.org/10.1016/J.MENCOM.2021.09.002

Ge, X., Chang, C., Zhang, L., Cui, S., Luo, X., Hu, S., Qin, Y., & Li, Y. (2018). Conversion of Lignocellulosic Biomass Into Platform Chemicals for Biobased Polyurethane Application. *Advances in Bioenergy*, *3*, 161–213. https://doi.org/10.1016/BS.AIBE.2018.03.002

Gerloff, N. (2021). Comparative Life-Cycle-Assessment analysis of three major water electrolysis technologies while applying various energy scenarios for a greener hydrogen production. *Journal of Energy Storage*, *43*(March), 102759. https://doi.org/10.1016/j.est.2021.102759

Gomes, J., Puna, J., Marques, A., Gominho, J., Lourenço, A., Galhano, R., & Ozkan, S. (2022). Clean Forest—Project Concept and Early Results. *Energies*, *15*(24). https://doi.org/10.3390/EN15249294

GSYF - Equipamentos para Energia, Lda | www.pvinfo.pl. (n.d.). Retrieved July 25, 2023, from https://www.pvinfo.pl/gsyf-equipamentos-para-energia-lda

Guerra, L., Moura, K., Rodrigues, J., Gomes, J., Puna, J., Bordado, J., & Santos, T. (2018). Synthesis gas production from water electrolysis, using the Electrocracking concept. *Journal of Environmental Chemical Engineering*, *6*(1), 604–609. https://doi.org/10.1016/j.jece.2017.11.033

Guerra, L., Rossi, S., Rodrigues, J., Gomes, J., Puna, J., & Santos, M. T. (2018). Methane production by a combined Sabatier reaction/water electrolysis process. *Journal of*

Environmental Chemical Engineering, *6*(1), 671–676. https://doi.org/10.1016/j.jece.2017.12.066

Güney, T. (2019). Renewable energy , non-renewable energy and sustainable development. *International Journal of Sustainable Development & World Ecology*, *26*(5), 389–397. https://doi.org/10.1080/13504509.2019.1595214

Han, J., He, X., Li, R., Wan, C., Yan, Q., & Yu, F. (2014). *Oxygen removal from syngas by catalytic oxidation of copper catalyst*. https://doi.org/10.1016/j.joei.2014.03.005

IPCC. (n.d.). *Climate Change 2022: Mitigation of Climate Change: Chapter 1 "Introduction and Framing."*

IRENA. (2020). *GREEN HYDROGEN COST REDUCTION SCALING UP ELECTROLYSERS TO MEET THE 1.5°C CLIMATE GOAL H 2 O 2*. www.irena.org/publications

Jarvis, A., Leedal, D., Taylor, C. J., & Young, P. (2009). Stabilizing global mean surface temperature: A feedback control perspective. *Environmental Modelling & Software*, *24*(5), 665–674. https://doi.org/10.1016/J.ENVSOFT.2008.10.016

Jiang, W., Kumar, A., & Adamopoulos, S. (2018). Liquefaction of lignocellulosic materials and its applications in wood adhesives—A review. *Industrial Crops and Products*, *124*, 325–342. https://doi.org/10.1016/J.INDCROP.2018.07.053

JRC. (2022). *CO2 emissions of all world countries*. https://doi.org/10.2760/07904

Junaedi, C., Hawley, K., Walsh, D., Roychoudhury, S., Abney, M. B., & Perry, J. L. (2011). Compact and lightweight sabatier reactor for carbon dioxide reduction. *41st International Conference on Environmental Systems 2011, ICES 2011*. https://doi.org/10.2514/6.2011-5033

Kelly, N. A. (2014). Hydrogen production by water electrolysis. *Advances in Hydrogen Production, Storage and Distribution*, 159–185. https://doi.org/10.1533/9780857097736.2.159

Khodakov, A. Y., Chu, W., & Fongarland, P. (2007). *Advances in the Development of Novel Cobalt Fischer−Tropsch Catalysts for Synthesis of Long-Chain Hydrocarbons and Clean Fuels*. https://doi.org/10.1021/cr050972v

Kim, J., & Park, K. (2016). *Financial development and deployment of renewable energy technologies ☆*. https://doi.org/10.1016/j.eneco.2016.08.012

Kvamme, O. A. (2023). Curriculum and the United Nations' sustainable development goals. *International Encyclopedia of Education: Fourth Edition*, 406–413.

https://doi.org/10.1016/B978-0-12-818630-5.03071-2

Lavate, S., Yalamati, H. P. S., & Srivastava, R. (2023). Application of hydrogen in various sectors. *Solar-Driven Green Hydrogen Generation and Storage*, 507–524. https://doi.org/10.1016/B978-0-323-99580-1.00002-9

Lehner, F., & Hart, D. (2022). The importance of water electrolysis for our future energy system. *Electrochemical Power Sources: Fundamentals, Systems, and Applications Hydrogen Production by Water Electrolysis*, 1–36. https://doi.org/10.1016/B978-0-12-819424-9.00008-2

Lu, S., Shi, Y., Meng, N., Lu, S., Yu, Y., & Zhang, B. (2020). Electrosynthesis of Syngas via the Co-Reduction of CO2 and H2O. *Cell Reports Physical Science*, *1*(11). https://doi.org/10.1016/J.XCRP.2020.100237

Lu, W. C. (2017). Greenhouse gas emissions, energy consumption and economic growth: A panel cointegration analysis for 16 Asian countries. *International Journal of Environmental Research and Public Health*, *14*(11). https://doi.org/10.3390/IJERPH14111436

Lundegard, P. D. (1964). Methane. *Environmental Forensics: Contaminant Specific Guide*, 97–110. https://doi.org/10.1016/B978-012507751-4/50028-8

Ma, X., & Fu, Q. (2020). The influence of financial development on energy consumption: Worldwide evidence. *International Journal of Environmental Research and Public Health*, *17*(4). https://doi.org/10.3390/ijerph17041428

Mamlouk, M. (2022). Alkaline Anion Exchange Membrane (AEM) Water Electrolysers—Current/Future Perspectives in Electrolysers for Hydrogen. *Comprehensive Renewable Energy, Second Edition: Volume 1-9*, *1–4*, 473–504. https://doi.org/10.1016/B978-0-12-819727-1.00103-5

Masyagina, O. V., & Menyailo, O. V. (2020). The impact of permafrost on carbon dioxide and methane fluxes in Siberia: A meta-analysis. *Environmental Research*, *182*. https://doi.org/10.1016/J.ENVRES.2019.109096

Mateus, M. M., Bordado, J. C., Galhano, R., & Santos, D. (2016). *Potential biofuel from liquefied cork-Higher heating value comparison*. https://doi.org/10.1016/j.fuel.2016.01.081

Mazzeo, D., Sacit Herdem, M., Matera, N., & Wen, J. Z. (2022). Green hydrogen production: Analysis for different single or combined large-scale photovoltaic and wind renewable systems. *Renewable Energy*, *200*, 360–378. https://doi.org/10.1016/j.renene.2022.09.057

Moulijn, J. A., Makkee, M., & Van Diepen, A. E. (2013). *Chemical Process Technology* (Second Edi). Wiley.

Museo Galileo - In depth - Methane. (n.d.). Retrieved January 18, 2023, from https://catalogue.museogalileo.it/indepth/Methane.html

Ott, J., Gronemann, V., Pontzen, F., Fiedler, E., Grossman, G., Burkhard Kersebohm, K., Weiss, G., & Witte, C. (2012). Methanol - An Industrial Review by Lurgi GmbH, Air Liquide GmbH and BASF AG. *Ullmann's Encyclopedia of Industrial Chemistry*.

Overview of greenhouse gases - NAEI, UK. (n.d.). Retrieved November 29, 2022, from https://naei.beis.gov.uk/overview/ghg-overview.php

Ozturk, M., Saba, N., Altay, V., Iqbal, R., Rehman Hakeem, K., Jawaid, M., & Hanum Ibrahim, F. (2017). *Biomass and bioenergy: An overview of the development potential in Turkey and Malaysia*. https://doi.org/10.1016/j.rser.2017.05.111

Primary, secondary, final, and useful energy: Why are there different ways of measuring energy? - Our World in Data. (n.d.). Retrieved July 17, 2023, from https://ourworldindata.org/energy-definitions

Provisional State of the Global Climate 2022. (n.d.). Retrieved December 14, 2022, from https://storymaps.arcgis.com/stories/5417cd9148c248c0985a5b6d028b0277

Qian, E. W. (2014). Pretreatment and Saccharification of Lignocellulosic Biomass. *Research Approaches to Sustainable Biomass Systems*, 181–204. https://doi.org/10.1016/B978-0-12-404609-2.00007-6

Rehman, M. U., Rashid, M., Zulfikar, S., & Bhutto, A. (2017). *Energy consumption to environmental degradation, the growth appetite in SAARC nations*. https://doi.org/10.1016/j.renene.2017.03.100

Saunois, M., R. Stavert, A., Poulter, B., Bousquet, P., G. Canadell, J., B. Jackson, R., A. Raymond, P., J. Dlugokencky, E., Houweling, S., K. Patra, P., Ciais, P., K. Arora, V., Bastviken, D., Bergamaschi, P., R. Blake, D., Brailsford, G., Bruhwiler, L., M. Carlson, K., Carrol, M., … Zhuang, Q. (2020). The global methane budget 2000-2017. *Earth System Science Data*, *12*(3), 1561–1623. https://doi.org/10.5194/ESSD-12-1561-2020

Scheiner, S. M. (2023). Greenhouse Effect. *Reference Module in Life Sciences*. https://doi.org/10.1016/B978-0-12-822562-2.00132-8

Senior, S. Ø. (2008). *Issue paper: Definition of primary and secondary energy*. http://www.iea.org/Textbase/publications/free_new_Desc.asp?PUBS_ID=1461

Shiva Kumar, S., & Lim, H. (2022). An overview of water electrolysis technologies for green hydrogen production. *Energy Reports*, *8*, 13793–13813. https://doi.org/10.1016/J.EGYR.2022.10.127

Shlesinger, T., & van Woesik, R. (2023). Oceanic differences in coral-bleaching responses to marine heatwaves. *Science of The Total Environment*, *871*, 162113. https://doi.org/10.1016/J.SCITOTENV.2023.162113

Speight, J. G. (2020). Synthesis gas and the Fischer–Tropsch process. *The Refinery of the Future*, 427–468. https://doi.org/10.1016/B978-0-12-816994-0.00012-9

Thangal, S. H., Muralisankar, T., Anandhan, K., Gayathri, V., & Yogeshwaran, A. (2022). Effect of CO 2 driven ocean acidification on the mud crab Scylla. *Environmental Pollution*, *312*(July), 119995. https://doi.org/10.1016/j.envpol.2022.119995

Thomassen, M. S., Reksten, A. H., Barnett, A. O., Khoza, T., & Ayers, K. (2022). PEM water electrolysis. *Electrochemical Power Sources: Fundamentals, Systems, and Applications Hydrogen Production by Water Electrolysis*, 199–228. https://doi.org/10.1016/B978-0-12-819424-9.00013-6

UN Enviroment Programme. (2022). *Emissions Gap report 2022*.

Vasseur, E. (1973). United Nations Conference on the Human Environment: Stockholm, 5–16 June 1972. *Water Research*, *7*(8), 1227–1233. https://doi.org/10.1016/0043-1354(73)90077-8

Wei, H., Yingting, Y., Jingjing, G., Wenshi, Y., & Junhong, T. (2017). Lignocellulosic Biomass Valorization: Production of Ethanol. *Encyclopedia of Sustainable Technologies*, 601–604. https://doi.org/10.1016/B978-0-12-409548-9.10239-8

Wei, X., Sharma, S., Marechal, F., & Van Herle, J. (2023). *Design and optimization of a shared heat exchanger network for an integrated rSOC system*. *52*, 1065–1070. https://doi.org/10.1016/B978-0-443-15274-0.50170-0

Yang, W., Shimanouchi, T., Iwamura, M., Takahashi, Y., Mano, R., Takashima, K., Tanifuji, T., & Kimura, Y. (2015). Elevating the fuel properties of Humulus lupulus, Plumeria alba and Calophyllum inophyllum L. through wet torrefaction. *Fuel*, *146*, 88–94. https://doi.org/10.1016/J.FUEL.2015.01.005

Yue, S., Lu, R., Shen, Y., & Chen, H. (2019). *How does financial development affect energy consumption? Evidence from 21 transitional countries*. https://doi.org/10.1016/j.enpol.2019.03.029

Zheng, Y., Wang, J., Yu, B., Zhang, W., Chen, J., Qiao, J., & Zhang, J. (2017). A review of high temperature co-electrolysis of H2O and CO2 to produce sustainable fuels using solid oxide electrolysis cells (SOECs): Advanced materials and technology. *Chemical Society Reviews*, *46*(5), 1427–1463. https://doi.org/10.1039/C6CS00403B

7. Annexes

Index of Annexes

7.1. Photos of the current prototype and equipment

Figure 7-1:Electrolyzer stack shell

Figure 7-2: Electrolyte feeding tank;

Figure 7-3: Pressure valve at the top of the feeding tank

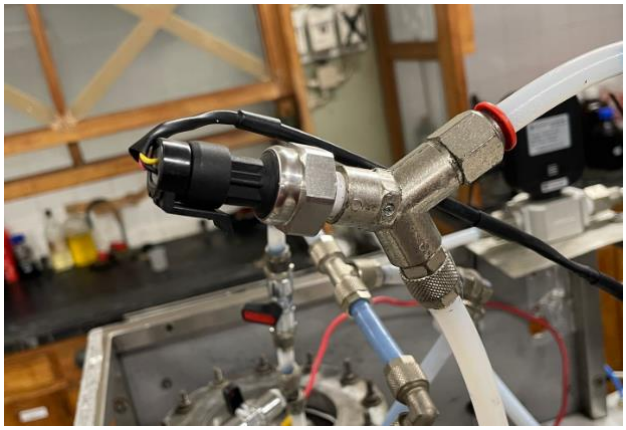

Figure 7-4:pressure sensor in the gas exit

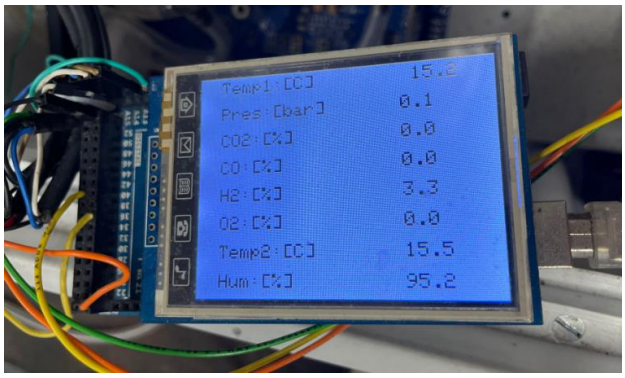

Figure 7-5: Gas analyser display;

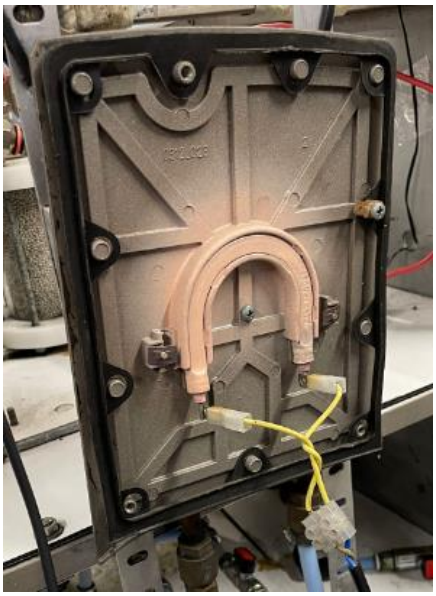

Figure 7-6: Heating coil responsible for heating;

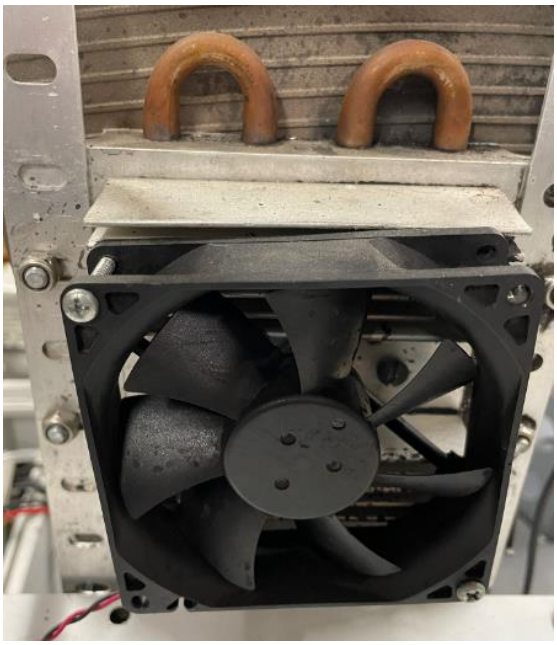

Figure 7-7: Cooling fan;

Figure 7-8:Power supply conected to the stack;

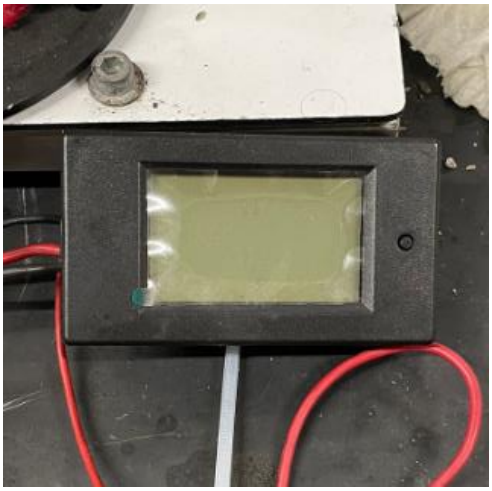

Figure 7-9: Voltage and current intensity display;

Figure 7-10: New set of sensors;

7.2. Biomass FTIR analysis

Throughout the set of tests using biomass, after finishing each group a sample of each used electrolyte (with the biomass diluted) was kept for Fourier Transform Infrared Spectroscopy (FTIR) analysis. The following Figure 7-11,Figure 7-12Figure 7-13Figure 7-14 andFigure 7-15 correspond to the absorbance spectra obtained for each sample.

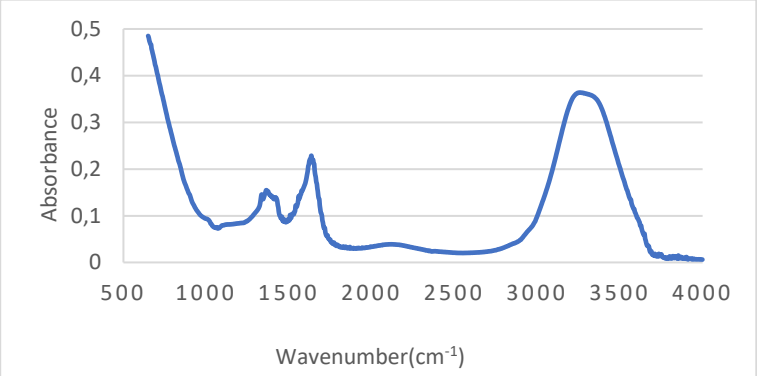

Figure 7-11: 2.5 % Acacia FTIR Absorbance spectra;

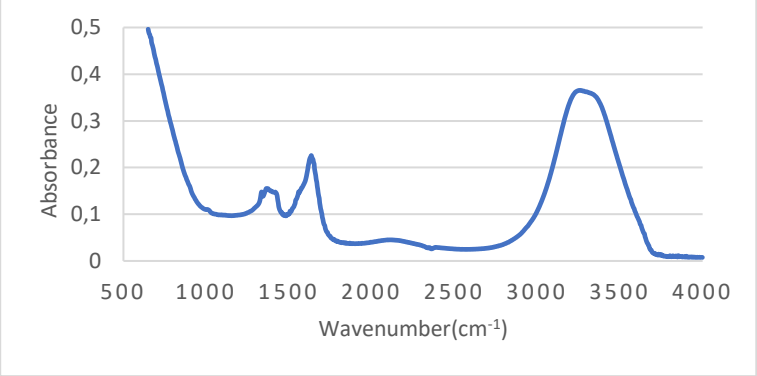

Figure 7-12: 5 % Acacia FTIR Absorbance spectra;

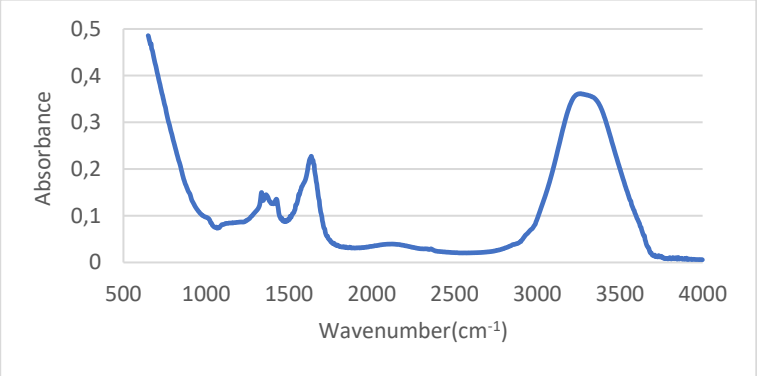

Figure 7-13: 2.5 % Energreen FTIR Absorbance spectra;

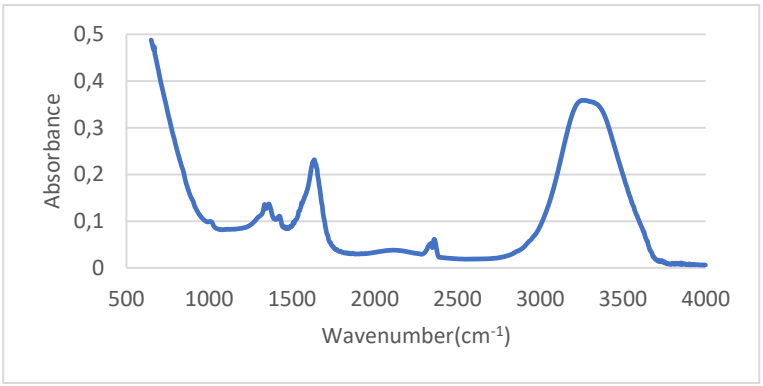

Figure 7-14: 5 % Energreen FTIR Absorbance spectra

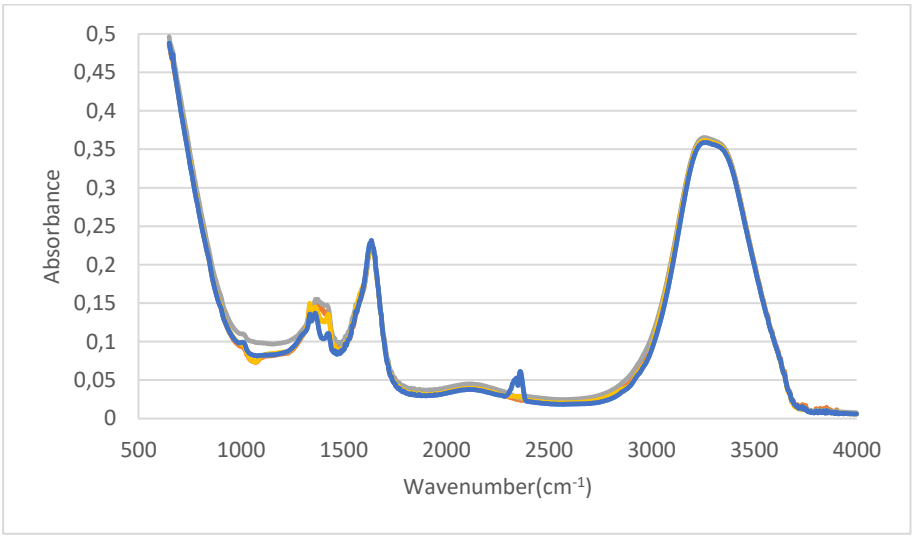

Figure 7-15: Compilation of all tests FTIR Absorbance spectra

From the analysis of the spectra and based on a similar study from Mateus et al., 2016 the following key bands were identified in all cases:

- a strong wide band between 3200 and 3500 cm^{-1} corresponding to the vibration of the $O-H$, associated with carboxylic acids and derivatives;
- a signal between 1600 and 1700 cm^{-1} corresponding $C=O$ stretching vibration characteristic of ester groups;
- A group of peaks between 1300 and 1450 cm^{-1} most likely corresponding to a combination of stretching $C-O-H$ of carboxylic acids and derivatives and $C-O-C$ stretch of cyclic ethers which is also quite common in carbohydrates.

7.3. Poster presented in IFEQB 2022

Utilização de biomassa florestal liquefeita na co-eletrólise da água para produção de gás de síntese

Martins, D. M.[1*], Troiano A.[1], Gonçalves A. D.[1] , Cabrita, T. M.[2], Rodrigues, J. C.[2], Puna[1,3], J. F., Gomes, J. F.[1,3]

[1]Departamentol de Engenharia Química, Instituto Superior de Engenharia de Lisboa, Instituto Politécnico de Lisboa, R. Conselheiro Emídio Navarro 1, 1959-007 Lisboa, Portugal

[2] GSyF, Lda, R. S. Sebastião, 11 2500-064 Fanadia, Caldas da Rainha

[3] CERENA – Centro de Recursos Naturais e Ambiente, Instituto Superior Técnico, Universidade de Lisboa, Av. Rovisco Pais, 1, 1949-001 Lisboa, Portugal

*a43720@alunos.isel.pt

Introdução

O aumento contínuo da necessidade energética mundial nas últimas décadas resultou num crescente consumo de fontes combustíveis não renováveis (petróleo, gás natural entre outros) e, consequentemente, maiores impactes ambientais. Por esta mesma razão, observa-se uma aposta cada vez maior no desenvolvimento de possíveis fontes de combustível sustentáveis (biomassa, energia solar, eólica, entre outras).

Desenvolvido no âmbito de um projeto I&DT pela start-up GSYF, Lda, (que tem trabalhado no Lab. Tec. Química do DEQ/ISEL), esta unidade piloto de 1 KW tem como objetivo a valorização de biomassa previamente liquefeita de resíduos florestais lignocelulósicos, a qual será posteriormente utilizada como fonte de carbono num processo de co-eletrólise, destinado à produção de gás síntese (H_2, CO, CO_2), também designado por *syngas*. Por sua vez, este *syngas* será transformado em outros produtos de valor acrescentado, nomeadamente, de biocombustíveis sintéticos.

A produção de syngas por via eletroquímica tem por base as seguintes reações:

Reações no cátodo:

$$2H_2O + 2e^- \rightarrow 2H_2 + 2OH^-$$

Reações no ânodo:

$$4OH^- \rightarrow O_2 + H_2O + 4e^-$$

$$2C + O_2 \rightarrow 2CO$$

$$2CO + O_2 \rightarrow 2CO_2$$

Reação global de processo:

$$2H_2O + C + W_e \rightarrow 2H_2 + CO_2$$

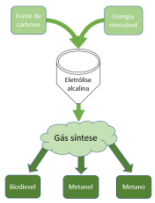

Figura 1. Processo de produção de gás síntese por via electroquímnica, patenteado pela GSYF.

Metodologia

Os trabalhos atuais focam-se no na realização de testes de otimização das condições de uma unidade protótipo constituída por um reservatório de eletrólito, um conjunto de sensores de pressão e temperatura, bomba de transporte, um radiador com ventoinha (de modo a controlar a temperatura de processo), uma resistência de aquecimento, uma coluna de adsorção de humidade e um eletrolisador constituído por um stack de 11 discos de grafite.

Relativamente ao eletrólito usado, nos testes de otimização recorreu-se primeiro a uma solução de KOH(1M), sendo que nos dois últimos conjuntos de testes fui usada uma solução de NaOH de igual concentração.

É importante referir que em testes futuros está planeada a adição de biomassa liquefeita. Esta irá servir como fonte secundária de carbono para a reação de conversão de O_2 em CO_2. O flowsheet deste processo encontra-se apresentado na figura 2.

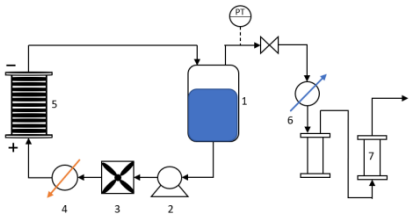

Figura 2. Flowsheet do processo protótipo: (1) Reservatório de eletrólito; (2) bomba; (3) Radiador com ventoinha; (4) Resistência de aquecimento; (5) Eletrolisador; (6) Depósito de condensados; (7) Coluna de adsorção de humidade, com sílica gel.

Resultados e Discussão

Teste	T (°C)	P (bar)	V (V)	I (A)	V/cell	CO2 (%)	H2 (%)	O2 p(%)	CO (%)	Fp (l/h)	Wh/l	R²
1	90,9	4,2	32,0	15,5	2,7	31,3	63,2	3,5	2,0	49,2	10,1	1,064
2	101,2	4,1	30,0	14,5	2,5	36,2	59,8	2,4	1,6	48,7	8,9	1,033
3	110,6	4,1	29,0	16,8	2,4	33,5	62,8	2,3	1,4	53,5	9,1	1,082
4	91,1	4,9	33,0	15,0	2,8	29,3	65,6	3,0	2,1	48,3	10,2	1,323
5	100,9	4,8	30,0	15,0	2,5	31,1	64,9	2,0	2,0	46,3	9,7	1,196
6	109,7	5,3	31,0	17,5	2,6	29,9	66,4	1,8	1,9	50,6	10,7	1,412
7	91,6	6,0	30,0	15,0	2,5	30,4	63,8	4,0	1,8	44,1	10,2	1,012
8	101,0	5,9	30,0	15,0	2,5	29,7	65,1	3,4	1,8	44,5	10,1	1,020
9	110,1	6,1	30,0	17,5	2,5	29,3	66,0	2,9	1,8	47,1	11,1	1,073
10	90,8	4,1	34,0	14,5	2,8	26,7	65,7	5,8	1,8	54,4	9,1	1,359
11	101,2	4,2	34,0	15,0	2,8	25,0	69,1	4,1	1,8	46,0	11,1	1,366
12	109,9	4,0	32,0	16,0	2,7	26,3	68,4	3,5	1,8	44,3	11,6	1,366
13	89,8	5,6	38,9	15,3	3,2	26,2	60,8	10,9	2,1	70,2	8,5	1,471
14	102,4	5,2	39,5	9,9	3,3	30,0	59,0	9,0	2,0	57,2	6,8	1,515
15	110,7	5,4	35,9	13,8	3,0	30,0	59,7	8,3	2,1	59,7	8,3	1,302

Tabela 1: Testes realizados no protótipo para os electrólitos KOH e NaOH: 1-1M de KOH, 4 bar, 90°C; 2-1M de KOH, 4 bar, 100°C; 3-1M de KOH, 4 bar, 110°C; 4-1M de KOH, 5 bar, 90°C; 5-1M de KOH, 5 bar, 100°C; 6-1M de KOH, 5 bar, 110°C; 7-1M de KOH, 6 bar, 90°C; 8-1M de KOH, 6 bar, 100°C; 9-1M de KOH, 6 bar, 110°C; 10-1M de NaOH, 4 bar, 90°C; 11-1M de NaOH, 4 bar, 100°C; 12-1M de NaOH, 4 bar, 110°C ; 13-1M de NaOH, 5 bar, 90°C; 14-1M de NaOH, 5 bar, 100°C; 15-1M de NaOH, 5 bar, 110°C

Antes de proceder á analise dos resultados obtidos é necessário referir que o ultimo conjunto de testes (1M de NaOH, 5 bar), foi realizado após a mudança dos discos de grafite e instalação de um novo conjunto de sensores de maior precisão.

Os testes efetuados podem ser divididos em dois conjuntos correspondentes ao eletrólito usado, sendo que nos primeiros nove foi utilizada uma solução de KOH (1M) e, nos restantes, uma solução de NaOH com a mesma concentração (sendo que ainda falta efetuar os testes referentes ás condições de 6 bars com este eletrólito).

Ao comparar a potência usada por caudal de gás síntese obtido (Wh/L), observa-se que, em geral, para as diferentes condições de pressão e temperatura, o NaOH apresenta um valor menor, o qual, por sua vez, irá corresponder a um menor custo de funcionamento de processo. Através dos dados obtidos deduz-se ainda que, o aumento da pressão de funcionamento traduz-se também no aumento da potência por caudal.

Relativamente á composição e, assumindo que o gás de síntese poderá ser direcionado para um reator de Metanação (*Sabatier*), é importante ter em conta especificamente a concentração de CO_2(irá ser convertido em metano como é mostrado na reação seguinte) e o O_2 que poderá desativar os catalisadores usados no processo. Para definir a composição foi usado um conjunto de sensores, que permitiram a monitorização continua do gás produzido ao longo de cada teste(exemplo na figura 2)

$$CO_2 + 4H_2 \rightarrow CH_4 + 2H_2O$$

$$CO + 3H_2 \rightarrow CH_4 + H_2O$$

Tendo em conta isto conclui-se que enquanto que o aumento da temperature de funcionamento resulta numa menor concentração de O_2, o aumento de pressão resulta num acréscimo deste valor. Por outro caso, relativamente ao CO_2 produzido, tambem é possivel observar que o aumento da pressão de funcionamento resulta num decréscimo da concentração deste.

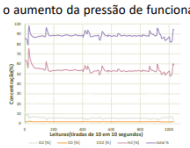

Figura 2. Exemplo da Variação das concentrações dos diferentes componentes do gás síntese ao longo de um dos testes(15-1M de NaOH, 5 bar, 110°C)

Conclusões

Este conjunto de testes teve como objetivo a comparação do desempenho de duas soluções de eletrólito distintas (1M de KOH e 1M de NaOH) sob diferentes condições de pressão (4, 5 e 6 bar) e temperatura de funcionamento (90, 100 e 110 ºC). Este procedimento irá possibilitar a otimização das condições de funcionamento do processo, introduzindo o uso de biomassa liquefeita enquanto fonte alternativa de carbono, de modo a maximizar a viabilidade económica deste e desta forma permitir assim o seu uso numa escala maior associada ao mercado atual.

Ao longo dos vários testes realizados, baixas percentagens de O_2 é benefico do ponto de vista processual porque, em caso de utilização do *syngas* produzido num processo de metanação, este irá traduzir-se num menor envenenamento do catalisador utilizado e, consequentemente, num processo mais rentável. Deste modo, é possível concluir que, as condições em que se observa uma menor percentagem de O_2 correspondem ao teste com 1M de KOH, a 5 bar e 110°C.

Relativamente á potência por caudal de gás produzido, é ideal que este valor seja o menor possível, visto que este irá traduzir em parte no custo energético associado à operação do processo. Sendo assim, observa-se que, o teste com o menor valor correspondeu às condições de 1M de NaOH, 5 bar e 100°C, com um Wh/L igual a 6,8.
Em testes futuros pretende-se avaliar o desempenho deste mesmo electrolizador com adição de biomassa liquefeita e, a sua eficiência enquanto meio sustentável alternativo aos processos termoquímicos já existentes.

Agradecimentos

Agradecimentos: Os autores agradecem à Fundação para a Ciência e Tecnologia (FCT, I. P.) pelo financiamento concedido, através do projeto "CLEANFOREST", ref.ª PCIF/GVB/0167/2018.

Referências

Guerra, L.; Rossi, S.; Rodrigues, J.; Gomes, J.; Puna, J.; Santos, M.T. Methane production by a combined Sabatier reaction/water electrolysis process. *Journal of Environmental Chemical Engineering*. **2018**, 671-676. **(Artigo).**

Guerra, L.; Moura, K.; Rodrigues, J.; Gomes, J.; Puna, J.; Bordado, J.; Santos, T. Synthesis gas production from water electrolysis, using the Electrocracking concept. *Journal of Environmental Chemical Engineering*. **2018**, 604-609. **(Artigo).**

Gonçalves, A.; Puna, J.; Guerra, L.; Rodrigues, J.; Gomes, J.; Santos, M.T.; Alves, D. Towards the Development of Syngas/Biomethane Electrolytic Production, Using Liquefied Biomass and Heterogeneous Catalyst. *Energies*.**2019**, 12, 3787. **(Artigo).**

7.4. Poster presented in IFEQB 2023 and Chempor 2023

Liquified biomass utilization in water co-electrolysis for Synthesis gas production

D.M. Martins [1,*], T.M. Cabrita [2], J.C. Rodrigues [2], J.F. Puna [1,3], J.F. Gomes [1,3]

[1] Instituto Superior de Engenharia de Lisboa, Instituto Politécnico de Lisboa, R. Conselheiro Emídio Navarro 1, 1959-007 Lisbon, Portugal;

[2] GSyF, Lda, R. S. Sebastião, 11 2500-064 Fanadia, Caldas da Rainha, Portugal;

[3] CERENA – Centro de Recursos Naturais e Ambiente, Instituto Superior Técnico, Universidade de Lisboa, Av. Rovisco Pais, 1, 1949-001, Lisbon, Portugal; *

diogo15martins@gmail.com

ChemPor 2023

Introduction

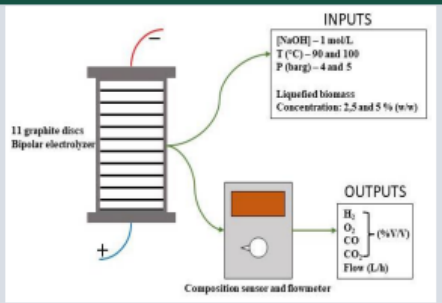

Figure 1: simplified visual system explanation.

Over the last decades, the continuous increase in the world's energy needs resulted in growing consumption of non-renewable fuel sources (oil, natural gas, among others) and, consequently, greater environmental impacts. For this same reason, there is an increasing commitment to the development of alternative sustainable energy sources (biomass, solar and wind energy, among others).[1]

Developed within the scope of an R&DT project by the start-up GSYF, Lda, this 1 kW pilot unit aims at the recovery of previously liquefied biomass from lignocellulosic forest residues, later used as a carbon source in a co-electrolysis process, intended for the production of synthesis gas (H_2, CO, CO_2), also known as syngas. In turn, this syngas will be transformed into other value-added products, namely synthetic biofuels such as methane, methanol or biodiesel. This prototype unit consists of an electrolyte reservoir, a set of pressure and temperature sensors, a transport pump, a radiator with a fan (in order to control the temperature of the process), a heating resistance, a moisture adsorption column and an electrolyzer consisting of a stack of 11 spaced graphite discs.[2], [3]

Process Theory

The production of synthesis gas via electrochemical means is based on the following reactions[2]:

Cathode reactions:

$$2H_2O + 2e^- \rightarrow 2H_2 + 2OH^-$$

Anode reactions:

$$4OH^- \rightarrow O_2 + H_2O + 4e^-$$

$$2C + O_2 \rightarrow 2CO$$

$$2CO + O_2 \rightarrow 2CO_2$$

Global reaction:

$$2H_2O + C + W_e \rightarrow 2H_2 + CO_2$$

Objective

Current experimental work focuses on optimizing syngas production to later be in the future used as feedstock for methane production. For this specific purpose, the syngas produced aims for: [3]

- oxygen concentrations as low as possible (to minimize the risk of catalyst deactivation during methanation);
- a CO_2:H_2 ratio ideally close to the one associated with the conversion of CO_2 into methane (1:4).

Two different biomasses were tested at two different concentrations (2.5 and 5% (w/w)) to compare with each other and the performance without using any liquified biomass. In all tests, the electrolyte was a 1M solution of NaOH.

Methodology

Three different groups of tests were executed:

- one without adding liquified biomass;
- one using a liquified sample of Acacia biomass
- another using a sample of non-specified composition designated as evergreen.

Within the following range of conditions:

- for each biomass they were diluted in the electrolyte solution at 2.5 and 5%;
- pressures of 4 and 5 bar gauge;
- and temperature of 100 and 110 ˚C.

They were executed over 3 hours with data being collected in intervals of 15 minutes. For simpler presentation the average of the 3 last collections in the stationary state was collected and presented as the shortened results for each test.

Results

As sample of the data collected, the following table present an example of a comparison of performance for the conditions of 4 bar gauge and 100 ˚C while the graph below displays the variation in syngas composition through out one of the tests in the same group:

Biomass used	O_2 (%)	CO (%)	CO_2 (%)	H_2 (%)	F (L/h)	CO_2:H_2 Ratio
Without Biomass	4.1	1.8	25.4	68.7	46.84	2.71
2.5% Acacia	3.9	2.0	34.5	59.6	67.53	1.72
5% Acacia	3.3	2.0	54.9	39.7	63.21	0.72
2.5% Energreen	6.2	2.0	40.6	51.2	56.83	1.26
5% Energreen	4.1	2.0	40.6	53.3	67.68	1.31

Table 1: Test results for the conditions of 4 barg and 100 ˚C.

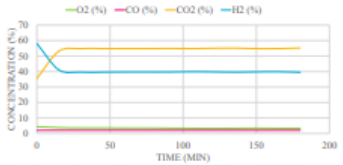

Figure 2: gas outlet composition over the duration of the teste, 5% Acacia biomass, at 4 barg and 100 ˚C.

Conclusion

From the data obtained through experimental work it can be concluded that the additions of liquified biomass causes significant increase in the CO_2 content in the gas outlet, resulting in a lower CO_2:H_2 ratio. Additionally, the higher CO_2 productions also requires more O_2 consumption, generating syngas with lower O_2 concentration.

Focusing on the production of syngas specifically for future use in methanation, the addiction of biomass, specifically Acacia shows favored results in the production of a syngas mixture while lowering its O_2 content. On the other hand, CO_2:H_2 ratios as expected are farther from the ideal value when compared to the ideal 0.25. Although, this can be easily resolved either by later addition of H_2 or alternatively the partial removal of its CO_2 (this still being an easier approach compared to removing the O_2).

References

[1] X. Ma and Q. Fu, "The influence of financial development on energy consumption: Worldwide evidence," *Int. J. Environ. Res. Public Health*, vol. 17, no. 4, 2020, doi: 10.3390/ijerph17041428.

[2] L. Guerra *et al.*, "Synthesis gas production from water electrolysis, using the Electrocracking concept," *J. Environ. Chem. Eng.*, vol. 6, no. 1, pp. 604–609, 2018, doi: 10.1016/j.jece.2017.11.033.

[3] L. Guerra, S. Rossi, J. Rodrigues, J. Gomes, J. Puna, and M. T. Santos, "Methane production by a combined Sabatier reaction/water electrolysis process," *J. Environ. Chem. Eng.*, vol. 6, no. 1, pp. 671–676, 2018, doi: 10.1016/j.jece.2017.12.066.

Acknowledgements

The authors would like to thank the *Fundação para a Ciência e Tecnologia* (FCT, I.P.) for funding granted through the project "CLEANFOREST", ref. PCIF/GVB/0167/2018.

7.5. Scientifically paper published in Excellence in Research & Innovation in Education (EIRAI) as part of CEMEERS-23 Online Proceeding

The article can be found through the following doi:

https://doi.org/10.17758/EIRAI19.F0623121